ECR plasma deposited SiO_2 and Si_3N_4 layers

a room temperature technology

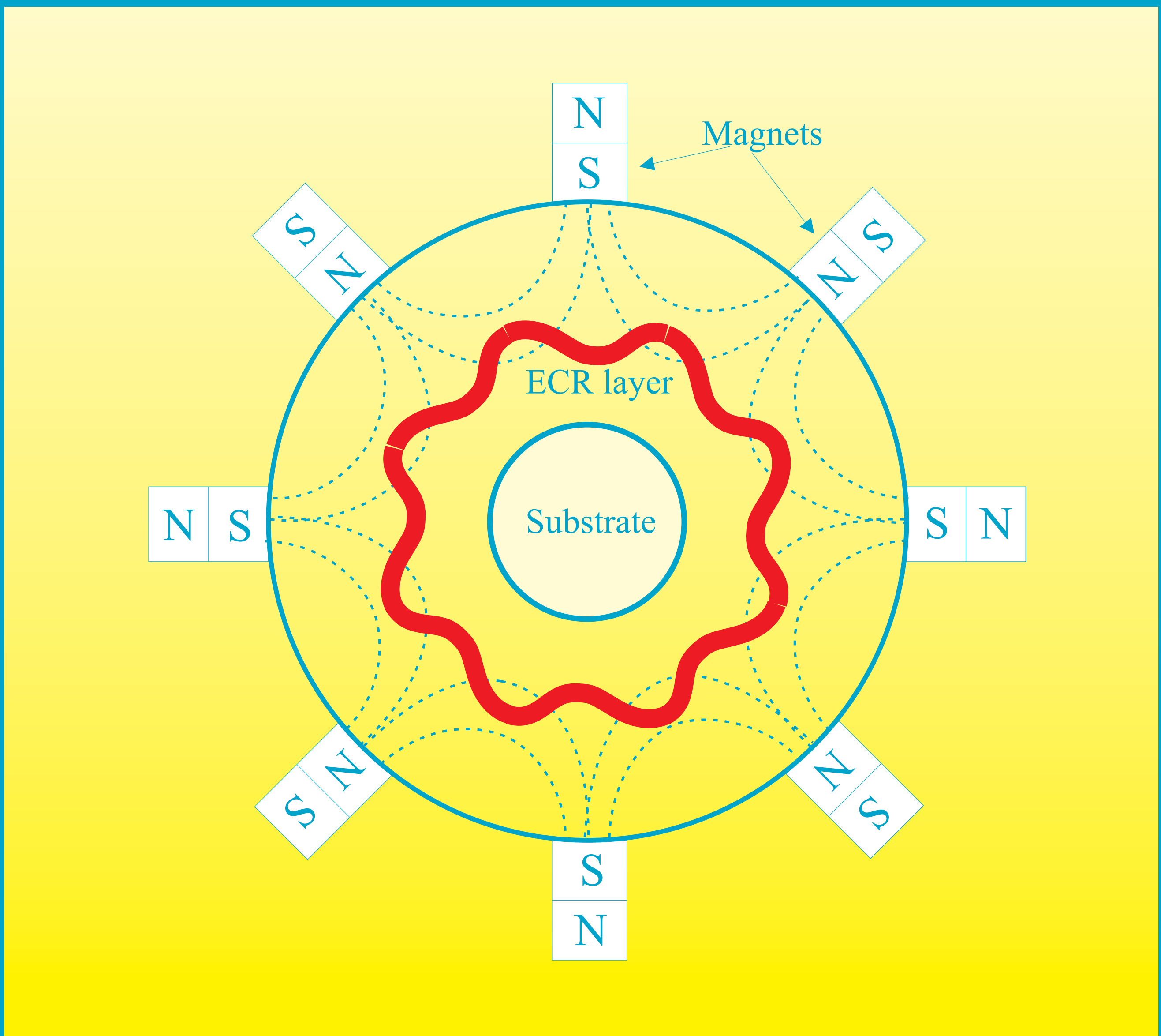

Gratiela Isai

ECR PLASMA DEPOSITED SiO_2 AND Si_3N_4 LAYERS

A ROOM TEMPERATURE TECHNOLOGY

Promotiecommissie:

Voorzitter:	
Prof. dr. W.H.M. Zijm	Universiteit Twente
Promotoren:	
Prof. dr. H. Wallinga	Universiteit Twente
Prof. dr. P.H. Woerlee	Philips Research Laboratories
Assistent promotor:	
Dr. J. Holleman	Universiteit Twente
Leden:	
Prof. dr. P.M. Sarro	TU Delft/DIMES
Prof. dr. ing. C. Cobianu	"Valahia" Univ. of Targoviste, Roemenië
Prof. dr. ing. D.H.A. Blank	Universiteit Twente
Prof. dr. J. Schmitz	Universiteit Twente

ISBN 90-365-1934-9

©Gratiela Isai, 2003

This research was financially supported by the Dutch Foundation for Fundamental Research on Matter (FOM).

ECR PLASMA DEPOSITED SiO_2 AND Si_3N_4 LAYERS

A ROOM TEMPERATURE TECHNOLOGY

PROEFSCHRIFT

ter verkrijging van
de graad van doctor aan de Universiteit Twente,
op gezag van de rector magnificus,
prof. dr. F.A. van Vught,
volgens besluit van het College voor Promoties
in het openbaar te verdedigen
op vrijdag 27 juni 2003 om 16.45 uur

door

Gratiela Ileana Isai

geboren op 24 september 1975

te Ploiesti, Romania

Dit proefschrift is goedgekeurd door:

de promotoren: Prof. dr. H. Wallinga

Prof. dr. P.H. Woerlee

en de assistant promotor: Dr. J. Holleman

To Ana and Bogdan

TABLE OF CONTENTS

1. Introduction 1

1.1. Gate dielectrics for thin film transistors 1

1.2. Low temperature deposition 2

1.3. Deposition techniques 3

1.4. Motivation 5

1.5. Outline of the thesis 6

1.6. References 6

2. Theoretical and experimental details 9

2.1. Electron cyclotron plasma 9

2.1.1. *Energy transfer* 11

Pressure influence upon plasma parameters 13

Microwave power influence upon plasma parameters 14

2.1.2. *Plasma chemistry* 15

Electron-impact processes 16

Neutral reaction chemistry 17

Plasma kinetics 18

2.1.3. *ECR deposition system* 21

2.2. Jet Vapour Deposition 22

2.3. Wafer preparation and deposition conditions 24

2.4. Physical and chemical characterisation equipment 24

2.5. Electrical characterisation 25

2.5.1. *Capacitance-Voltage characteristics* 26

2.5.2. *Current-Voltage characteristics* 28

2.6. References 31

3. Physical properties of ECR SiO_2 35

3.1. Introduction 35

3.2. Deposition kinetics 36

3.2.1. *SiH_4 flow role* 37

3.2.2. *Pressure role* 39

3.2.3. *Microwave power role* 40

3.2.4. *N_2O flow role* 41

3.2.5. *Temperature role* 42

3.3. Refractive index ... 43

3.3.1. SiH_4 flow role ... 44

3.3.2. Pressure role ... 45

3.3.3. Microwave power role ... 46

3.3.4. N_2O flow role ... 47

3.3.5. Temperature role ... 48

3.4. Atomic composition ... 49

3.4.1. SiH_4 flow role ... 50

3.4.2. Microwave power role ... 53

3.4.3. Pressure role ... 54

3.4.4. N_2O flow role ... 57

3.4.5. Annealing role ... 58

3.5. Film roughness ... 59

3.6. Summary ... 60

3.7. References ... 60

4. Electrical properties of ECR SiO_2 ... 63

4.1. Introduction ... 63

4.2. Interface properties ... 64

4.2.1. SiH_4 flow role ... 65

4.2.2. Pressure role ... 66

4.2.3. Microwave power role ... 69

4.2.4. N_2O flow role ... 70

4.2.5. Temperature role ... 71

4.2.6. Thickness role ... 71

4.2.7. Annealing role ... 73

4.2.8. Comparison between various dielectrics ... 74

4.3. Dielectric strength ... 75

4.3.1. SiH_4 flow role ... 76

4.3.2. Pressure role ... 77

4.3.3. Microwave power role ... 78

4.3.4. N_2O flow role ... 79

4.3.5. Temperature role ... 80

4.3.6. Thickness role ... 80

4.3.7. Annealing role ... 81

4.4. Conduction mechanism ... 81

4.4.1. Superior oxides conduction mechanism ... 82

4.4.2. Non-stoichiometric oxides conduction mechanism ... 84

4.5. Charge trapping during electric stress ... 87

4.6. Reliability 92
4.7. Summary 94
4.8. References 94
5. ECR-PECVD Silicon Nitride 99
5.1. Introduction 99
5.2. Deposition kinetics 101
5.2.1. Pressure role 101
5.2.2. Microwave power role 102
5.2.3. N_2 flow role 103
5.2.4. The effect of consecutive depositions 104
5.3. Refractive index 105
5.3.1. Pressure role 105
5.3.2. Microwave power role 107
5.3.3. N_2 flow role 108
5.3.4. The effect of consecutive depositions 109
5.4. Atomic composition 110
5.4.1. Pressure role 110
5.4.2. Microwave power role 114
5.4.3. N_2 flow role 115
5.4.4. The effect of consecutive depositions 116
5.5. C-V characteristics 116
5.5.1. Pressure role 117
5.5.2. N_2 flow role 119
5.5.3. Microwave power role 120
5.5.4. Thickness role 120
5.6. J-E characteristics 121
5.6.1. Pressure role 122
5.6.2. N_2 flow role 124
5.6.3. Thickness role 126
5.7. Summary 127
5.8. References 127
6. Jet Vapour Deposition of SiO_2 131
6.1. Introduction 131
6.2. Nozzle design 132
6.3. Film composition and refractive index 134
6.3.1. Pressure influence 135
6.3.2. SiH_4 flow influence 136

6.3.3. N_2O flow influence ... 137
6.3.4. Thickness role ... 138
6.4. J-E characteristics ... 138
6.5. C-V characteristics ... 141
6.6. Annealing effect ... 142
6.7. Summary ... 145
6.8. References ... 145
7. Transistors with low temperature gate dielectric ... 147
7.1. Introduction ... 147
7.2. MOSFET fabrication ... 148
7.2.1. Transistors with low temperature gate dielectric ... 148
7.2.2. Transistors with near room temperature gate dielectric ... 149
7.3. MOSFET structures ... 151
7.4. Transistors characteristics ... 152
7.4.1. Gate dielectrics deposited at 500°C ... 153
7.4.2. Room temperature gate dielectrics ... 157
7.5. Thin film transistors ... 158
7.6. Summary ... 160
7.7. References ... 160
8. Conclusions and recommendations ... 161
8.1. Conclusions ... 161
8.2. Recommendations ... 164
Annex A.1 ... v
Annex A.2 ... vii
Samenvatting ... ix
Summary ... xiii
Acknowledgments ... xv
List of publications ... xvii
About the author ... xix

Chapter 1 Introduction

Abstract

In this chapter, the reader is introduced into the world of low temperature dielectrics. Their importance as gate dielectrics in thin film transistors (TFTs) for flat panel displays and the desired film properties are shown. The processes that occur in plasma enhanced chemical vapour deposition (PECVD) are discussed. The main low temperature PECVD methods of dielectrics are compared. The motivations behind this research and the outline of this thesis are presented.

1.1. Gate dielectrics for thin film transistors

A thin film transistor (figure 1.1) is a semiconductor device composed of thin layers with different conductivities, deposited on top of an insulating substrate. TFTs are used mainly as switching devices in liquid crystal displays. The gate dielectrics for MOSFETs are traditionally grown at 800 - 1000ºC, but this temperature is too high for temperature-unstable substrates such as glass or plastic, which are employed in flat panel displays. Therefore, there is a high demand for low-temperature, high-quality gate dielectrics for TFTs.

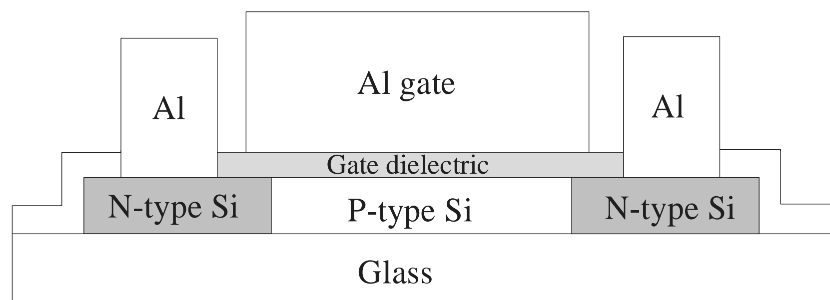

Figure 1.1. Schematic representation of a thin film transistor.

Plastic displays may replace the glass screens in the future due to their several advantages: lower cost, lower power consumption, lower weight and

better flexibility [1]. Consequently, a lot of research is performed nowadays with deposition temperatures as low as 100°C [2].

Another point of interest in recent years is producing flat panel display with large area, high resolution and reduced costs. In order to minimise the production costs, the number of connections can be reduced by integrating a part of the pixel addressing circuitry on the glass substrates [3]. However, the electron mobility of amorphous-hydrogenated silicon (a-Si:H) thin film transistors (TFTs) that are currently employed in display fabrication is too low (1 cm^2/Vs) for the circuit's requirements. Consequently, TFTs with high mobility, formed inside a large silicon grain [4], as shown in figure 1.2, are a potentially attractive solution. Because the carrier mobility is affected not only by the silicon (Si), but also by the traps situated at the interface with the gate insulator, these devices require thin gate dielectrics deposited at low temperature and with very good chemical and electrical properties. It is an experimental fact however, that a low deposition temperature results in a degradation of the film properties.

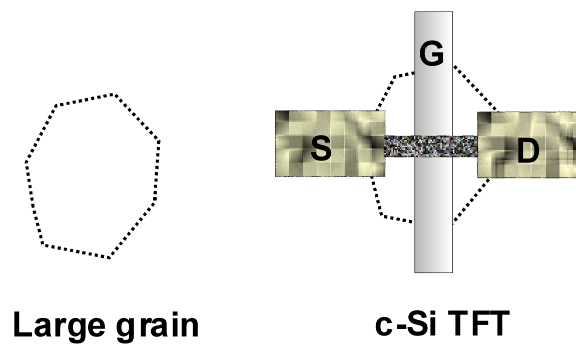

Figure 1.2. Single large grain c-Si TFT.

The insulators have to possess low trap density at the interface with Si for high-mobility TFTs. The leakage current has to exhibit low values so that the off-current of the TFT is smaller than 10^{-12} A. Furthermore the thin films have to show good reliability, so that the devices will maintain their performance for a long time. It is not easy to obtain layers that possess all these qualities, thus a study of how these film properties are influenced by different deposition conditions is required.

1.2. Low-temperature deposition

Chemical vapour deposition (CVD) is a method of obtaining solid thin films by chemical reactions between components chemisorbed on a surface from the gas phase [5]. In case of thermal deposition, the energy needed for

molecules to adsorb on the surface, to diffuse and to react is given by heating the gas and the substrate. In case of plasma-enhanced chemical vapour deposition (PECVD) however, the source of energy is nonthermal. Due to the high chemical reactivity of the radicals formed in the plasma, the film can be deposited at a much lower temperature than required for thermal reactions.

The principal steps that occur in a PECVD chamber are shown in figure 1.3. In the plasma, molecules are dissociated forming free radicals and ions by interactions with electrons. The radicals may react with other radicals or molecules in the gas-phase and form precursor molecules. Plasma particles diffuse toward the substrate and some are adsorbed on the surface. The radicals migrate on the surface and react, forming the film. The by-products of the reaction are desorbed. Some of the particles that were not adsorbed together with the by-products are pumped away.

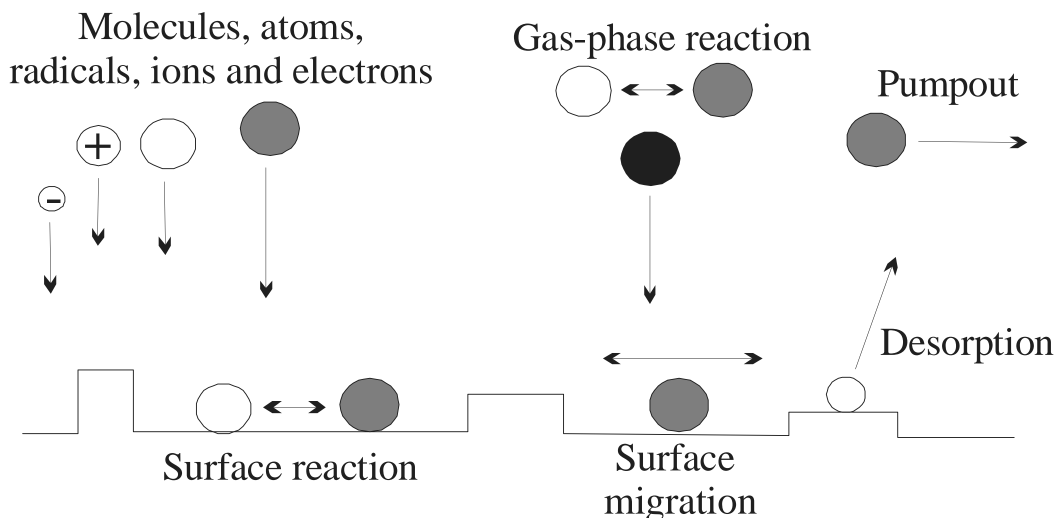

Figure 1.3. Schematic representation of thin film deposition.

In PECVD, the radicals can react in the gas-phase and produce large particles, which can become incorporated in the growing film. The effects are highly deleterious for the film properties. PECVD therefore needs better tuning than CVD in order to avoid particle formation in the gas phase.

1.3. Deposition techniques

The standard gate dielectric nowadays for amorphous TFTs is silicon nitride (S_3N_4) deposited by PECVD with radio-frequency excitation, but the processing temperature of 300°C is too high for flexible displays.

Furthermore, these layers exhibit high hydrogen content up to 20% [6], low dielectric strength, high interface trap density and high defect densities due to the high-energy ions impinging on the film surface during the film growth.

Several studies have succeeded in improving the dielectric properties, while reducing further the deposition temperature until almost room temperature, by experimenting with other deposition techniques [7].

A promising approach for realising such films is electron cyclotron resonance (ECR) microwave plasma deposition [8, 9]. The plasma is generated by coupling the movement of the electrons in a static magnetic field with a microwave power source. At resonance, when the microwave frequency equals the electron cyclotronic frequency, electrons absorb very efficiently energy from the microwave power and ionise the precursor gases. ECR plasma is an electrodeless, noncollisional plasma that has several advantages over the conventional rf plasma sources. Electrodeless plasma has the advantage of avoiding high-voltage sheath, i.e. high ion-bombardment. ECR plasma operates at low pressure, has low electron and ion energy, and high degree of ionisation [10]. Because of these "soft" and "dense" characteristics of ECR plasma [11], it is possible to lower the deposition temperature, without degrading the film quality. Furthermore, the plasma damage to the growing film is lower, due to the fact that the substrate is remote from the plasma.

Several works have reported that electron cyclotron resonance plasma source either in its classical configuration (electromagnetic energy introduced by a circular waveguide and magnetic field perpendicular on the substrate) or in the distributed configuration (microwave power distributed by eight antennas and magnetic field parallel with the substrate) [12] is a powerful tool for obtaining device-quality SiO_2 at low temperatures. However, the focus of this study is a less known ECR discharge configuration, called multipolar ECR [13], which has been shown to produce layers with extremely low hydrogen content. It acquired the name "multipolar" from the multipolar magnetic field, created by a row of permanent magnets around the plasma chamber. This new technique has certain advantages such as a magnetic field parallel to the substrate, which minimises the plasma damage, a tuneable microwave cavity, and a quartz dome that reduces the metal contamination.

Another deposition that was reported in literature to be successful in obtaining very thin S_3N_4 layers is Jet Vapour Deposition [14]. Highly diluted silane (SiH_4) in helium is introduced downstream of the plasma region, through a small nozzle (figure 1.4). The huge difference between the pressure in the gas line and the pressure in the reaction chamber insures a supersonic jet of reactive gas. This technique can be used to ensure extra energy transfer to the growing film, eliminating the need to heat the wafer. It further

increases the probability of reaction at or near the surface rather than in the gas phase.

A more detailed description of the principles and experimental set-ups of both ECR PECVD and JVD is made in chapter 2.

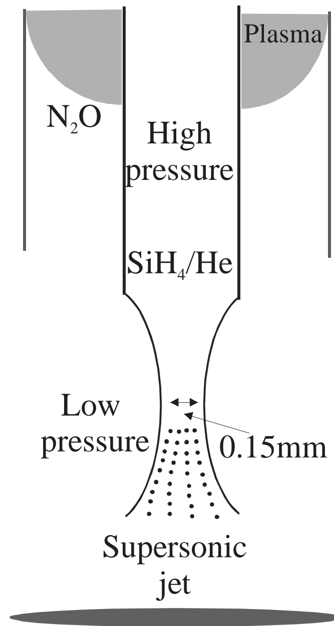

Figure 1.4. Jet Vapour Deposition.

1.4. Motivation

Deposition of dielectrics at temperatures close to room temperature but with properties similar to the ones grown at 1000ºC is very important for the new generation of flat panel displays and other applications.

Although several studies were performed on low-temperature dielectrics, multipolar ECR plasma was not previously investigated in detail, despite its advantages. Much research was done on physical and chemical properties of low-temperature dielectrics deposited by ECR plasma, but the influence of all deposition parameters on electrical properties was not exhausted. The main challenge in depositing low-temperature gate dielectrics is to obtain layers that exhibit both high breakdown field and low interface trap density. Furthermore the reliability, conduction mechanism and trapping performance of low-temperature deposited dielectrics have not been researched until now, especially in case of ECR PECVD and JVD. Hydrogen bonds are still present in layers obtained at room temperature, but it is possible to eliminate them by optimising the deposition conditions. Jet Vapour Deposition has proved to

be a powerful tool for Si_3N_4 layers, but JVD silicon oxide (SiO_2) films for TFTs were not yet investigated, despite their very good quality.

1.5. Outline of the thesis

This thesis presents the deposition and characterisation of SiO_2 and Si_3N_4 layers by different deposition methods. Chapter 2 describes the two deposition techniques that were employed for dielectric layer production and the energy transfer and chemistry in ECR plasma. Also the principal film characterisation methods are shown. Chapter 3 presents the influence of various deposition parameters upon the physical and chemical properties of SiO_2 obtained by multipolar ECR PECVD. In chapter 4 the interface properties, the dielectric strength, the conduction mechanism and film reliability of the same layers are shown. Optimisation of silicon nitrides deposited by ECR plasma is presented in chapter 5. Chapter 6 describes the properties of jet vapour deposition oxides obtained at room temperature and chapter 7 shows the performances of transistors made with low temperature gate dielectrics. Thermally grown oxide, rf-PECVD and LPCVD oxides and nitrides were used as references, and their properties were compared with the characteristics of ECR and JVD room temperature insulators.

1.6. References

1. C.S. Yang, L.L. Smith, C.B. Arther, G.N. Parsons, "Stability of low-temperature amorphous silicon thin film transistors formed on glass and transparent plastic substrates", J. Vac. Sci. Technol. B, **18**, pp. 683-689 (2000).
2. P.G. Carey, P.M. Smith, S.D. Theiss, P. Wickboldt, "Polysilicon thin film transistors fabricated on low temperature plastic substrates", J. Vac. Sci. Technol. A **17**, pp. 1946-1949 (1999).
3. J.S. Im, R.P. Sposili, "Crystalline Si films for integrated active-matrix liquid-crystal displays", Materials Research Society Bulletin **21**, pp. 39-48 (1996).
4. R. Ishihara and M. Matsumura, "Excimer-laser-produced single-crystal silicon thin-film transistors", Jpn. J. Appl. Phys. **36**, pp. 6167-6170 (1997).
5. S. Sivaram, "Chemical Vapor Deposition Thermal and Plasma Deposition of Electronic Materials", International Thomson Publishing Inc. 1995, pp. 1.

6. A.J. Flewitt, A.P. Dyson, J. Robertson, W.I. Milne, "Low temperature growth of silicon nitride by electron cyclotron resonance plasma enhanced chemical vapour deposition", Thin Solid Films **383**, pp. 172-177 (2001).
7. J. Lee, C. Han, C. Kim, "High performance low temperature polysilicon thin film transistor using ECR plasma thermal oxide as gate insulator", IEEE El. Dev. Lett., **15**, pp. 301-303 (1994).
8. N. Jiang, B. Agius, M. C. Hugon, J. Olivier, M. Puech, "Radio-frequency bias effects on SiO_2 films deposited by distributed electron cyclotron resonance plasma enhanced chemical vapor deposition", J. Appl. Phys. **76**, pp. 1847-1855 (1994).
9. J.W. Lee, N.I. Lee, S.H. Hur, C.H. Han, "Oxidation of silicon using electron cyclotron resonance nitrous oxide plasma and its application to polycrystalline silicon thin film transistors", J. Electrochem. Soc. **144**, pp. 3283-3287 (1997).
10. M. Dahimene, J. Asmussen, "The performance of a microwave ion source immersed in a multicusp static magnetic field", J. Vac. Sci. Technol. B **4**, pp. 126-130 (1986).
11. S. Garcia, I. Martil, G. Gonzalez Diaz, E. Castan, S. Duenas, M. Fernandez, "Deposition of SiN_x:H thin films by the electron cyclotron resonance and its application to Al/SiN_x:H/Si structures", J. Appl. Phys. **83**, pp. 332-338 (1998).
12. M. Firon, M. C. Hugon, B. Agius, Y. Z. Hu, Y. Wang, and E. A. Irene, "Comparison of the physical and electrical properties of electron cyclotron resonance and distributed electron cyclotron resonance SiO_2", J. Vac. Sci. Technol. B **14**, pp. 2543-2549 (1996).
13. J. Hopwood, J. Asmussen, "Neutral gas temperatures in a multipolar electron cyclotron resonance plasma", Appl. Phys. Lett. **58**, pp. 2473-2475 (1991).
14. T.P. Ma, "Making silicon nitride film a viable gate dielectric", IEEE Trans. on El. Devices **45**, pp. 680-690 (1998).

Chapter 2 Theoretical and experimental details

Abstract

In this chapter, the two main deposition methods: Electron Cyclotron Resonance Plasma Enhanced Chemical Vapour Deposition (ECR-PECVD) and Jet Vapour Deposition (JVD) are described. ECR plasma is a high-density plasma created by superposing a magnetic field and a microwave source. It has several advantages over the rf-PECVD. The deposition system permits deposition at low pressures and temperatures. JVD technique is also tested by modifying the manner of introducing SiH_4*. By creating a high speed* SiH_4*/He jet, it is believed that the film properties can be improved. The chemical and physical film properties of the deposited dielectrics have been investigated and the required measurement equipment is presented in this chapter. Electrical film properties such as oxide charge concentration, interface trap density, equivalent oxide thickness, dielectric constant are determined from the capacitance-voltage curves of the MOS capacitors. The main conduction mechanisms exhibited by dielectrics are studied by investigating the current-voltage measurements.*

2.1. Electron Cyclotron Resonance Plasma

Electron Cyclotron Resonance (ECR) plasma is an electrodeless plasma generated by superposing a static magnetic field and a microwave power source. In ECR plasmas, microwave energy is used to accelerate the electrons. The electric field of a microwave can be written as:

$$\boldsymbol{E} = \boldsymbol{E}_0 \cos(\omega_0 t) \tag{2.1}$$

where ω_0 is the microwave frequency. In vacuum, without any collisions, the electric field and velocity are phase-shifted by $\pi/2$. In the presence of a magnetic field, electrons experience a force perpendicular to their direction of

motion, which will make them rotate around the magnetic field lines (figure 2.1) with the cyclotronic frequency (ω_c):

$$\omega_c = \frac{e}{m_e} B \tag{2.2}$$

where B is the intensity of the magnetic field and e and m_e the charge and the mass of the electron, respectively. Therefore the electron phase will be modified. If ω_0 is equal to ω_c, then electrons will move in phase with the electric field and the field will accelerate them continuously. This phenomenon is called electron cyclotron resonance [1]. Because of the electron trajectory around the magnetic field lines, the electrons can collide with gas molecules and ionise them before loosing their energy at the walls, even at low pressures when the mean free path is similar to the reactor size. Therefore ECR is efficient for low pressures; at high pressures due to many collisions, the resonance is lost.

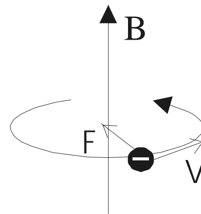

Figure 2.1. The electron movement in a magnetic field.

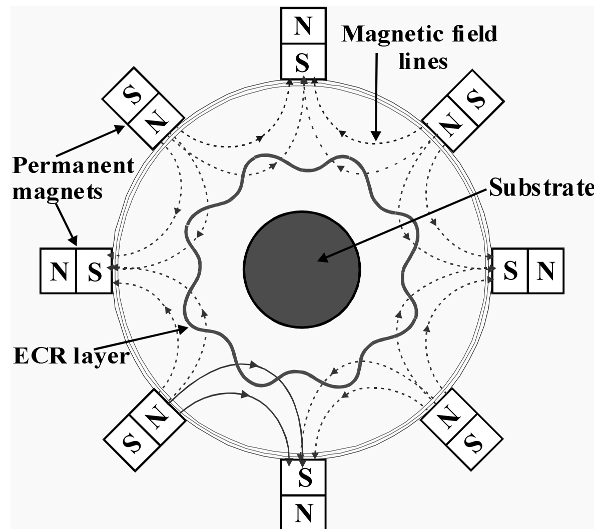

Figure 2.2. Top view of the multipolar ECR.

There exist at least five types of ECR system configurations [1], but most of the studies have been concentrated on only two of them. The first one is the conventional or divergent ECR plasma source [2], which is characterised

by a magnetic field created by a solenoid positioned perpendicular to the substrate plane. The second one is the distributed ECR plasma source [3], in which the microwave source power is introduced through eight antennas symmetrically distributed inside the chamber.

A distinct ECR configuration, called multipolar ECR or microwave plasma disk reactor (MPDR-300) has been investigated. A top view of the system as designed by Asmussen [4, 5] is presented in figure 2.2.

A multipolar magnetic field is created by eight permanent magnets distributed outside the plasma dome as in figure 2.2. In the ECR layer shown in figure 2.2, the intensity of the magnetic field is 875 Gauss, and the corresponding cyclotronic frequency is 2.45 GHz, equal to the frequency of the microwave source. Therefore, this is the area where the electrons are highly accelerated and the dissociation and ionisation of the gas occurs. The ions have a higher mass than the electrons and their cyclotronic frequency in the magnetic field will be much lower than the frequency of the microwave source. As a result they will gain lower velocity and can escape more easily from the magnetic field. In the middle of the quartz dome, the magnetic field is zero, thus the ions will migrate in this region toward the substrate.

In comparison with other PECVD systems, ECR plasma can be ignited at lower pressure, therefore gas-phase reactions can be avoided. Furthermore, at low pressure, the electrons have large mean free paths and absorb very efficiently energy from the microwave source. Therefore, ECR plasma is a high-density plasma (electron density $\geq 10^{11} cm^{-3}$). Another advantage of the ECR plasma constitutes the low plasma damage brought to the film.

2.1.1. Energy transfer

The energy of the plasma particles that arrive at the substrate is important for the deposited film. The main stages of energy transfer from the plasma toward the substrate are:

1. acceleration of free electrons in the applied electric field
2. collisions of electrons with gas molecules, which generate ions, free radicals, excited molecules and electrons
3. diffusion of these particles to the film surface and walls where they dissipate their energy
4. acceleration of ions towards the film and walls by the plasma potential.

Because electrons have higher velocity, they will diffuse at the plasma edge much faster than the ions. As a consequence, the plasma will become more positive (plasma potential) in comparison with any surface and the positive ions will be accelerated toward the surfaces. Most of the ion energy is

obtained from the acceleration of ions in the plasma sheath, therefore the ion energy can be calculated based on the plasma potential (V_p). If the surface is floating, as is the case of deposited dielectrics, the surface will have a floating potential V_f and the voltage drop can be written [6] as in expression 2.3:

$$\Delta V_p = V_p - V_f = \frac{\tilde{T}_e}{e}(2.84 + \frac{1}{2}\ln M_+) \quad (2.3)$$

where M_+ is the ion molecular weight and $\tilde{T}_e$ the electron "temperature" in eV, which is an indicative of electron kinetic energy. $\tilde{T}_e(\text{eV}) = k_B T_e$, where T_e is the electron temperature in K. For a gas like N_2O with the total mass of 44, $\Delta V_p \approx 4.7\ \tilde{T}_e/e$.

In case of ECR remote plasma, the particles diffusing from the plasma to the substrate suffer collisions downstream of the plasma, while the electrons are not receiving anymore energy from the microwave. Therefore, the plasma potential, electron energy and ion energy decrease with the distance from the plasma. The radical energy increases because of elastic collisions with ions and therefore both radicals and ions will collide with the film surface. The effect of electron bombardment is small, because of the small electron mass and the electrons deceleration in the plasma sheath.

It is important to have an idea of how the deposition conditions such as pressure and microwave power influences the plasma parameters: ΔV_p, $\tilde{T}_e$, ion energy, plasma density in order to estimate the energy transfer from the plasma to the growing film at various conditions. Plasma density is equal to the electron density (n_e), which is approximately equal to the ion density for quasineutral plasma.

Several authors have measured and modelled the plasma parameters in ECR plasma [6-12]. However, most of the plasma parameter measurements were performed in Ar plasma, not in SiH_4/N_2O or SiH_4/N_2 mixtures, in order to avoid deposition upon the measurement equipment. Unfortunately plasma parameters such as ΔV_p and $\tilde{T}_e$ are influenced also by the type of gas introduced in the chamber as shown by Hopwood et al. [8]. The main influences upon plasma parameters, supported by measurements and simulations in Ar ECR plasmas from literature are presented below.

Pressure influence upon plasma parameters

The mean free path for molecular collisions (the mean distance between two collisions of a molecule) can be written as [13]:

$$l = \frac{1}{\sqrt{2}\pi a^2 n} \tag{2.4}$$

where n is the gas concentration and a the molecule diameter. If the gas concentration is expressed as a function of pressure from the ideal gas law, the mean free path can be written:

$$l(\text{cm}) \approx \frac{7}{p(\text{mTorr})} \tag{2.5}$$

For the pressure ranged used in our ECR system (5-20 mTorr), the mean free path is 0.35 – 1.4 cm. Because the wafer is situated at a distance of 4 cm from the quartz dome where plasma is generated, the ions will collide with neutrals in average for three times in case of low pressure, loosing a part of their energy. In case of high pressure, the frequency of collisions is much higher, thus ions will have much lower energy.

In addition, $\tilde{T}_e$ will also decrease at high pressure due to the lower efficiency of ECR plasma. Therefore, in accordance with expression 2.3, ΔV_p and ion energy will also decrease. Uhm *et al.* [6] have calculated the relation between $\tilde{T}_e$ and pressure for an Ar ECR plasma:

$$\sqrt{\tilde{T}_e}\exp\left(-\frac{15.76}{\tilde{T}_e}\right) \sim \frac{1}{p} \tag{2.6}$$

Expression 2.6 shows how $\tilde{T}_e$ decreases with increasing the total pressure in the ECR plasma.

The measurements inside the ECR region [6] confirmed the theoretical calculations. For Ar plasma with 700 W incident microwave power, the $\tilde{T}_e$ decreased from 30 eV to 5 eV when pressure increased from 0.2 to 20 mTorr. For the same experimental conditions, the plasma density (n_e) increases with increasing the pressure until 10 mTorr ($2 \cdot 10^{12}$ cm^{-3}) and decreases for pressures higher than 10 mTorr, due to inefficiency of the ECR plasma at high pressures.

Similar results were obtained for the values of $\tilde{T}_e$ in a multipolar ECR plasma by Hopwood et al. [8]. Because of $\tilde{T}_e$ decrease, ΔV_p decreases also

from 40 V to 10 V with increasing the pressure from 0.2 to 10 mTorr, as measured by Weng *et al.* [9] in an Ar ECR plasma at 150 W. The increase in plasma density with pressure was also measured in multipolar ECR plasma by Mak *et al.* [10]. The neutral gas density increases 10 times while raising the pressure from 6 to 70 mTorr, due to the increase in gas concentration, as calculated by Kinder [11] for ECR plasma. The same author calculated the average ion flux and electron density and both registered a maximum at the same pressure of 1 mTorr.

Microwave power influence upon plasma parameters

The microwave influence upon the plasma parameters has been modelled and measured for ECR plasma in the literature. Weng *et al.* [10] have extracted the value for the plasma density n_e from the dissipation of input power into the plasma:

$$\kappa P = e^2 n_e \overline{E^2} / (m_e \nu_m) \tag{2.7}$$

where P is the microwave power, κ the microwave absorption coefficient in the plasma, $\overline{E}$ an effective electric field, ν_m the momentum transfer collision frequency. Obviously, the plasma density increases with increasing the incident microwave power.

Uhm *et al.* [9] have shown that also the electron temperature and ion energy increase with the microwave power:

$$n_e \sqrt{\tilde{T}_e} \varepsilon_L \sim \kappa P \tag{2.8}$$

where ε_L indicates the energy dissipated in the plasma per ion injected in the plasma sheath and can be written as a sum of:

$$\varepsilon_L = \varepsilon_c + 2\tilde{T}_e + \varepsilon_i \tag{2.9}$$

ε_c is the energy lost by collisions and ε_i is the ion energy gained in the plasma sheath.

The calculations were confirmed by experiments performed by Mak *et al.* [12] with 20 sccm Ar multipolar ECR plasma at different pressures. The ion density which is more or less equal to the electron density increases from $1.5 \cdot 10^{11}$ cm^{-3} to $2.5 \cdot 10^{11}$ cm^{-3}, when microwave power increases from 250 W to 800 W [10] for 0.78 mTorr.

All the plasma parameters, including the ion energy, $\tilde{T}_e$ and ΔV_p increase with increasing the microwave power due to the fact that more power is

absorbed by electrons from the microwave source. Weng *et al.* [9] have modelled $\tilde{T}_e$ and V_p between microwave powers of 75 and 250 W for Ar ECR plasma at 1 mTorr; $\tilde{T}_e$ increases from 7 eV to 10 eV and V_p increases from 12 V to 23 V. Measurements confirmed that the ion energy increases from 19 eV to 22 eV in a 0.77 mTorr Ar plasma, while the microwave power increases from 150 to 750 W [8]. For the same deposition conditions, the Ar neutral temperature increases from 500 K to 800 K.

To summarize, high pressure decreases the electron temperature, plasma potential and ion energy; it increases the plasma density and radical concentration. However, the n_e and the ion flux exhibit a maximum at pressures between 1 and 10 mTorr, depending on other deposition conditions. Microwave power increases the energies and densities of all the particles created in the plasma.

2.1.2. Plasma chemistry

In order to give an idea of what happens in the reactor chamber and which process dominates for the chosen range of pressure and power, an estimation of different process rates was realised. The chemical reactions that occur in a plasma are complex and in order to make a precise analysis, a database processor, a global plasma model and a database with all reaction mechanisms and coefficient rates are required. Because modelling the plasma was not the research goal, this rough and qualitative analysis was done only for a better understanding of the deposition kinetics and film modifications at various conditions.

Deposition of silicon oxide (SiO_2) from silane (SiH_4) and nitrous oxide (N_2O) was studied. A schematic representation of the reactor can be seen in figure 2.3. The chamber was separated in three parts:

- plasma chamber, where N_2O is introduced and plasma is ignited (see also figure 2.5).
- gas-phase reaction chamber where SiH_4 is introduced and reacts with radicals and ions arriving from the plasma.
- diffusion chamber where various SiO_2 precursor molecules (SiH_3, SiH_2O, HSiO) diffuse to the substrate and are adsorbed at the surface; surface reactions occur and SiO_2 is formed.

These processes are competing with each other and their approximate rates will be estimated.

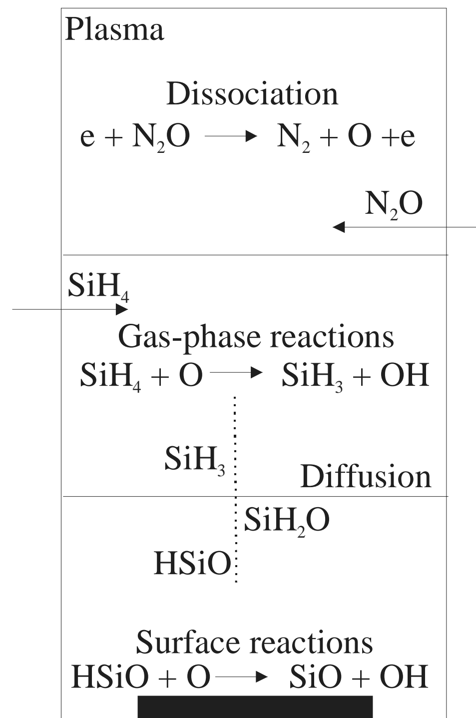

Figure 2.3. Schematic representation of SiO_2 deposition in a remote PECVD reactor.

Electron-impact processes

Supposing for the beginning that only an insignificant quantity of SiH_4 diffuse inside the plasma chamber, let us look at the elastic and inelastic collisions between the electrons and N_2O molecules. For low energy electrons (< 2 eV), the collisions are elastic:

$$N_2O + e \rightarrow N_2O + e \tag{2.10}$$

Electrons with higher energy can undergo inelastic collisions, thus exciting the molecules, which can either relax while emitting a photon or dissociate:

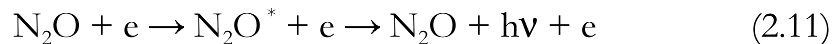

$$N_2O + e \rightarrow N_2O^* + e \rightarrow N_2O + h\nu + e \tag{2.11}$$

$$N_2O + e \rightarrow N_2 + O^* + e \tag{2.12}$$

The energy required for the dissociation of N_2O molecule is 4 eV or 9 eV depending on the degree of excitation of the resulted O radical.

The electron needs a high energy ($\tilde{T}_e > 13$ eV) in order to ionise the N_2O molecule:

$$N_2O + e \rightarrow N_2O^+ + 2e \tag{2.13}$$

The ionisation processes are very important for sustaining the plasma by extracting more electrons from gas molecules. The reactions written above are just some examples of dissociation and ionisation phenomena. The complete electron-impact processes in N_2O discharges and the energy required for each reaction are described by Kline *et al.* [14].

SiH_4 may also diffuse back into the plasma and be dissociated in the plasma chamber, forming SiH_x radicals. This occurs especially for Knudsen number (Kn) > 1, while backstream diffusion is minimized for Kn < 0.01 [13]. For a typical ECR PECVD conditions (low pressure and average flow), Kn is ~ 0.1 thus there is a strong possibility that SiH_4 is dissociated by collisions with electrons.

Neutral reaction chemistry

The radicals, ions and electrons resulted from the processes described above will diffuse from the plasma and react with SiH_4 as shown in figure 2.3. The exact reaction mechanism is not known. Kushner [15] has reviewed the process and simulated the deposition of SiO_2 from SiH_4, N_2O and He in a remote plasma where SiH_4 is introduced downstream. The reactions with higher reaction rate that will mostly consume the supply available are:

$$SiH_4 + O^* \rightarrow SiH_3 + OH \quad (2.14)$$

$$SiH_3 + O \rightarrow SiH_2O + H \quad (2.15)$$

$$SiH_2O + O \rightarrow HSiO + OH \quad (2.16)$$

These radicals with high reactivity and high sticking coefficient will diffuse toward the substrate and will be adsorbed at the surface. The oxidising reaction will continue with oxygen atoms or hydroxyl groups until SiO_2 is produced. Possible reactions pathways are:

$$HSiO + O \rightarrow SiO + OH \quad (2.17)$$

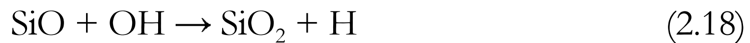

$$SiO + OH \rightarrow SiO_2 + H \quad (2.18)$$

These are only a few possibilities, the complete list of reactions together with the reaction rates can be found in Kushner's work [15]. The ions can also contribute to the formation of precursors, however their concentrations are much lower due to the fact that more energy is required for the ionisation processes. Kushner [10] has calculated the fluxes of different precursors to the substrate for the following deposition conditions: 300 mTorr, total flow

of 210 sccm and 0.3 W cm^{-3} input power. The simulation has shown that SiO and SiO_2 are formed at the substrate, not in the gas-phase. In the case of ECR plasma, at much lower pressures, the probability of forming SiO_2 in the reactor is even lower. Kushner has calculated the following fluxes of the precursors to the substrate when using $He/N_2O/SiH_4$ chemistry: $SiH_3/SiH_2O/HSiO/O$ = 7/2/5/3 [10].

Plasma kinetics

In order to determine which processes are limiting the deposition rate and which dominate at different pressure and power, the frequency of different processes such as electron-impact reaction, reaction with a free radical, diffusion to the wall and pumpout were calculated.

Smith [13] has written the reaction rate for N_2O dissociation by collisions with electrons as in expression 2.19.

$$R_{\mathrm{N_2O}} = n_{\mathrm{e}} n_{\mathrm{N_2O}} \int_0^{\infty} \sqrt{\frac{2E_{\mathrm{e}}}{m_{\mathrm{e}}}} \sigma_{\mathrm{N_2O}}(E_{\mathrm{e}}) f(E_{\mathrm{e}}) dE_{\mathrm{e}} \tag{2.19}$$

where E_e is the electron energy, n_{N_2O} the concentration of N_2O, σ_{N_2O} (E_e) the collision cross section of N_2O molecules and $f(E_e)$ the electron energy distribution. With this expression it is possible to estimate the generation of oxygen radicals. In order to simplify the calculations, the N_2O dissociation is considered to happen when an electron of 9 eV [14] collides with an N_2O molecule. The maximum dissociation-collision cross section for this reaction is $3.3 \cdot 10^{-16}$ cm^2 [14]. From the measured plasma parameters in similar ECR systems found in literature [9], the average electron temperature was estimated to be 5 eV. If the electron-energy-distribution-term $f(E_e)$ is considered of Maxwellian form, it can be approximated that 10% of the total electron population have enough energy to dissociate N_2O molecules. Introducing these values in expression 2.19 and calculating the velocity of an electron with $\tilde{T}_e$ = 9 eV, the frequency at which an N_2O molecule is dissociated will be:

$$\nu_{\mathrm{d}} = R_{\mathrm{N_2O}} / n_{\mathrm{N_2O}} = n_{\mathrm{e}} \sqrt{\frac{2E_{\mathrm{e}}}{m_{\mathrm{e}}}} \sigma_{\mathrm{N_2O}} \cdot 0.6 = 2.7 \cdot 10^{-8} n_{\mathrm{e}} = 834 \ \mathrm{s^{-1}} \tag{2.20}$$

The value for n_e ($2 \cdot 10^{11} cm^{-3}$) was taken from ref. [8] in which the electron density was measured in a similar ECR system.

ν_d depends on the concentration of electrons that have enough energy to dissociate the N_2O molecules, which increases with both n_e and T_e. With

increasing the pressure, n_e increases and T_e decreases. Therefore it can be considered that due to the opposite effects of pressure upon the electron density and energy, the dissociation frequency is more or less independent of pressure.

The second event estimated is the reaction frequency of a SiH_4 molecule with the oxygen radicals (see reaction 2.14). The reaction rate can be written as the product of oxygen radicals' concentration (n_O), SiH_4 concentration (n_{SiH_4}) and the rate coefficient for this reaction $k_r = 3\cdot10^{-10}cm^3s^{-1}$ [15]:

$$R_{SiH_4} = k_r n_{SiH_4} n_O \tag{2.21}$$

The rate coefficient corresponds to a reaction probability of near to 1 for a SiH_4+O^* collision. The reaction probability with unexcited oxygen radicals is much lower. n_O was considered to be 10% of the total N_2O concentration, but its real value can be much higher, depending on the plasma parameters. The reaction frequency of an individual SiH_4 molecule with oxygen radicals in a mixture of 20 sccm N_2O and 5 sccm 2% SiH_4 diluted in He is:

$$\nu_r = R_{SiH_4} / n_{SiH_4} = 3\cdot10^{-10}\, 0.1 n_{N_2O} = 8.3\cdot10^2 p \ \ (s^{-1}) \tag{2.22}$$

where p is the value of the total pressure expressed in mTorr. The reaction frequency increases at higher electron densities due to an increased dissociation factor and decreases if the gases are diluted with an unreactive gas.

Two physical processes can also influence the deposition: diffusion to the wall and pumpout. The frequency at which a molecule reaches the wall can be estimated as:

$$\nu_D = 4D/\Lambda^2 = 5.4\cdot10^5 / p \ \ (s^{-1}) \tag{2.23}$$

where D is the diffusion coefficient, which is inversely proportional with the pressure and Λ the diffusion length, typically 1 cm.

Finally, the pumpout frequency is the inverse of the residence time in the plasma:

$$\nu_P = W/V = 143/p \ \ (s^{-1}) \tag{2.24}$$

where V is the volume of the plasma chamber (500 cm^3) and W the total flow rate of 25 sccm.

All the calculated frequencies are presented in figure 2.4 versus the total pressure. By comparing these frequencies, it can be qualitatively estimated which process dominates at various deposition conditions.

For high pressures ≈ 50 -100 mTorr, the fastest event is the reaction with radicals, due to high collision rate. Therefore, for this pressure range, gas-phase chemistry will dominate and the deposition will be limited by the diffusion to the substrate of precursor molecules and radical formation by dissociation.

At pressures lower than 25 mTorr, the diffusion frequency becomes larger than the frequency of reaction with radicals, thus the radicals once formed will diffuse toward the substrate and react with other molecules. This pressure regime was used for ECR deposition. Surface chemistry starts to dominate at $p < 10$ mTorr, for which ν_r is 10 times smaller than ν_D. At high microwave power, with increasing the electron temperature and density the crossover between diffusion and reaction frequencies can occur at lower pressures, thus film deposition starts to be limited by diffusion of molecules to the substrate even for low pressures.

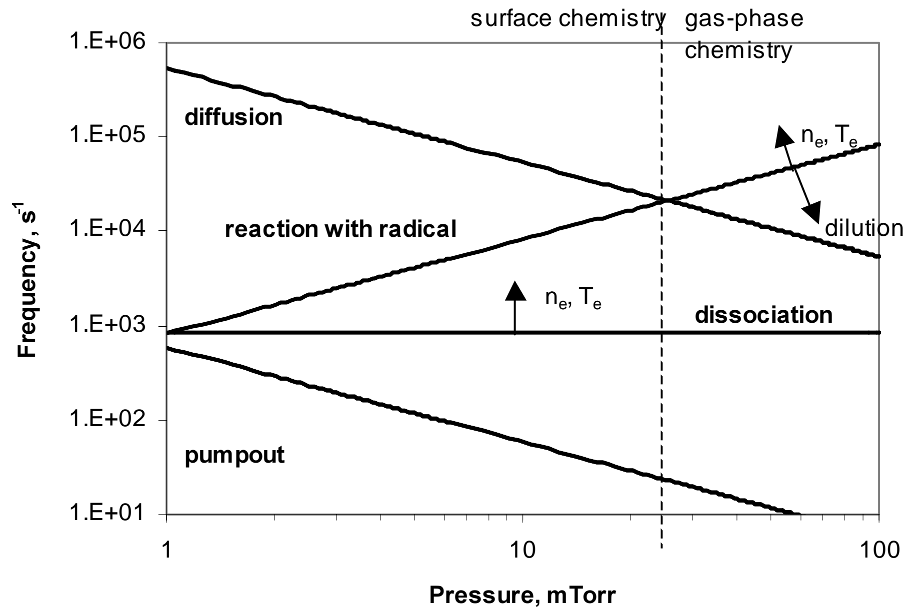

Figure 2.4. Frequencies of different processes that occur in the reaction chamber to a molecule.

It can be observed that the dissociation processes occur faster than pumping away the gas, thus it can be considered that the reactant gas utilization fraction is very high for our ECR system. The cause for this phenomenon is the high electron density and energy in case of ECR plasma, which enhance the dissociation process.

To summarize, it can be concluded from the qualitative analyses made that the surface chemistry dominates at low pressure and low microwave power

while gas-phase chemistry and diffusion limited deposition occurs mainly at high pressure and high microwave power.

For Si_3N_4 deposition, similar calculations can be made. N_2 is a much more stable molecule than N_2O, thus the energy required for an electron to dissociate the molecule is higher (12 eV). Therefore, the concentration of electrons that possess sufficient energy to dissociate an N_2 molecule is lower and the dissociation frequency may be one or two orders lower. Also the reaction rate between nitrogen radicals and SiH_4 is lower, therefore the reaction frequency for a SiH_4 molecule with radicals is shifted to lower values.

2.1.3. ECR deposition system

The deposition system consists of a microwave plasma disk reactor (MPDR-300), comparable with the one described by Asmussen [5] and it is shown in figure 2.5.

Microwave radiation of 2.45 GHz is introduced through an input probe into the chamber where multipolar ECR plasma is created. The quartz dome has the role of maintaining the vacuum and minimising the contamination of the film. The permanent magnets surround the dome, creating a magnetic field parallel to the substrate. A cooling system was built to avoid overheating of the components from the plasma and a resonant tuner is used for minimising the reflected power.

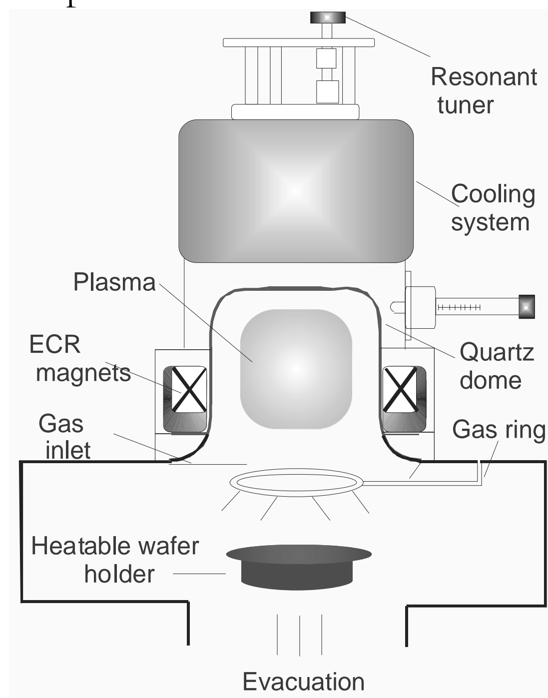

Figure 2.5. Experimental set-up.

A 500 l/s turbo pump in series with a mechanical pump was used to evacuate the deposition chamber and the base pressure was $3\cdot10^{-6}$ Torr. The wafers were introduced in the chamber through a load lock chamber, in which vacuum was maintained also by a turbo pump.

2.2. *Jet Vapour Deposition*

Jet Vapour Deposition (JVD) [16] is another technique used with success in depositing gate dielectrics. Ma [16] has reported silicon nitrides with a very good interface with silicon and good dielectric strength, obtained by JVD. Although the layers were obtained at room temperature, they were annealed at 800ºC after deposition. Also the film thickness was only a few nanometers. Our challenge is to obtain thicker dielectrics for TFTs and without high temperature annealing, but with the same high quality.

The principal novelty in JVD is the fact that SiH_4 is introduced in the reaction chamber through a small nozzle (figure 1.4). If SiH_4 is highly diluted with a light carrier gas like helium and there is a large pressure difference across the two ends of the nozzle, then according to the principles of fluid dynamics, the molecules will be injected into the chamber with a high velocity. This technique ensures extra energy transfer to the growing film, eliminating the need to heat the wafer in order to achieve good dielectric strength. The other precursor (nitrogen, oxygen, nitrous oxide) is dissociated in a microwave plasma [16] and plasma particles react with the SiH_4 molecules.

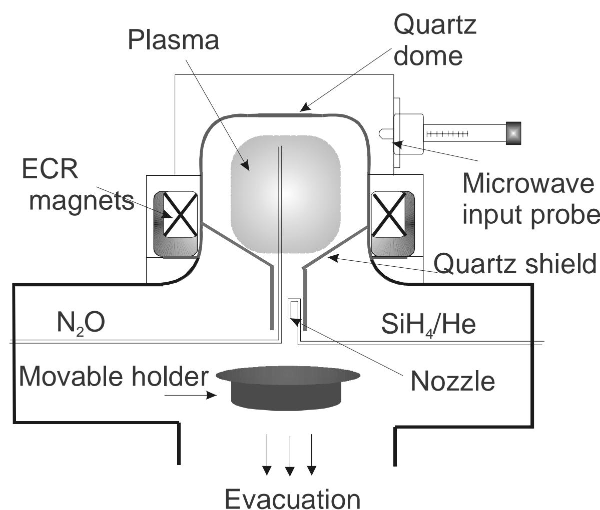

Figure 2.6. JVD experimental set-up.

The ECR deposition system has been modified in order to experiment with JVD (figure 2.4.). The 2% SiH_4 diluted in helium was introduced in the

chamber not through a shower ring as in the case of ECR-PECVD (figure 2.5), but through a quartz line bonded with a small nozzle of 0.2 mm, downstream the plasma (figure 2.6). The nozzle has the role of accelerating the gas by converting its static enthalpy into kinetic energy.

The shape and dimensions of the nozzle were calculated based on the fluid mechanics principles [17], to ensure a jet with high velocity. In order to achieve supersonic speeds, the nozzle has a convergent-divergent shape (see figure 1.4). With a convergent nozzle, the jet would only reach sonic speeds. Due to the a 170 Torr difference between the pressure in the inner SiH_4/He gas line and the pressure in the deposition chamber, the fluid expands and is accelerated from a negligible velocity to a supersonic velocity at the nozzle outlet. A nozzle of 2 mm length with a 150 μm throat was manufactured from quartz and bonded to the gas line in the deposition chamber, as shown in figure 2.6.

A quartz shield was bonded to the dome (figure 2.6) in order to avoid backstream diffusion of SiH_4 into the plasma and to insure that SiH_4 is not dissociated inside the plasma, but through remote collisions with radicals and ions flowing out of the plasma source. Due to the SiH_4/He high-speed jet and the system configuration, the deposition is localised, underneath the nozzle. In order to ensure good film uniformity over the whole wafer, a movable holder with two independent movements was designed. The holder rotates around its own axis and has an independent translational movement on a segment of a circle, as presented in figure 2.7.

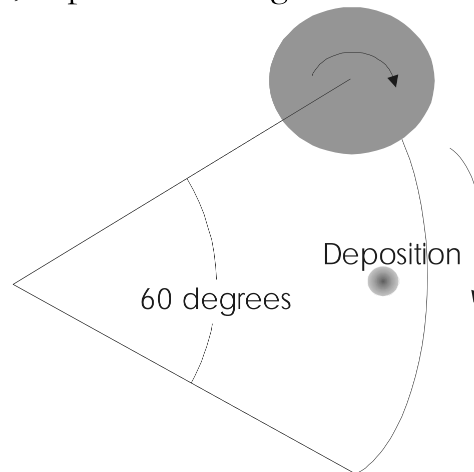

Figure 2.7. Holder movements.

2.3. Wafer preparation and deposition conditions

3-inch and 4 inch (100) or (111)-oriented n-type Si wafers with a resistivity of 1-10 Ωcm were used as substrates. The wafer preparation included 10 minutes in 100% fuming HNO_3, 10 minutes in boiling 69% HNO_3, followed by rinsing in DI water and finally a 1% HF etch of 25 s in order to remove the native oxide.

For deposition of SiO_2, electronically pure N_2O and SiH_4 were used as the gas precursors. N_2O was introduced in the quartz dome, in the plasma region, while SiH_4 was injected downstream of the plasma, in order to avoid diffusion of SiH_4 in the ECR region. SiH_4 is less stable than N_2O, so it is preferably to be dissociated through collisions with particles diffusing from the plasma, in order to obtain a stoichiometric SiO_2 film. For some experiments, SiH_4 was diluted in helium, in order to decrease the deposition rate and investigate the effects of helium upon the film properties [18].

For deposition of Si_3N_4, N_2 was chosen as gas precursor because it was reported that layers obtained from N_2 are denser and contain less hydrogen, compared to Si_3N_4 deposited from NH_3.

The films were deposited at near room temperature, without external heating. Due to plasma heating, the substrate temperature, measured by a thermocouple bonded inside the sample holder reached a maximum of 60°C. The wafer temperature might be higher however.

2.4. Physical and chemical characterisation equipment

The thickness and refractive index of the deposited layers were determined by an automatic Plasmos ellipsometer with fixed wavelength of 633 nm. In the case of thin dielectrics (10-20 nm), spectroscopic ellipsometry (SE) measurements were made at NMRC, Ireland, using a variable angle spectroscopic phase modulated ellipsometer (UVISEL from Jobin-Yvon) in the 1-4.5 eV spectral range. The angle of incidence (φ) was varied between 70° and 80° in order to obtain a maximum sensitivity of the SE measurements. The SE spectra were fitted using the Bruggemann Effective Medium Approximation (B-EMA) [10] for multicomponent films. Using the B-EMA, the deposited SiO_2 thin films have been modelled as a mixture of SiO_2 and voids. The quality of the fit was evaluated using the reliability of the fit (χ^2) obtained from the Marquardt-Levenberg regression analysis [19]. The values of the refractive index presented in chapter 6 were the ones measured with the spectral energy of 2 eV.

The etch rate of the films in Buffered Oxide Etch (BOE) solution (6 parts 40% NH_4F and 1 part 49% HF) was measured in order to obtain information about the layers density and composition. The chemical composition of the films was obtained by a Scanning Auger Microscopy (SAM), with a Perkin-Elmer PHI600 SAM multiprobe and by X-ray photoelectron spectroscopy (XPS) performed with a PHI Quantum 2000 Scanning ESCA Microprobe. Both equipments were calibrated with stoichiometric thermally grown SiO_2 and Si_3N_4 samples.

Chemical bonds in the film were studied by Fourier-transform infrared spectroscopy (FTIR) measurements realized with a BioRad FTS-60A FTIR spectrometer in the mid-infrared region (400-40000 cm^{-1}). The absorption coefficient for various chemical bonds was calculated as $\ln(10)\times \text{Absorbance}/\text{film thickness}$. The hydrogen content in the films was analysed by elastic recoil detection (ERD) measurements. The film roughness was measured by atomic force microscopy (AFM).

2.5. Electrical characterisation

Metal-insulator-silicon (MIS) capacitors were manufactured by sputtering 1 μm thick aluminium on the dielectric surface. Capacitors with different sizes and shapes were fabricated, using one mask and a lithography step (figure 2.8). The aluminium was then wet etched by introducing the wafer for 1-2 min in H_2SO_4 at 55°C. The native oxide was removed from the backside of the Si wafer with 1% HF etch solution and an aluminium layer of 1 μm was also sputtered in order to form the back electrode.

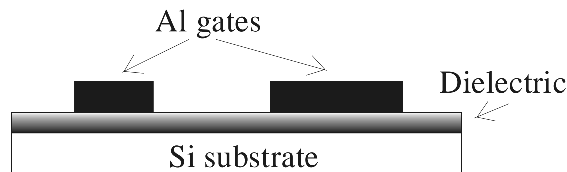

Figure 2.8. MIS capacitors.

The samples were subjected to a post-deposition anneal (PDA) step of 60 min, at 500°C, in wet N_2 ambient (N_2 bubbled through DI water at room temperature). Most of the samples received an aluminium-sintering step (post-metallization annealing - PMA) of 5 min, at 400°C, in wet N_2 ambient to ensure a good ohmic contact. The effects of both annealing processes on the physical and electrical film properties will be discussed in chapter 3, chapter 4 and chapter 6.

2.5.1. Capacitance-Voltage characteristics

From the capacitance measurement of MIS structures, a lot of information such as the dielectric capacitance, the equivalent oxide thickness, the silicon doping, the interface trap density and the concentration of the charge situated in the dielectric can be extracted.

The high-frequency capacitance of metal-oxide-semiconductor (MOS) structures was measured by superimposing a small ac signal with a frequency of 10 kHz on a ramped dc bias between the gate and the substrate. The high-frequency capacitance was measured with a Hewlett-Packard 4275A multi-frequency meter. The quasistatic *C-V* curve was measured with a Hewlett-Packard 4140B pA meter, by applying only a dc bias with a sweep rate of 0.1 V/s. The bias was applied on the metal gate. For an n-type substrate, the silicon layer will be in accumulation (higher concentration of electrons at the interface than in the bulk) for positive voltages, in inversion (hole concentration at interface greater than electron concentration in the bulk) for negative biases and in depletion (carrier concentration at interface lower than in the bulk) for intermediate biases (figure 2.9).

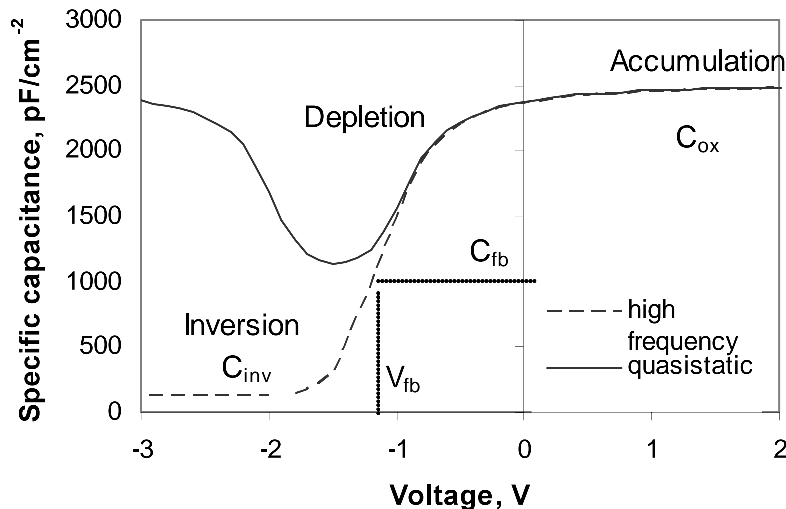

Figure 2.9. Capacitance-Voltage characteristics for a MOS structure.

The conduction band and the valence band are flat in the bulk, but curved at the interface due to the difference in work function (Φ_{MS}) between the metal and silicon and to the oxide charge present at the interface. The flatband voltage (V_{fb}) is the voltage applied to the gate in order to level the band bending in the silicon layer [20]. Using the value of the flatband voltage, the net charge density in the dielectric can be calculated based on the expressions given by Nicollian *et al.* [20]:

$$N = \frac{C_{\mathrm{ox}}}{e}\left(V_{\mathrm{fb}} - \Phi_{\mathrm{MS}}\right) \tag{2.25}$$

C_{ox} is the capacitance of the oxide in accumulation. In order to find the flatband voltage, the MOS capacitance in case of flatband condition can be calculated:

$$C_{\mathrm{fb}} = \frac{1}{1/C_{\mathrm{ox}} + 1/C_{\mathrm{Si,fb}}} \tag{2.26}$$

The silicon capacitance in the flatband condition is given by:

$$C_{\mathrm{Si,fb}} = \frac{\varepsilon_{\mathrm{Si}}\varepsilon_0}{\lambda_{\mathrm{d}}} \tag{2.27}$$

where $\varepsilon_{\mathrm{Si}}$ is the silicon dielectric constant (11.9), ε_0 the vacuum permittivity (8.854 pF/m) and λ_{d} the Debye length, which has the expression:

$$\lambda_{\mathrm{d}} = \sqrt{\frac{2\varepsilon_{\mathrm{Si}}\varepsilon_0 kT}{q^2 N_{\mathrm{Si}}}} \tag{2.28}$$

If the silicon doping is not precisely known, it can be calculated from the width of the silicon depletion layer:

$$w_{\mathrm{Si}} = \sqrt{\frac{4\varepsilon_{\mathrm{Si}}\varepsilon_0 kT \ln\left(N_{\mathrm{Si}}/n_{\mathrm{i}}\right)}{q^2 N_{\mathrm{Si}}}} = \frac{\varepsilon_{\mathrm{Si}}\varepsilon_0}{C_{\mathrm{Sinv}}} \tag{2.29}$$

where k is Boltzmann's constant ($1.38 \cdot 10^{-23}$ J/K), T the substrate temperature. C_{Sinv} is the silicon capacitance in inversion and it can be easily estimated from the high-frequency MOS capacitance in inversion:

$$C_{\mathrm{Sinv}} = \frac{1}{1/C_{\mathrm{inv}} - 1/C_{\mathrm{ox}}} \tag{2.30}$$

C_{inv} is the dielectric capacitance in inversion, as shown in figure 2.9. All the capacitances mentioned above are the capacitances per unit area.

The sources of charges found in the dielectric are numerous, most common are the silicon or oxygen dangling bonds or the contaminants.

The interface traps have the ability of exchanging charges (electrons or holes) with the silicon layer and can also be detected by evaluating the *C-V*

curves. One method to determine the interface trap density (D_{it}) using both quasistatic and high-frequency capacitance is the Castagne method [21]. The expression for D_{it} at an applied gate voltage is:

$$D_{it} = \frac{1}{e}\left(\frac{1}{1/C_{LF} - 1/C_{ox}} - \frac{1}{1/C_{HF} - 1/C_{ox}}\right) \tag{2.31}$$

where C_{LF} and C_{HF} are the quasistatic and the high-frequency capacitance respectively, at the applied voltage.

2.5.2. Current-Voltage characteristics

Besides good interface properties, the dielectric needs to possess low leakage current, high breakdown field and preferably a conduction mechanism that is not trap-related. All these properties can be extracted from the current-voltage (*I-V*) characteristics or current density-electric field (*J-E*) curves.

The measurements were performed with a Hewlett-Packard 4156B parameter analyser. A positive voltage was applied on the gate, thus electrons were injected from the substrate and the silicon substrate was in accumulation. The substrate temperature was controlled by a Temptronic thermo-chuck. Typical *J-E* curves are presented in figure 2.10. The electric field applied was calculated as:

$$E_{ox} = \frac{V - V_{fb}}{t_{ox}} \tag{2.32}$$

or extracted from the integrated area below the quasistatic *C-V* curve between V_{fb} and the measuring voltage in case of the thinner dielectrics [20]. The last method also corrects for the band bending in accumulation. The critical field was calculated as the electric field that causes a current with the density of 1 nA/cm^2 to pass through the film. Breakdown is reached for currents higher than 0.01 A/cm^2. The film resistivity is calculated between 1 and 5 MV/cm, in the area where the current dependence with voltage is linear, as in expression 2.33.

$$\rho = \frac{\Delta E}{\Delta J} \tag{2.33}$$

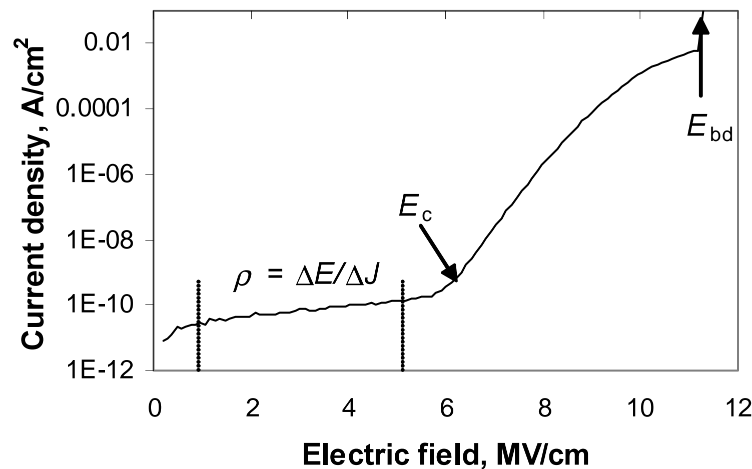

Figure 2.10. Current density versus electric field for a MOS structure.

The critical and breakdown fields were extracted by averaging the I-V curves of 25 capacitors of 0.1 mm^2.

Several conduction mechanisms have been investigated in order to identify the main transport mechanism for our dielectrics. Figure 2.11 shows the electron movement from the silicon towards the aluminium gate when positive voltage is applied on the gate.

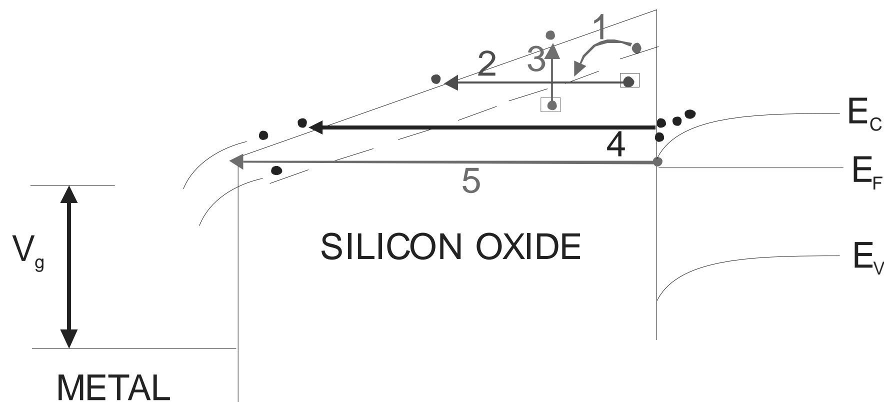

Figure 2.11. Electron transport through a SiO_2 layer.

Table 2.1 shows the expressions for the five currents investigated, where C_1, C_2, C_3 are constants, h the Plank's constant, m_0 the electron mass, ε_R the dielectric constant, r the Poole-Frenkel coefficient ($1 < r < 2$), ϕ the barrier height between the conduction band in the semiconductor and the conduction band in the dielectric.

Table 2.1. Principal conduction mechanisms.

	Conduction mechanism	Expression
1	Electron hopping	$J_1 = C_1 E \exp\left(-\frac{q\phi_a}{kT}\right)$
2	Field assisted emission	$J_2 = C_2 E^2 \exp\left(-\frac{8\pi(2m_e q\phi_T)^{1/2}}{3hE}\right)$
3	Poole-Frenkel effect	$J_3 = C_3 E \exp\left(-\frac{q\phi_T}{kT}\right)\exp\left(E^{1/2}\frac{\sqrt{q^3/(\pi\varepsilon_0\varepsilon_R)}}{rkT}\right)$
4	Fowler-Nordheim tunnelling	$J_4 = \frac{q^2 m_0}{8\pi h\phi m_e} E^2 \exp\left[-\frac{8\pi(2m_e q\phi^3)^{1/2}}{3hE}\right]$
5	Direct tunnelling	$J_5 = \frac{q^2 m_0}{8\pi h\phi m_e} E^2 \exp\left\{-\frac{8\pi(2m_e q\phi^3)^{1/2}\left[1-\left(1-\frac{t_{ox}E}{\phi}\right)^{3/2}\right]}{3hE}\right\}$

J_1 is caused by electrons jumping from one trap to another and is characterized by an exponential dependence on temperature with a thermal activation energy ϕ_a and an ohmic *J-E* characteristic [22]. The second conduction mechanism, J_2 represents the field-assisted emission and is attributed to tunnelling of electrons from traps to the dielectric conduction band [23]. Poole-Frenkel effect is expressed by J_3 and is the thermal emission of charge carriers due to a decrease in the trap barrier height (ϕ_T) under the influence of an electric field [24, 25]. The first three mechanisms are attributed to the presence of traps in the dielectric bandgap.

Current J_4 is the expression of Fowler-Nordheim tunnelling which is due to electrons tunnelling from silicon to the dielectric conduction band [26, 27]. In case of direct tunnelling (J_5), electrons pass directly from silicon into the metal conduction band [28].

Constant current stress (CCS) measurements were performed in order to evaluate the dielectric integrity. Through 0.01 mm^2 capacitors, a constant current of 1 mA/cm^2 was forced until breakdown was reached i.e. the applied voltage drops to a small fraction of the original value (figure 2.12). The charge-to-breakdown was calculated as current multiplied by the time to breakdown. Charge-to-breakdown distributions (Weibull plots) were drawn

from 50 CCS measurements performed with the silicon substrate in accumulation.

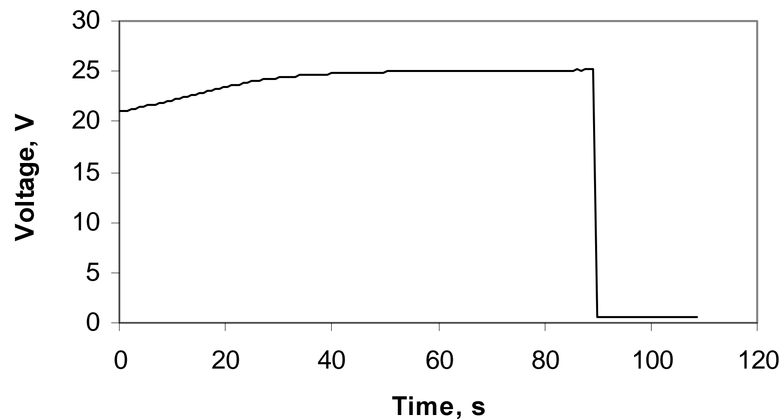

Figure 2.12. Constant current measurement for a 25 nm oxide.

The transistors fabrication is described in chapter 7.

2.6. References

1. O.A. Popov, Physics of thin films, Vol. 18, Plasma sources for thin film deposition and etching, p. 126.
2. S. Dzioba, R. Rousina, "Dielectric thin film deposition by electron cyclotron resonance plasma chemical vapor deposition for optoelectronics", J. Vac. Sci. Technol. B **12**, pp. 433-440 (1994).
3. S. Sitbon, M.C. Hugon, B. Agius, F. Abel, J.L. Courant, M. Puech, "Low temperature deposition of silicon nitride films by distributed electron cyclotron resonance plasma-enhanced chemical vapor deposition", J. Vac. Sci. Technol. A **13**, pp. 2900-2907 (1995).
4. J. Hopwood, J. Asmussen, "Neutral gas temperatures in a multipolar electron cyclotron resonance plasma", Appl. Phys. Lett. **58**, pp. 2473-2475 (1991).
5. J. Asmussen, "Electron cyclotron resonance microwave discharges for etching and thin-film deposition", J. Vac. Sci. Technol. A, **7,** pp. 883 (1989).
6. H.S. Uhm, P.H. Lee, Y.I. Kim, J.H. Kim, H.Y. Chang, "A Study of Density in Electron-Cyclotron-Resonance Plasma", IEEE Transactions on Plasma Science **23**, pp. 628-635 (1998).
7. G. King, F.C. Sze, P.Mak, T.A. Grotjohn, J. Asmussen, "Ion and neutral energies in a multipolar electron cyclotron resonance plasma source", J. Vac. Sci. Technol. A **10**, pp. 1265-1269 (1992).

8. J. Hopwood, D.K. Reinhard, J. Asmussen, "Charged particle densities and energy distributions in a multipolar electron cyclotron resonant plasma etching source", J. Vac. Sci. Technol. A **8**, pp. 3103-3112 (1990).
9. Y. Weng, M. Kushner, "Electron energy distributions in electron cyclotron resonance discharges for material processing", J. Appl. Phys. **72**, pp. 33-42 (1992).
10. P. Mak, M.-H. Tsai, J. Natarajan, B.L. Wright, T.A. Grotjohn, F.M.A. Salam, M. Siegel, J. Asmussen, "Investigation of multipolar electron cyclotron resonance plasma source sensors and models for plasma control", J. Vac. Sci. Technol. A **14**, pp. 1894-1900 (1996).
11. R.L. Kinder, "Consequences of mode structure on plasma parameters in electron cyclotron resonance sources used for materials processing", Master thesis, University of Illinois at Urbana-Champaign, 1998.
12. P. Mak, G. King, T.A. Grotjohn, J. Asmussen, "Investigation of the influence of electromagnetic excitation on electron cyclotron resonance discharge properties", J. Vac. Sci. Technol. A **10**, pp. 1281-1287 (1992).
13. D.L. Smith, "Thin film deposition, principles and practice", McGraw-Hill, 1995.
14. L.E. Kline, W.D. Partlow, R.M. Young, R.R. Mitchell, T.V. Congedo, "Diagnostics and modeling of RF discharge dissociation in N_2O", IEEE Trans. Plasma Sci. **19**, pp. 278-285 (1991).
15. M.J. Kushner, "Plasma chemistry of $He/O_2/SiH_4$ and $He/N_2O/SiH_4$ mixtures for remote plasma-activated chemical-vapor deposition of silicon oxide", J. Appl. Phys. **74**, pp. 6538-6553 (1993).
16. T.P. Ma, "Making silicon nitride film a viable gate dielectric", IEEE Trans. on El. Devices **45**, pp. 680-690 (1998).
17. R.W. Fox and A.T. McDonald, Introduction to Fluid Mechanics, p. 614.
18. S. Garcia, I. Martil, G. Gonzalez Diaz, E. Castan, S. Duenas, M. Fernandez, "Deposition of SiN_x:H thin films by the electron cyclotron resonance and its application to Al/SiN_x:H/Si structures", J. Appl. Phys. **83**, pp. 332-338 (1998).
19. W. H. Press, B.P.Falnnery, S.A. Teukolshy, W.T. Vetterling, Numerical Recipe in C, Cambridge University Press, Cambridge, 1998.
20. E.H. Nicollian, J.R. Brews, MOS (metal oxide semiconductor) physics and technology, Chapter 3.
21. R. Castagne, A. Vapaille, "Description of the SiO_2-Si interface properties by means of very low frequency MOS capacitance measurements", Surface Science, **28**, pp. 157-193 (1971).
22. S.M. Sze, "Current transport and maximum dielectric strength of silicon nitride films", J. Appl. Phys. **38**, pp. 2951-2956 (1967).

23. C. Chaneliere, J.L. Autran, R.A.B. Devine, "Conduction mechanisms in Ta_2O_5/SiO_2 and Ta_2O_5/Si_3N_4 stacked structures on Si", J. Appl. Phys. **86**, pp. 480-486 (1999).
24. E. Kameda, T. Matsuda, Y. Emura, T. Ohzone, "Fowler–Nordheim tunneling in MOS capacitors with Si-implanted SiO_2", Solid-St. Electron. **42**, pp. 2105-2111 (1998).
25. M. Depas, B. Vermeire, P. W. Mertens, R. L. Van Meirhaenghe, M. Heyns, "Determination of tunnelling parameters in ultra-thin oxide layer poly-Si/SiO_2/Si structures", Solid-St. Electron. **38**, pp. 1465-1471 (1995).
26. J.R. Yeargan, H.L. Taylor, "The Poole-Frenkel effect with compensation present", J. Appl. Phys. **39**, pp. 5600-5604 (1968).
27. W.R. Harrell, J. Frey, "Observation of Poole-Frenkel effect saturation in SiO_2 and other insulating films", Thin Solid Films **352**, pp. 195-204 (1999).
28. P. Gentil, Instabilities in Silicon Devices – Silicon Passivation and Related Instabilities, edited by G. Barbottin and A. Vapaille (Elsevier, Amsterdam, 1989).

Chapter 3 Physical properties of ECR SiO_2

Abstract

In this chapter a study of the deposition of silicon dioxide layers by multipolar Electron Cyclotron Resonance Plasma Enhanced Chemical Vapour Deposition (ECR-PECVD) from N_2O and SiH_4 is presented. The influences of different deposition parameters (gas flow rates, total pressure, microwave power, annealing processes and substrate temperature) on deposition kinetics and physical properties were investigated and explained. Low pressure, low SiH_4 flow and high power produce films with a higher refractive index, lower etch rate, good stoichiometry and fewer hydrogen bonds. High quality SiO_2 films were obtained not only at high deposition temperature of 500°C, but also at near room temperature with increased microwave power. The electrical properties of the films are discussed in chapter 4 of this thesis.

3.1. Introduction

Silicon dioxide (SiO_2) is one of the most used materials in electronics manufacturing. SiO_2 layers are traditionally grown by oxidising the silicon in oxygen ambient at around 1000°C; they are amorphous and possess a refractive index of 1.46 and a density of 2.2 g/cm^3 [1]. Due to the fact that SiO_2 is an excellent insulator and has a very good interface with silicon, it is the preferred gate dielectric for high-mobility, fast devices.

The tendency to fabricate electronics on glass or plastic has triggered huge advances in low temperature deposition of SiO_2. However, a low deposition temperature degrades the gate insulator properties. The challenge is to develop at ambient temperature, high-quality dielectrics comparable in terms of both physical and electrical properties, to the SiO_2 grown at 1000°C. The films need to exhibit a stoichiometric ratio Si:O of 1:2 in order to avoid creation of dangling bonds i.e. trap centers, high density, strong Si-O bonds, unstrained interface and to lack contaminants.

The main problem is reducing the hydrogen content and densifying the layer at low deposition temperature. Due to the higher density of ECR plasma compared to radio frequency plasma it is believed that the hydrogen

content can be limited. Studies have shown that by increasing the ratio between the flux of impinging ions and the flux of particles, it is possible to reduce the concentration of Si-OH bonds [2].

Device-quality SiO_2 has been obtained by ECR PECVD in the past [3], but the influences of various deposition parameters on film composition and density were not systematically investigated. Also highly diluted SiH_4 was not frequently employed, in contrast with pure SiH_4 or low diluted SiH_4, despite its advantage in eliminating hydrogen bonds in the rf-PECVD layers [4].

In order to determine the optimal deposition conditions for dense stoichiometric oxides and to understand better the plasma phenomena, the influence of pressure, SiH_4 and N_2O flow, microwave power, temperature and annealing process upon the deposition kinetics, the film's physical and chemical properties were studied. The content of this chapter is organised in such a way that each subsection covers only one film property and the major factors that affect this property.

Both pure and diluted SiH_4 were tested as source gases, but significantly improved film quality was obtained with diluted SiH_4. However the deposition rate was lowered with diluted SiH_4, which can also explain the better quality. Denser films were obtained at lower pressure, lower flows and higher microwave power. Although a higher temperature in general improved the film properties, layers without hydrogen bonds were obtained at near room temperature by adjusting the deposition parameters.

3.2. Deposition kinetics

In case of SiO_2 deposition, SiH_4 and N_2O are usually used as precursor gases due to the lower reactivity of N_2O compared to O_2, and therefore smaller probability of gas-phase reactions. The N_2O dissociation and the reaction mechanism with SiH_4 were described in section 2.1.2. A global reaction for the film deposition can be written:

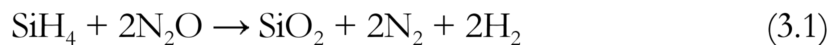

$$SiH_4 + 2N_2O \rightarrow SiO_2 + 2N_2 + 2H_2 \qquad (3.1)$$

Nitrogen atoms are also present in the plasma, and although the likelihood of them reacting with silane molecules is much smaller than for oxygen, it is nevertheless different from zero, therefore Si-N-H bonds are also present in the oxide film.

If the oxidation is not complete, in the end there will remain hydrogen atoms in the film, bonded to silicon, nitrogen or oxygen. It can be viewed as a plus, because hydrogen may passivate the dangling bonds, however hydrogen

bonds can constitute also a disadvantage due to their poor thermal stability and tendency to degrade the structural and electrical properties of the dielectric at high biases and temperatures.

High deposition rates are desired in industry in order to reduce deposition time and production costs. However, fast growing dielectrics have poor quality, due to insufficient time for particles to migrate on the film surface and form strong bonds between atoms. In case of gate dielectric for high mobility TFTs, thin films with higher quality are preferred over fast deposited layers.

The influence of each parameter upon the deposition kinetics was analysed; each deposition parameter is treated separately while keeping the other conditions constant.

Both pure SiH_4 and 2% SiH_4 diluted in helium was used. 5 sccm diluted SiH_4 contains actually only 0.1 sccm pure SiH_4.

3.2.1. SiH_4 flow role

Two series of experiments were performed in order to investigate the SiH_4 role in deposition kinetics; one in which pure SiH_4 was employed and one with (2%) SiH_4 diluted in helium. Figure 3.1 shows the deposition rate as a function of the SiH_4 partial pressure and flow. It can be seen that the deposition rate can be written as a linear function of the SiH_4 partial pressure, which passes through zero, confirming other results [5-10].

The SiH_4 concentration (n_{SiH_4}) at constant volumetric flow can be written according to the ideal gas law, as a function of SiH_4 partial pressure (p_{SiH_4}), Boltzmann's constant (k_B) and temperature (T) [11]:

$$n_{SiH_4} = \frac{p_{SiH_4}}{k_B T} \tag{3.2}$$

By replacing n_{SiH_4} in equation 2.21 with the above expression, the reaction rate between SiH_4 and oxygen radicals becomes proportional with the partial pressures of SiH_4 and oxygen:

$$R = k_r n_{SiH_4} n_O \sim p_{SiH_4} p_O \tag{3.3}$$

With increasing the SiH_4 flow, p_{SiH_4} increases and the deposition rate increases proportionally. This indicates that the deposition of the film is controlled mainly by the concentration of SiH_4. The slope of the growth rate

was higher for the experiments performed with diluted SiH_4, due to the influence of other parameters, such as higher total pressure. The layers obtained with pure SiH_4 exhibited a deposition rate too high for our application; the main difficulty in depositing thin films at a high rate is achieving a good reproducibility.

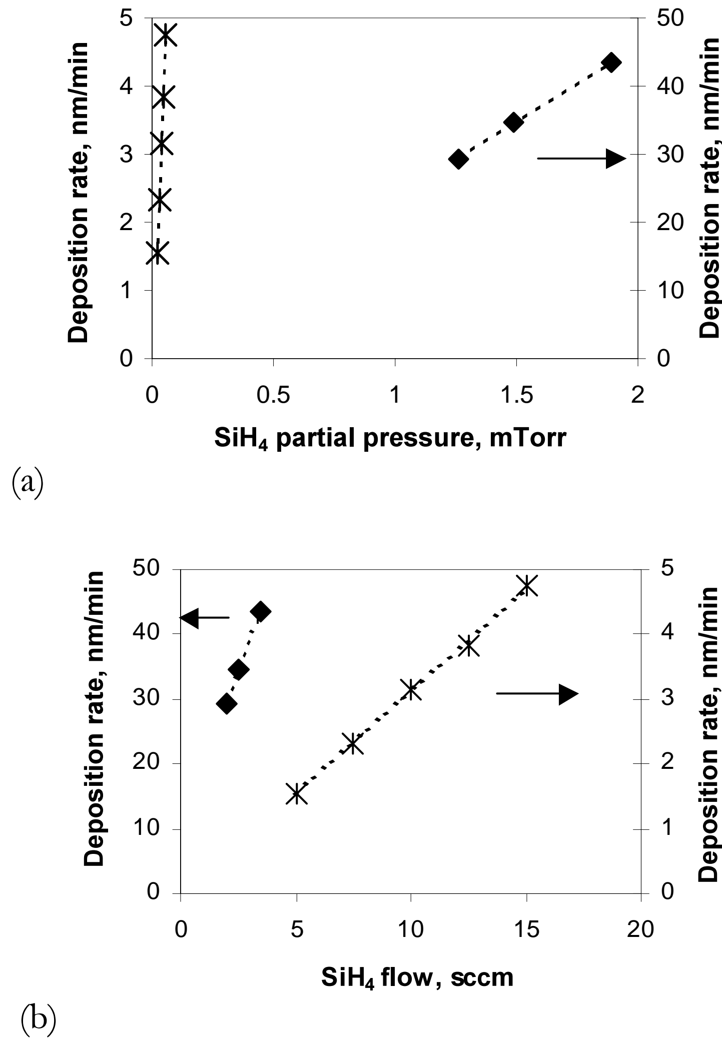

Figure 3.1. (a) Deposition rate versus SiH_4 partial pressure and (b) deposition rate versus SiH_4 flow for near room temperature layers (◆) obtained at 7 mTorr, 500 W, with 10 sccm N_2O and pure SiH_4 between 2 and 4 sccm, and (✳) obtained at 12 mTorr, 400 W with 50 sccm N_2O and 2% diluted SiH_4 in He between 5 and 15 sccm.

3.2.2. Pressure role

The influence of pressure upon deposition kinetics was studied for different series of experiments, using both pure (figure 3.2) and diluted SiH_4 (figure 3.3). The deposition rate gradually increases with increasing the pressure in the chamber. By taking into consideration expressions 3.2, the concentrations of the reactive gases will increase as a result of raising the total pressure, and therefore the deposition rate will be higher (see expression 3.3).

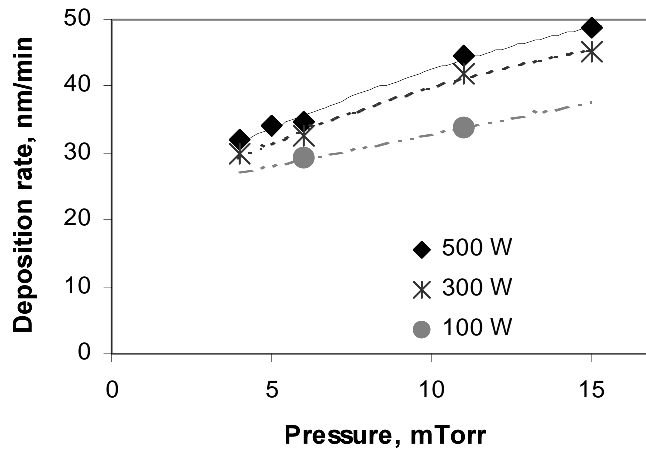

Figure 3.2. Deposition rate versus pressure for near room temperature layers deposited with 2 sccm pure SiH_4, 25 sccm N_2O at (◆) 500 W, (✳) 300 W and (●) 100 W.

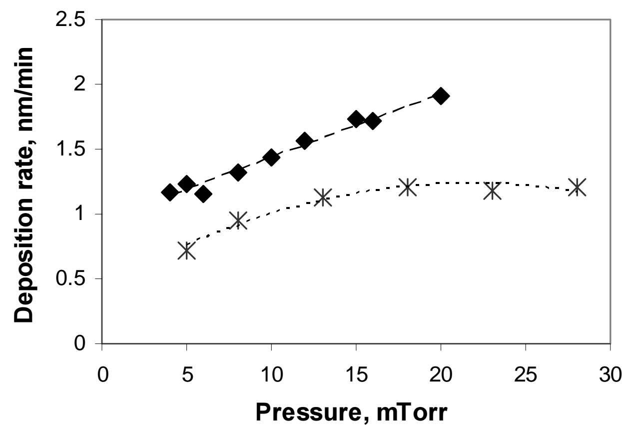

Figure 3.3. Deposition rate versus total pressure for oxides deposited with 5 sccm diluted SiH_4, (◆) with 20 sccm N_2O, at 400 W and at near room temperature, (✳) with 5 sccm N_2O, 150 W and at 500°C.

The film grows much faster at lower pressures, while at higher pressures there is a saturation tendency in deposition rate versus pressure (see figure 3.2

and figure 3.3). This trend was observed also by other authors [12]. In the high-pressure region due to frequent collisions, the ECR plasma is not so efficient and therefore the radicals' concentration is not linear anymore with the gas concentration introduced in the chamber (see expression 2.19). Also the diffusion coefficient decreases at high pressure (see expression 2.23) and the deposition rate becomes affected by the supply of molecules and radicals as it was explained in section 2.1.2.

3.2.3. Microwave power role

The deposition rate gradually increases with enhancing the microwave power for films deposited with pure SiH_4 (figure 3.4).

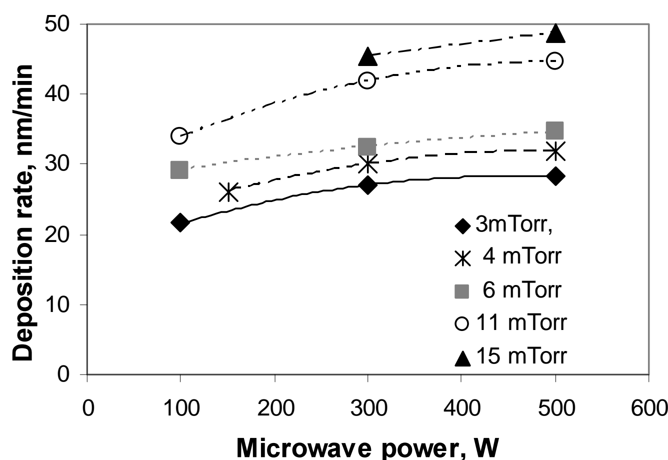

Figure 3.4. Deposition rate vs. microwave power for near room temperature layers deposited with 2 sccm SiH_4 and 25 sccm N_2O, at several pressures (◆) 3 mTorr, (✳) 4 mTorr, (■) 6 mTorr, (○) 11 mTorr and (▲) 15 mTorr.

An increase in the input microwave power results in a higher concentration of radicals and ions as measured by some authors in similar equipment set-ups (see section 2.1.1). This is to be expected because the electron density and temperature, the two factors that control the dissociation of molecules as explained by expression 2.19, are amplified by the larger dissipated power [13]. Consequently, if the radicals' concentration increases, the reaction rate will also increase and the film is deposited faster (see expression 3.3).

For layers deposited with diluted SiH_4 (figure 3.5) it can be observed that the effect of microwave power between 300 W and 500 W is insignificant upon the deposition rate. Apparently the dissociation degree increases very slowly with the input power for these microwave powers [14, 15].

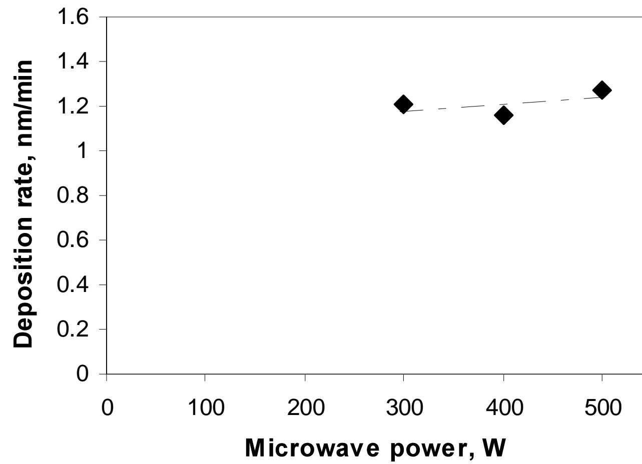

Figure 3.5. Deposition rate versus microwave power for near room temperature layers deposited with 5 sccm diluted SiH_4 and 20 sccm N_2O, at 6 mTorr.

3.2.4. N_2O flow role

Figure 3.6 shows how the deposition rate varies with N_2O flow, for layers deposited with pure and diluted SiH_4. As observed also by other authors [16], at high N_2O flows, the deposition rate decreases slightly, for the films obtained with pure SiH_4. When higher N_2O flow is introduced in the chamber, the partial pressure of SiH_4 will decrease, therefore the deposition rate will also be decreased (see expression 3.3).

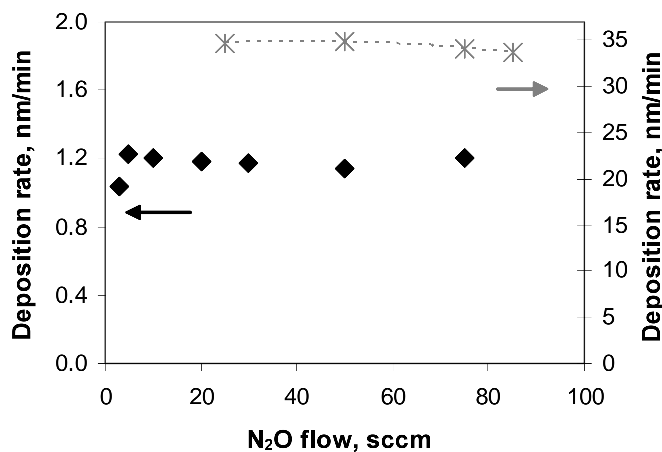

Figure 3.6. Deposition rate versus N_2O flow rate for oxides deposited (◆) with 5 sccm diluted SiH_4, at 18 mTorr, 150 W and 500°C, and (✳) with 2 sccm SiH_4, at 14 mTorr, 300 W and 300°C.

However, the deposition rate does not vary very much, considering the fact that SiH_4 partial pressure is reduced four times. The deposition rate may be limited by the supply of SiH_x radicals to the wafer.

At high N_2O flow less SiH_4 will diffuse backstream in the quartz dome and be deposited in the plasma dome and therefore the concentration of SiH_4 molecules at the substrate will be constant despite high dilution with N_2O gas. Diffusion of SiH_4 in the plasma was confirmed by monitoring the deposition of silicon oxide on the dome walls by in-situ reflectometry. In figure 3.7 the small waves are caused by a SiO_2 layer deposited in the dome, while the large wave is produced by the deposition on the wafer. Figure 3.7 shows that the deposition on the quartz dome becomes weaker for a high N_2O flow of 100 sccm, due to suppression of SiH_4 backstream diffusion.

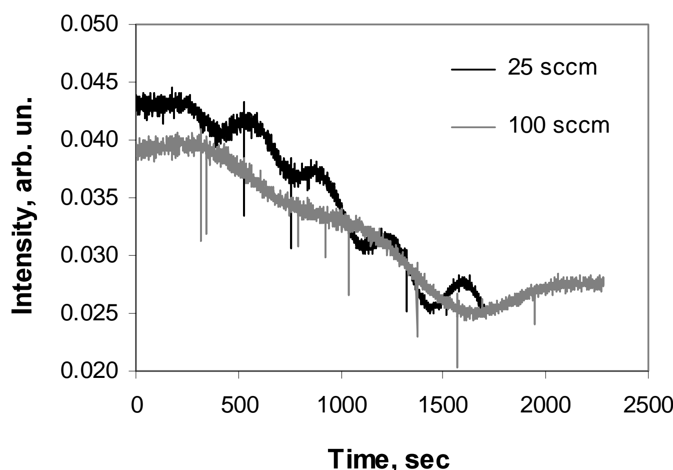

Fig. 3.7. Influence of N_2O flow upon upstream diffusion for RT layers deposited with 2 sccm SiH_4, at 14 mTorr, 30 W and (—) 100 sccm N_2O or (—) 25 sccm N_2O.

The amount of SiH_4 introduced was comparable with the amount of SiH_4 deposited on the walls and substrate, taking into account a surface of 1000 cm^2 and the SiO_2 density of $2{\cdot}10^{22}$ molecules/cm^3. Therefore it can be concluded that SiH_4 is the main factor that influences the deposition rate, while N_2O flow and microwave power show little influence for the conditions chosen for deposition.

3.2.5. Temperature role

Deposition decreases at high substrate temperatures, as can be observed in figure 3.8 for various series of experiments. Usually the chemical reactions are enhanced by temperature. However in the case of reactions between radicals, temperature has mostly no effect upon the reaction rate. Another explanation

would be the fact that the reaction that limits the deposition (the reaction with the slowest coefficient rate) takes place in the gas-phase where the substrate temperature has no influence. In both these cases, it would be expected that the deposition rate is constant with temperature.

The decrease in deposition rate with substrate temperature can be explained in terms of increasing the film density at higher temperature. A higher temperature will increase the energy of the particles migrating on the surface and will furthermore help desorb the hydrogen contained in the film. Both these events result in a denser and thinner film, which can be translated into a lower deposition rate.

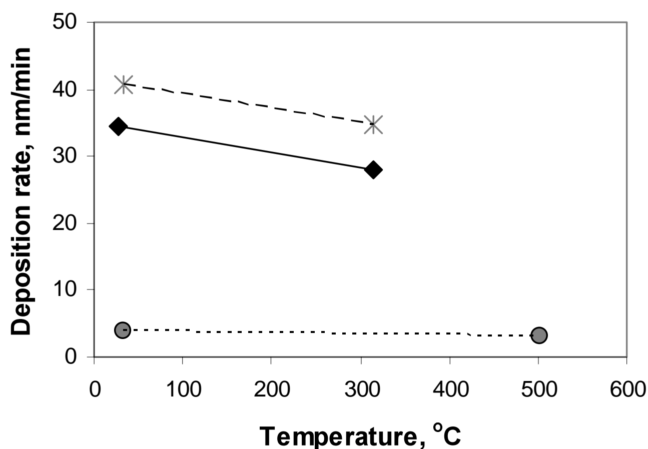

Figure 3.8. Deposition rate versus substrate temperature for oxides deposited with 2 sccm SiH_4, (◆) 25 sccm N_2O, at 7 mTorr and 300 W; (✳) 50 sccm N_2O, at 15 mTorr and 300 Watts; (●) 100 sccm N_2O, at 15 mTorr and 30 W.

3.3. Refractive index

The value of refractive index reflects two of the film properties: the film density and the atomic composition. Refractive indexes lower than the one of thermally grown oxide (1.46) can be a symptom of a porous film or a layer with hydrogen or water contamination. A refractive index higher than 1.46 is an indication of nitrogen contamination or silicon excess in the film. Because more than one factor influences the SiO_2 refractive index, it is difficult to determine the film quality based only upon the refractive index value. For example, a layer that has a refractive index of 1.46 and apparently is comparable to thermal oxide can experience both excess silicon and low hydrogen incorporation in the same time and possess very bad electrical properties. Therefore, the composition was investigated also in section 3.4 by Auger sputtering and infrared spectra.

3.3.1. SiH_4 flow role

The dependence of the refractive index with the SiH_4 flow was studied using both pure SiH_4 (figure 3.9) and diluted SiH_4 (figure 3.10). The refractive index clearly rises from 1.45 to 1.57 while the SiH_4 volumetric flow is increased, due to excess silicon incorporated in the films [17, 12]. This was confirmed by composition measurements (see section 3.4.1).

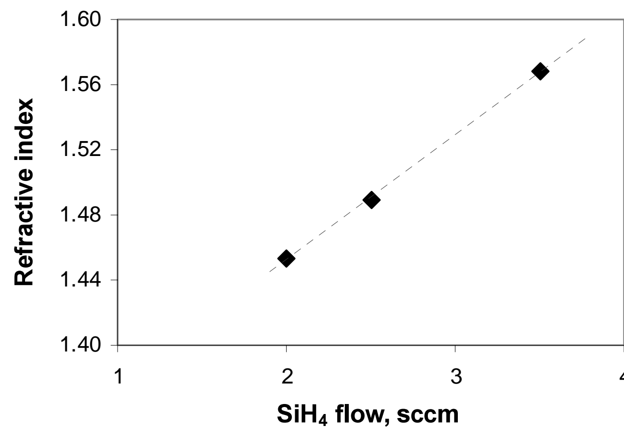

Figure 3.9. Refractive index versus SiH_4 flow for layers obtained at near room temperature, 7 mTorr, with 10 sccm N_2O, 500 W.

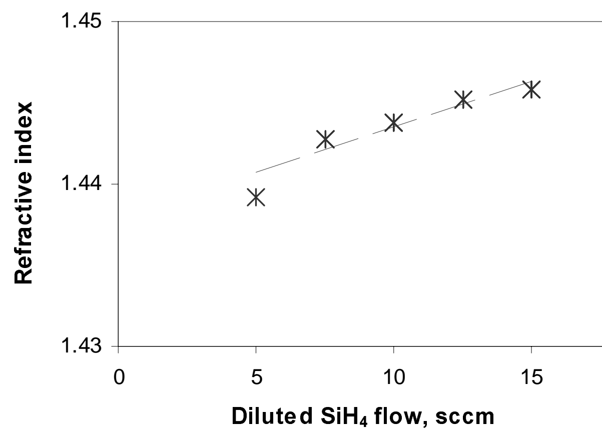

Figure 3.10. Refractive index versus diluted SiH_4 flow for layers deposited at near room temperature, 12 mTorr, with 50 sccm N_2O and 400 W.

One can see in figure 3.10 that the refractive index for the layers deposited with highly diluted SiH_4 is lower, around 1.44 - 1.45. The trend for these films is the same, the refractive index is higher for the layers obtained with higher SiH_4 flow, indicating a higher Si/O ratio in these layers [12].

3.3.2. Pressure role

For the films deposited at room temperature, the refractive index sharply falls down with increasing the total pressure (figure 3.11 and figure 3.12) [18].

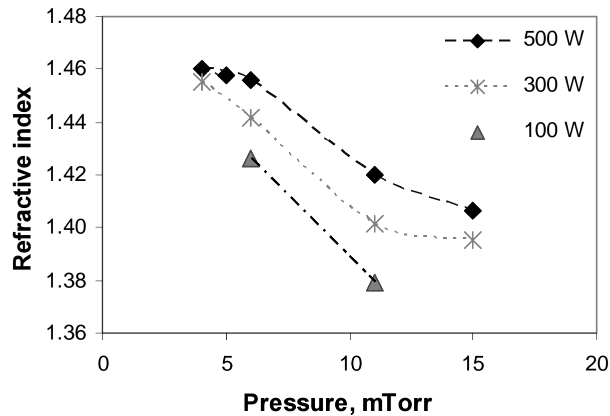

Figure 3.11. Refractive index versus pressure for layers deposited at near room temperature, with 2 sccm pure SiH_4, 25 sccm N_2O at (◆) 500 W, (✳) 300 W and (▲) 100 W.

ECR plasma is more efficient at low pressures, as shown in section 2.1. Because the ion energy and flux increase at low pressure as measured and simulated by other authors (see section 2.1.1), there is a higher energy transfer from the plasma to the film. When the insulators are deposited at near room temperature, the ion bombardment is important for effective hydrogen desorption from the growing film, as well as for adsorbed species to migrate on the surface [19]. Consequently, denser films with less hydrogen and higher refractive index will be obtained at lower pressures. For pressures around 5 mTorr, the refractive index is in the range of 1.45-1.46, which is comparable with the values of the thermally grown SiO_2 refractive index.

The refractive index for the oxides deposited at 500ºC decreases much slower than the refractive index of layers obtained at near room temperature (figure 3.12). A possible cause is the additional energy received from heating the substrate, which is used for breaking the hydrogen bonds and eliminating the hydrogen from the film.

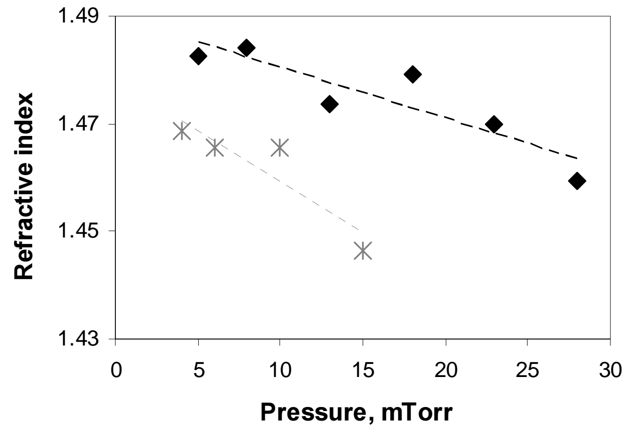

Figure 3.12. Refractive index versus total pressure for layers deposited with 5 sccm diluted SiH_4, (◆) 5 sccm N_2O, at 150 W and 500°C, and (✳) with 20 sccm N_2O at 400 W, at room temperature.

3.3.3. Microwave power role

As it can be seen in figure 3.13, the refractive index increases at an elevated microwave power. In section 2.1.1 it was shown that the ion energy and plasma density rises with the input microwave power. Consequently, the film deposited at 500 W will be subjected to an elevated flux of highly energetic radicals and ions and will therefore have a lower hydrogen content, higher density and higher refractive index.

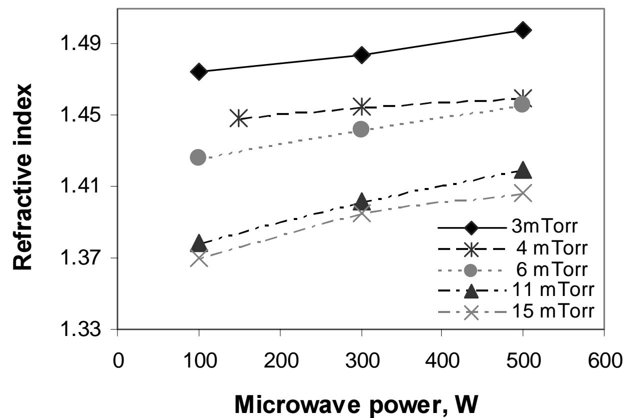

(a)

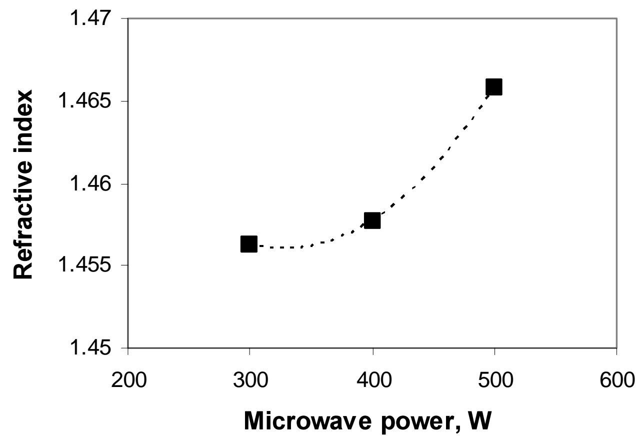

(b)

Figure 3.13. Refractive index versus microwave power for layers deposited at near room temperature (a) with 2 sccm SiH_4 and 25 sccm N_2O and several pressures: (◆) 3 mTorr, (✻) 4 mTorr, (●) 6 mTorr, (▲) 11 mTorr, (×) 15 mTorr and (b) with 5 sccm diluted SiH_4, 20 sccm N_2O and at 6 mTorr.

3.3.4. N_2O flow role

An increase in the N_2O flow for room temperature deposition results in a decreasing film density leading to a decrease of the refractive index (figure 3.14), especially for the layers obtained with pure SiH_4 and extremely low microwave power.

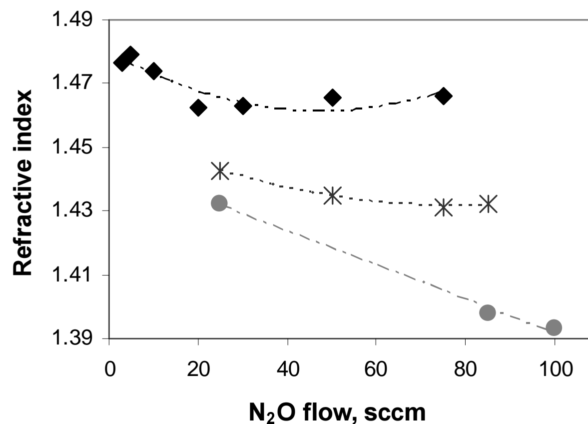

Figure 3.14. Refractive index versus N_2O flow rate for oxides deposited (◆) with 5 sccm diluted SiH_4, at 18 mTorr, 150 W and 500°C, (✻) with 2 sccm SiH_4, at 14 mTorr, 300 W and 300°C and (●) with 3.15 sccm SiH_4, at 14 mTorr, 30 W and room temperature.

The decrease of refractive index with increasing the N_2O flow can be considered an effect of lower energy transfer from the plasma toward the growing film. The energy arriving from the plasma is very important for

chemical activation of surface reactions such as hydrogen desorption and enhanced surface diffusion. Ion bombardment, which is mainly responsible for energy transfer from the plasma toward the substrate, depends upon the ion energy and concentration. If we consider the production of ions limited by the concentration of electrons with sufficient energy to ionise N_2O molecules, then at high flows the ions concentration decreases due to dilution. Therefore, the ion bombardment decreases, increasing the film porosity, diminishing the film density and the refractive index. For example, by varying the N_2O flow from 25 to 100 sccm the density calculated as the mass gained by the wafer divided by the wafer area and the film thickness, decreases by 7 %.

For high temperatures of 300ºC or 500ºC and powers of 150-300 W a rise in N_2O flow results in a very small decrease of the refractive index compared to the films deposited at room temperature at low power of 30 W (figure 3.14). This is quite understandable because the elevated temperature and power enhances both the hydrogen desorption and the surface-adsorbed species migration, therefore the growth of denser films.

3.3.5. Temperature role

Temperature role upon the refractive index was discussed in the last sections, when different series of experiments were realised. However the other deposition parameters were not always kept constant. In this subsection all the parameters were maintained constant, except for the temperature.

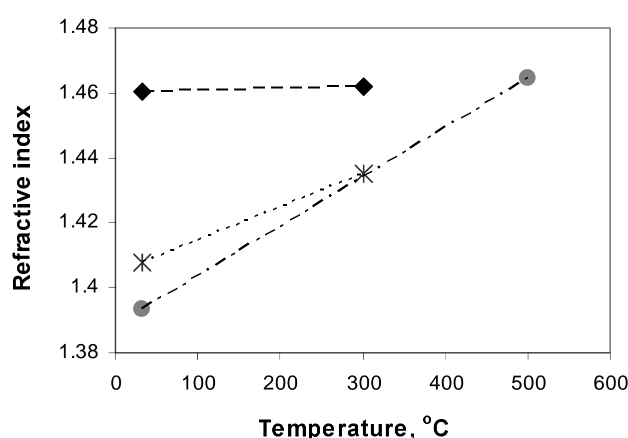

Figure 3.15. Refractive index versus substrate temperature layers deposited with 2 sccm SiH_4, (◆) 25 sccm N_2O, at 7 mTorr and 300 W; (✳) 50 sccm N_2O, at 15 mTorr and 300 W; (●) 100 sccm N_2O, at 15 mTorr and 30 W.

As one can see in the figure 3.15, the refractive index dramatically increases when the substrate is heated until 300°C or 500°C, if the deposition pressure is 15 mTorr. At this high pressure the ion bombardment is lower (see section 2.1.1) and insufficient for hydrogen desorption at room temperature, thus the refractive index is lower. Heating the substrate provides additional energy for densifying the film and destroying the hydrogen bonds [20].

At lower pressures however, the role of temperature is insignificant due to a more efficient transfer of energy from the ECR plasma to the growing film, and the refractive index is not substantially modified. Therefore, in order to obtain films at room temperature with properties similar with the ones obtained at higher temperatures, a rise in electron temperature has to occur, either by decreasing the pressure or by increasing the microwave power (see section 2.1.1).

3.4 Atomic composition

The film composition and bonding was investigated by means of Auger sputtering profiles, elastic recoil detection, etch rate in buffered oxide etchant (BOE) solution and Fourier Transform Infrared absorption spectra (see section 2.4). The film composition was homogeneous in depth, as it can be seen in figure 3.16. The atomic concentration was calculated by averaging the concentration at different depths inside the bulk of the layer.

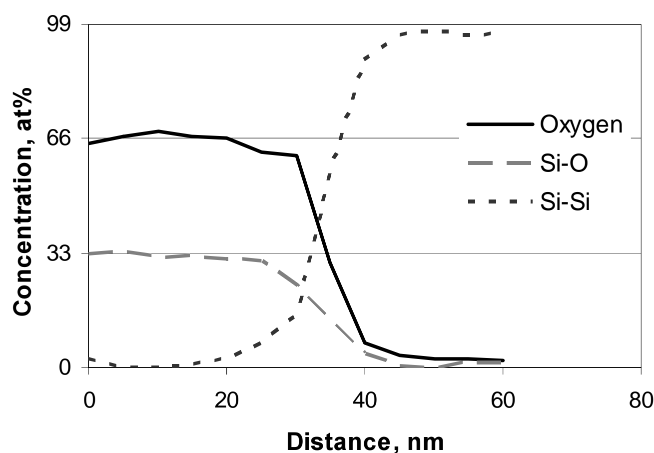

Figure 3.16. Auger sputter profile for an ECR film deposited at near room temperature, with 5 sccm diluted SiH_4, 20 sccm N_2O, at 400 W and 10 mTorr; Si-O represents the concentration of the silicon bonded to oxygen, Si-Si represents the concentration of silicon bonded to silicon.

3.4.1. SiH_4 flow role

The etch rate of SiO_2 layers in buffered oxide etching solution can provide useful information regarding the film porosity and composition. Figure 3.17 shows that the layer deposited with more SiH_4 flow is etched faster.

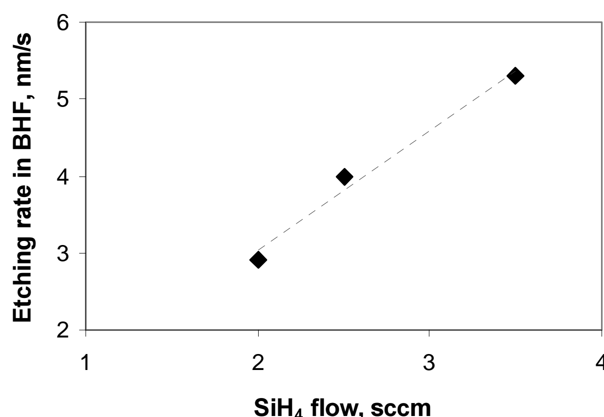

Figure 3.17. Etch rate versus SiH_4 flow layers deposited at near room temperature, 7 mTorr, with 10 sccm N_2O and 500 W.

It is known that if the SiO_2 layer contains excess silicon its etching rate is lower and if the layer is porous or contains hydrogen, the etching rate is higher. The silicon content as measured by Auger spectrometry increases from 34% to 40% with increasing the SiH_4 flow from 2 to 3.5 sccm, therefore the rise in etch rate can be explained only by a higher hydrogen content. For high concentrations of SiH_4 in gas-phase and high deposition rates, hydrogen is not replaced by oxygen radicals in the SiH_2O radicals adsorbed at the surface, therefore a nonstoichiometric film with high concentration of hydrogen and a high etch rate is deposited.

The Fourier transform infrared (FTIR) transmission spectrum confirms the higher concentration of hydrogen in case of high SiH_4 flow usage. In figure 3.18 the nitrogen-hydrogen (N-H) bonds are observed at around 3370 cm^{-1}.

A representative infrared spectrum for a high-quality ECR film is presented in figure 3.19. As it can be observed, there are no observable peaks for Si-H stretching mode at 2200 cm^{-1} [21]. This is a positive sign, considering that these bonds are easily destroyed during stress or high temperature, and deleterious silicon dangling bonds are created. Also the O-H vibration peak at 3670 cm^{-1} (1) and N-H stretching peak at 3370 cm^{-1} (2) are barely visible. Only if the scale is modified (see figure 3.18) they can be analysed. The absorption peak that corresponds to the Si-O stretching mode (4) observable

at 1078 cm^{-1} gives information about the film stoichiometry and density. The peak observed at around 2400 cm^{-1} (5) corresponds to the absorption due to CO_2 in the measurement chamber.

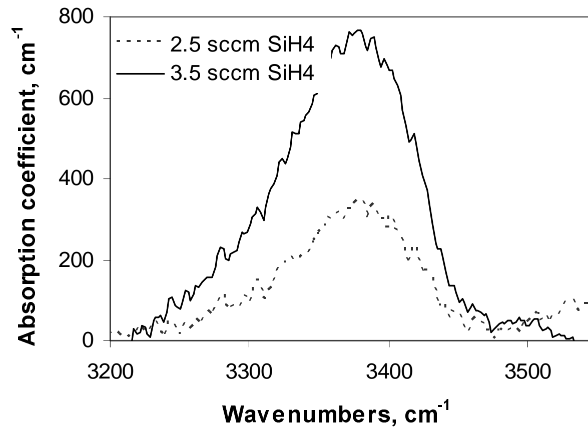

Figure 3.18. Infrared absorption spectra showing hydrogen bonds for oxides obtained at near room temperature, 7 mTorr with 10 sccm N_2O, 500 W and 2.5 sccm SiH_4 (----) or 3.5 sccm SiH_4 (—).

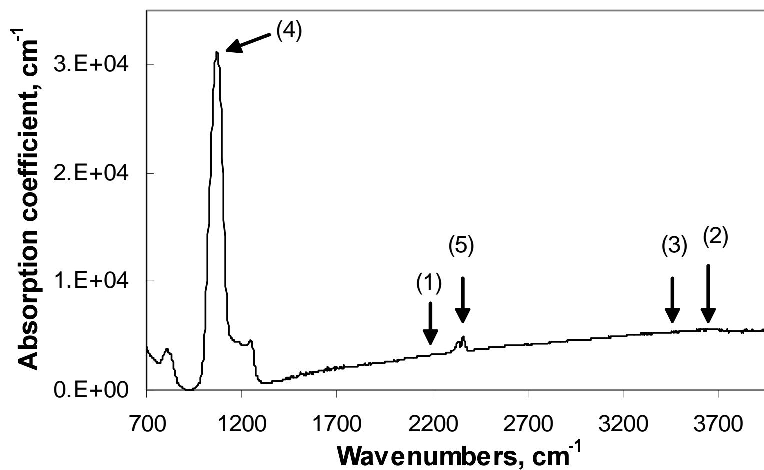

Figure 3.19. Infrared absorption spectrum for an ECR oxide deposited with 20 sccm N_2O, 5 sccm diluted SiH_4, at 400 W and 4 mTorr; (1) – (5) : see text.

The absorption spectra of two SiO_2 films deposited at room temperature and diluted SiH_4 flow were compared with the FTIR of a thermally grown oxide (figure 3.20). The frequency (ν), the full width at half maximum (FWHM) and the absorption coefficient (α) of the Si-O stretching mode were extracted from the spectra in figure 3.20 and were reported in table 3.1. One can observe that all the three parameters for the film deposited with lower SiH_4 flow, have values closer to the ones extracted for thermally grown

oxide. Similar results were obtained for films deposited with pure SiH_4. It has been shown that the decrease in stretching frequency and the rise of FWHM is usually the consequence of excess silicon in the layer [22-24] but it may be caused also by a lower film density [23, 25] and a lack of film bombardment [26].

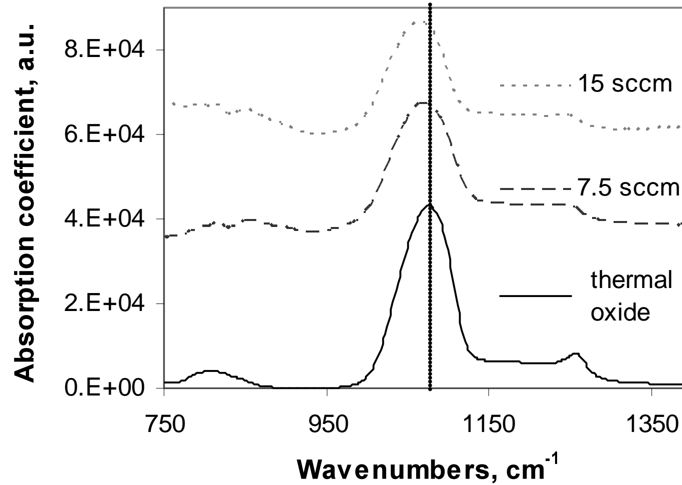

Figure 3.20. Infrared absorption spectra of thermal oxide and two ECR SiO_2 deposited at room temperature, with 50 sccm N_2O, at 400 W, 12 mTorr and with various diluted SiH_4 flow; the spectra are translated on the vertical axis for clarity reasons.

Table 3.1. The peak frequency, full width at half maximum and maximum absorption coefficient for Si-O stretching mode and also the N-H absorption coefficient for thermally grown oxide and ECR oxides. The films were deposited with 7.5 sccm and 15 sccm diluted SiH_4 (at 12 mTorr, 400 W and with 50 sccm N_2O).

Film	Si-O ν cm^{-1}	FWHM cm^{-1}	Si-O α cm^{-1}	N-H α cm^{-1}
7.5 sccm SiH_4	1072	85	29800	300
15 sccm SiH_4	1066	92	20150	400
Thermal SiO_2	1078	76	42500	50

Elastic recoil detection (ERD) measurements confirmed that a rise in the Si content from 33 at.% to 34.2 at.% occurs with increasing the diluted SiH_4 flow from 7.5 sccm till 15 sccm.

3.4.2 Microwave power role

The lowest etch rate was registered for SiO_2 films deposited at elevated microwave power (figure 3.21). Due to a higher energy absorbed from the microwave source, there is amplified particle bombardment upon the wafer (see section 2.1.1) and consequently, more hydrogen is eliminated and a denser film is produced. It is well known that denser layers have lower etch rate.

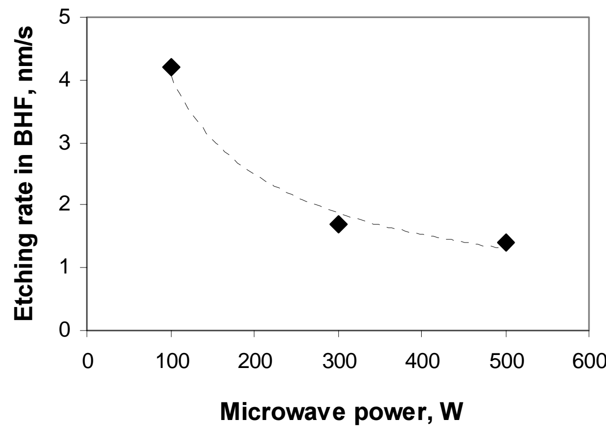

Figure 3.21. Etch rate versus microwave power for layers obtained at near room temperature, 7 mTorr with 10 sccm N_2O and 2 sccm SiH_4.

The FTIR spectra confirmed that less N-H bonds (3370 cm^{-1}) and O-H bonds (3670 cm^{-1}) were present in room-temperature films deposited at 500 W than in dielectrics obtained at 100 W (figure 3.22) due to a more efficient bombardment with ions and radicals (see section 2.1.1).

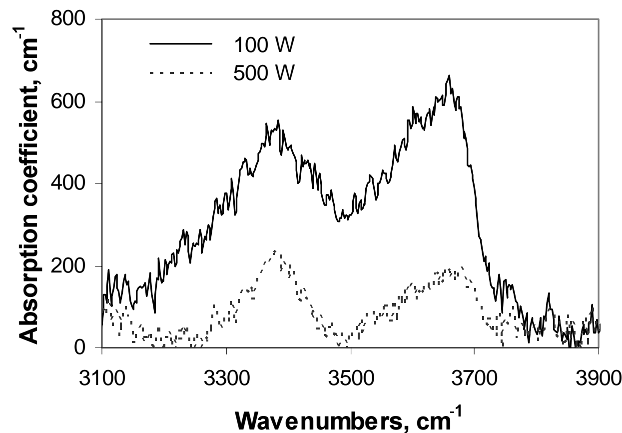

Figure 3.22. Infrared absorption spectra showing hydrogen bonds for oxides obtained at near room temperature, 7 mTorr, with 10 sccm N_2O and 2 sccm SiH_4 and 100 W or 500 W.

The hydrogen content measured by ERD, for the films produced by diluted SiH_4 rises from 0.8% to 1.1% when modifying the microwave power from 250 W until 500 W.

Besides hydrogen, also excess silicon was found to be present in films deposited at lower microwave power (table 3.2), indicating that the oxygen radicals had insufficient energy to migrate on the surface and oxidise completely the silicon bonds. On the contrary, at 500 W, the electron energy was so high that the dissociation coefficient for nitrogen molecules increased and the nitrogen incorporation in the layer doubled from 0.4 to 0.8 at.%.

Table 3.2. The composition of two ECR layers deposited at near room temperature, with 5 sccm diluted SiH_4, 20 sccm N_2O, at 6 mTorr and for various microwave power.

Microwave power, W	Si at.%	O at.%	N at.%	H at.%
250	35.3	63.2	0.4	1.1
500	32	66.4	0.8	0.8

From absorption spectra of Si-O_x bonds in layers obtained at various microwave power, the best SiO_2 film in terms of Si-O stretching mode frequency and FWHM was the one obtained at 400 W.

3.4.3 Pressure role

The pressure has an important influence upon the etching rate, (figure 3.23). While at low pressures, the etching rate is similar to the one of thermally grown oxide, an evidence of dense films, at high pressure the etching rate increases until 30 nm/sec. This phenomenon can be explained by an increase in hydrogen content at high processing pressure. Due to ECR inefficiency at high pressure (see section 2.1.1), the total energy received by the film is lower, therefore the insulator contains more hydrogen and is less dense.

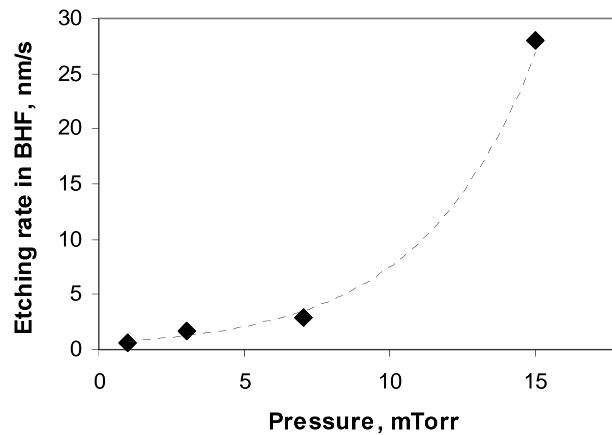

Figure 3.23. Etch rate versus pressure for layers obtained at near room temperature, with 10 sccm N_2O and 2 sccm SiH_4 and 500 W.

Because the etching rate for the oxide obtained at the lowest pressure, is even lower than 1.33, the etch rate of thermally grown oxide, the film composition was investigated by Auger spectroscopy. While for the film deposited at 3 mTorr, there is only 1.5 at.% nitrogen, at 1 mTorr, the nitrogen contamination measured by Auger sputtering reaches 10 at.%. A higher amount of nitrogen was incorporated at lower pressures, due to a higher dissociation efficiency of N_2 in the plasma. The increased nitrogen corporation caused also the decrease in the etch rate.

The increase of hydrogen content at high pressures was confirmed by the infrared spectra of layers (figure 3.24).

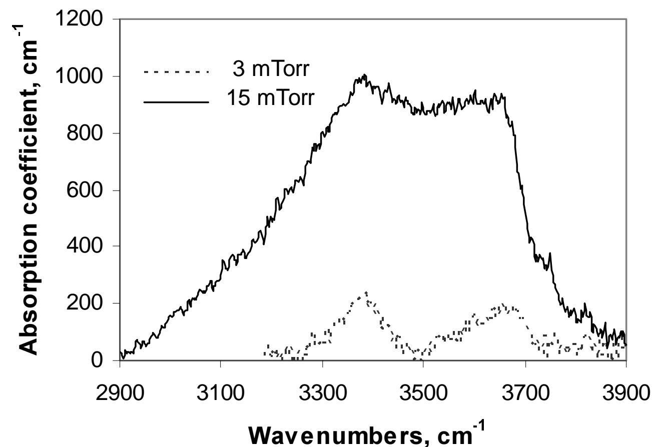

Figure 3.24. Infrared absorption spectra showing hydrogen bonds for layers obtained at near room temperature, with 10 sccm N_2O, 2 sccm SiH_4, at 500 W and 3 mTorr or 15 mTorr.

A similar trend of decreasing hydrogen bonds concentration with decreasing pressure was observed also for SiO_2 prepared with diluted SiH_4 as the reactive gas precursor (figure 3.25).

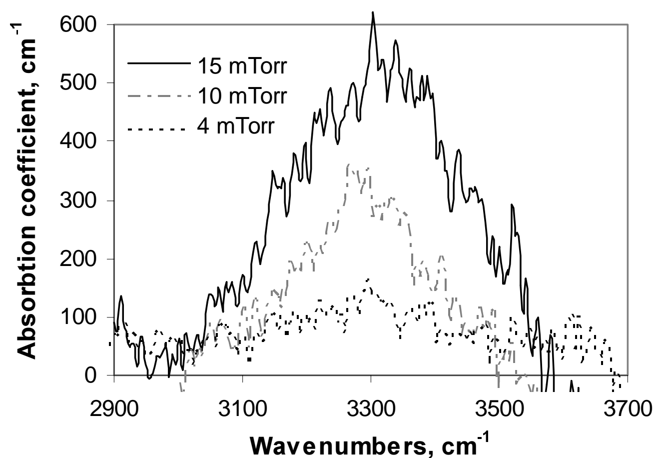

Figure 3.25. Infrared absorption spectra showing N-H bonds for layers obtained at near room temperature, with 20 sccm N_2O and 5 sccm diluted SiH_4, at 400 W and various pressures.

The absorption spectra of Si-O stretching mode for two ECR SiO_2 films deposited at total pressures of 4 and 15 mTorr are shown in figure 3.26. In addition, for comparison, the spectrum of thermally grown oxide is also represented and the extracted data is presented in table 3.3.

The Si-O absorbance peak has higher intensity, is less broad and occurs at higher frequency for the oxide deposited at lower pressure. Also the film is closer to the thermal oxide in terms of Si-O stretching mode frequency and FWHM. This suggests that the bonding structure of ECR low-pressure films is similar to that of thermal films, even if the films were deposited at near room temperature.

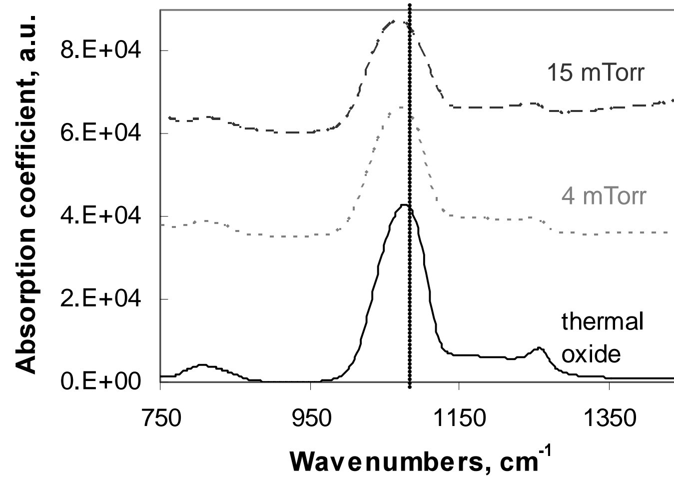

Figure 3.26. Infrared absorption spectra of thermal oxide and two ECR layers obtained at near room temperature, with 20 sccm N_2O and 5 sccm diluted SiH_4 flow, at 400 W and at (---) 4 mTorr or (—) 15 mTorr; the spectra are translated on the vertical axis for clarity reasons.

Table 3.3. The peak frequency, full width at half maximum and maximum absorption coefficient for Si-O stretching mode and also the N-H absorption coefficient for thermally grown oxide and ECR oxides. The films were deposited at pressures of 4 mTorr and 15 mTorr (with 5 sccm diluted SiH_4 and 20 sccm N_2O, at 400 W).

Film	Si-O ν cm^{-1}	FWHM cm^{-1}	Si-O α cm^{-1}	N-H α cm^{-1}
4 mTorr	1072	81	30800	150
15 mTorr	1066	85	24200	500
Thermal SiO_2	1078	76	42500	50

Auger spectrometry indicated excess silicon for oxides deposited with pure SiH_4 and good stoichiometry (Si: 33 at.%, O: 66 at.%) for the ones deposited with diluted SiH_4, independent of pressure.

Table 3.4. The composition of two ECR layers deposited at near room temperature, with diluted SiH_4 and various pressure determined by ERD.

Pressure, mTorr	Si, at.%	O, at.%	N, at.%	H, at.%
15	34.2	64.6	0.4	0.8
4	33.2	66.3	0.2	0.3

ERD has a better resolution and showed small silicon excess of 1% in the layer produced at high pressure of 15 mTorr (table 3.4). Also the hydrogen

content in the layer was 0.8 at.%, higher than in the film deposited at low pressure of 4 mTorr that had only 0.3 at.%. This confirms the observations made from infrared spectra of better hydrogen desorption at low processing pressure.

3.4.4 N_2O flow role

It is interesting to notice that while the N_2O flow is increased, the oxygen concentration measured with Auger and the Si-O bonds concentration extracted from FTIR spectra (figure 3.27) decrease. It is possible that at high flows, more bonds remained unsaturated due to the fact that there is a decrease of energy transfer from the plasma toward the growing film (see section 3.3.4).

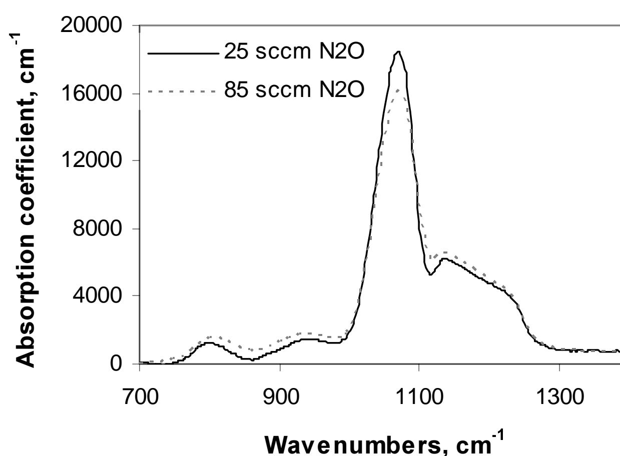

Figure 3.27. Infrared absorption spectra of ECR layers obtained at near room temperature, with 2 sccm SiH_4, at 14 mTorr, 30 Watts, and with (—) 25 or (---) 85 sccm N_2O.

3.4.5. Annealing role

The influences of post-deposition annealing in wet ambient at 500°C (see section 2.6) on the film properties have been investigated. This treatment has the effect of decreasing the N-H bonds concentration and creating extra Si-O bonds (figure 3.28). Apparently, due to the high temperature some of the hydrogen bonds were destroyed and extra Si-O bonds were formed in the film. The layer was deposited with pure SiH_4 and at very low microwave

power, thus it contained a lot of hydrogen and silicon dangling bonds before annealing. The effect of annealing on high-quality oxides was not observable.

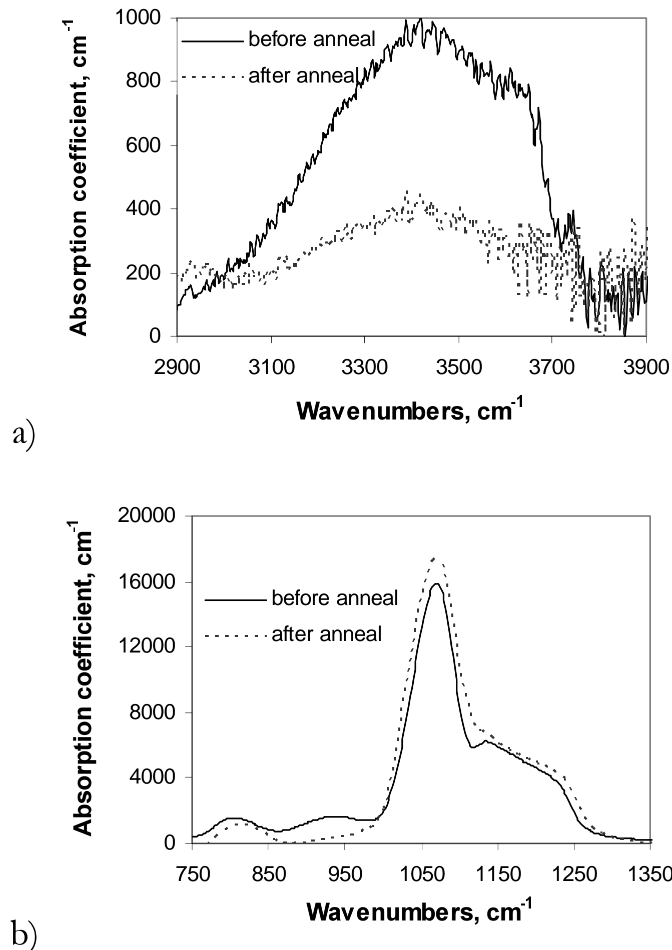

Figure 3.28. N-H stretching mode peak (a) and Si-O stretching mode peak (b) for ECR PECVD SiO_2 before and after 60 minutes wet anneal at 500°C. The layer was deposited with 2 sccm SiH_4, 85 sccm N_2O, at 14 mTorr, 30 W and near room temperature.

3.5. Film roughness

A high roughness can be a serious problem for thin gate dielectrics. Due to the fact that there are spots with lower thickness, the electric field can increase locally. Consequently, early breakdown can occur and the film integrity can be degraded.

Atomic force microscopy was used to measure the film roughness. The calculated mean roughness had values around 0.2 nm for thermally grown oxide and 0.3 nm for an ECR oxide with the same thickness of 50 nm. The similar values indicate the high quality of the ECR films. The roughnesses of

the films obtained at different conditions were compared, but only small differences within the measurement error were observed.

3.6. Summary

Stoichiometric SiO_2 films with a refractive index of 1.46, low etch rate of 1.7 nm/s in BOE, O/Si ratio of 2 and low hydrogen and nitrogen contaminations of 0.3 at.% and 0.2 at.% respectively, were deposited at rates around 1 nm/min by a multipolar ECR plasma source at different temperatures. In order to optimise the process, the effects of different deposition parameters on the films physical and chemical properties were studied. It is difficult to determine the exact optimal deposition conditions only after characterisation of physical properties, electrical characterisation performed in chapter 4 will bring more insight. The best films were obtained at low pressure (4-6 mTorr), highly diluted SiH_4 flow (5 sccm), low N_2O flow (5-20 sccm) and high microwave power (400-500 W). The quality of the films was explained based on the energy transfer from the plasma to the layers. Si-H bonds were not present in the layer and only N-H bonds were visualised in the infrared spectra, proving the high quality of the layer. Porous layers with high silicon concentration were obtained with pure SiH_4, while the usage of diluted SiH_4, decreased the deposition rate and improved considerably the film properties. By decreasing the temperature from 500°C to near room temperature, the film quality was not degraded, proving that the multipolar ECR plasma is very successful at low pressures.

3.7. References

1. B. El-Kareh, R.J. Bombard, Introduction to VLSI Silicon Devices – Physics, Technology and Characterisation, Kluwer Academic Publishers, 1985.
2. K.L Seaward, J.E. Turner, K. Nauka, A.M.E. Nel, "Role of ions in electron cyclotron resonance plasma-enhanced chemical vapor deposition of silicon dioxide", J. Vac. Sci. Technol. B **13**, pp. 118-124 (1995).
3. J.W. Lee, N.I. Lee, S.H. Hur, C.H. Han, "Oxidation of silicon using electron cyclotron resonance nitrous oxide plasma and its application to polycrystalline silicon thin film transistors", J. Electrochem. Soc. **144**, pp. 3283-3287 (1997).
4. S. Garcia, I. Martil, G. Gonzalez Diaz, E. Castan, S. Duenas, M. Fernandez, "Deposition of SiN_x:H thin films by the electron cyclotron

resonance and its application to $Al/SiN_x:H/Si$ structures", J. Appl. Phys. **83**, pp. 332-338 (1998).

5. M. Firon, M. C. Hugon, B. Agius, Y. Z. Hu, Y. Wang, and E. A. Irene, "Comparison of the physical and electrical properties of electron cyclotron resonance and distributed electron cyclotron resonance SiO_2", J. Vac. Sci. Technol. B **14**, pp. 2543-2549 (1996).
6. T. Fukuda, K. Saito, M. Ohue, K. Shima, N. Momma, "High-quality, high-rate SiO_2 and SiN films formed by 400 kHz bias electron cyclotron resonance-chemical vapor deposition", Jpn. J. Appl. Phys. **34**, L937-L940 (1995).
7. T.V. Herak, T.T. Chau, D.J. Thomson, S.R. Mejia, D.A. Buchanan, K.C. Kao, "Low-temperature deposition of silicon dioxide films from electron cyclotron resonant microwave plasmas", J. Appl. Phys. **65**, pp. 2457-2463 (1989).
8. O.A. Popov, H. Waldron, "Electron cyclotron resonance plasma stream source for plasma enhanced chemical vapor deposition", J. Vac. Sci. Technol. A **7,** pp. 914-917 (1989).
9. N. Jiang, M.C. Hugon, B. Agius, T. Kretz, F. Plais, D. Pribat, T. Carriere, M. Puech, "Device quality SiO_2 deposited by distributed electron cyclotron resonance plasma enhanced chemical vapor deposition without substrate heating", Jpn. J. Appl. Phys. **31**, pp. 1404-1407 (1992).
10. M.J. Hernandez, J. Garrido, J. Piqueras, "Silicon dioxide deposition by electron cyclotron resonance plasma: kinetic and ellipsometric studies", J. Vac. Sci. Technol. B **12,** pp. 581-584 (1994).
11. D.L. Smith, "Thin film deposition, principles and practice", McGraw-Hill, 1995.
12. P. Bulkin, N. Bertrand, B. Drévillon, "Deposition of SiO_2 in integrated distributed electron cyclotron resonance microwave reactor", Thin Solid Films, **296**, pp. 66-68 (1997).
13. P. Mak, G. King, T. A. Grotjohn, J. Asmussen, "Investigation of the influence of electromagnetic excitation on electron cyclotron resonance discharge properties", J. Vac. Sci. Technol. A **10,** pp. 1281-1284 (1992).
14. Y. Weng, M. Kushner, "Electron energy distributions in electron cyclotron resonance discharges for material processing", J. Appl. Phys. **72**, pp. 33-42 (1992).
15. P. Mak, M.-H. Tsai, J. Natarajan, B.L. Wright, T.A. Grotjohn, F.M.A. Salam, M. Siegel, J. Asmussen, "Investigation of multipolar electron cyclotron resonance plasma source sensors and models for plasma control", J. Vac. Sci. Technol. A **14**, pp. 1894-1900 (1996).
16. F. Plais, B. Agius, F. Abel, J. Siejka, M. Puech, G. Ravel, P. Alnot, N. Proust, "Low temperature deposition of SiO_2 by distributed electron

cyclotron resonance plasma-enhanced chemical vapor deposition", J. Electrochem. Soc. **139**, pp. 1489-1495 (1992).

17. T. Fukuda, M. Ohue, N. Momma, K. Suzuki, T. Sonobe, "Effects of excited plasma species on silicon oxide films formed by microwave plasma CVD", Jpn. J. Appl. Phys. **28**, pp. 1035-1940 (1989).
18. K.H. Chew, J. Chen, R.C. Woods, J.L. Shohet, "Silicon oxide deposition in an electron cyclotron resonance plasma with microwave spectroscopic monitoring of SiO", J. Vac. Sci. Technol. A **13,** pp. 2483-2489 (1995).
19. O. Joubert, R. Burke, L. Vallier, and C. Martinet, R. A. B. Devine, "Influence of ion energy on the physical properties of plasma deposited SiO_2 films", Appl. Phys. Lett. **62**, pp. 228-230 (1993).
20. T.V. Herak, D.J. Thompson, "Effects of substrate temperature on the electrical and physical properties of silicon dioxide films deposited from electron cyclotron resonant microwave plasmas", J. Appl. Phys. **67**, pp. 6347-6352 (1990).
21. Z. Yin and F. W. Smith, **"**Optical dielectric function and infrared absorption of hydrogenated amorphous silicon nitride films: Experimental results and effective-medium-approximation analysis", Phys. Rev. B **42**, pp. 3666-3675 (1990).
22. P. G. Pai, S. S. Chao, Y. Takagi, and G. Lucovsky, "Infrared spectroscopic study of SiO_x films produced by plasma enhanced chemical vapor deposition", J. Vac. Sci. Technol. A **4**, pp. 689-694 (1986).
23. H. Nakashima, K. Furukawa, Y.C. Liu, D.W. Gao, Y. Kashiwazaki, K. Muraoka, K. Shibata, T. Tsurushima, "Low-temperature deposition of high-quality silicon dioxide films by sputtering-type electron cyclotron resonance plasma", J. Vac. Sci. Technol. A **15**, pp. 1951-1954 (1997).
24. K.A. Buckle, K. Pastor, C. Constantine, D. Johnson, "Parametric evaluation of electron cyclotron resonance deposited SiO_2 using a multicusp plasma applicator", J. Vac. Sci. Technol. B **10,** pp. 1133-1138 (1992).
25. D. Landheer, L.Å. Ragnarsson, S. Belkouch, "Physical and electrical analysis of silicon dioxide thin films produced by electron-cyclotron resonance chemical-vapour deposition", Microelectronic Engineering, **36**, pp. 53-60 (1997).
26. R. G. Andosca, W. J. Varhue, "Silicon dioxide films deposited by electron cyclotron resonance plasma enhanced chemical vapor deposition", J. Appl. Phys. **72**, pp. 1126-1132 (1992).

Chapter 4 Electrical properties of ECR SiO_2

Abstract

In this chapter the investigation of the electrical properties of SiO_2 layers, grown by multipolar ECR-PECVD from N_2O and SiH_4 are presented. The physical properties of the layers were discussed in the previous chapter. The following electrical properties have been analysed: the interface trap density, the fixed oxide charge, the critical and breakdown field, the resistivity and the charge-to-breakdown. Furthermore, the trapping behaviour and the conduction mechanism have been studied. The dependencies of electrical properties on deposition parameters (gas flow rates, total pressure, microwave power, annealing processes and substrate temperature) have been analysed. Low pressure and high microwave power appear to have a beneficial influence upon the bulk properties and a damaging effect upon the interface with silicon. High quality SiO_2 films, comparable to thermally grown oxide were obtained at near room temperature, low SiH_4 flow, low pressures and intermediate microwave powers. Fowler-Nordheim tunnelling was found to be the dominant mechanism in dense SiO_2 layers, whereas the Poole-Frenkel effect is responsible for the high leakage current in the inferior dielectrics.

4.1. Introduction

The previous chapter has shown that multipolar ECR PECVD can deliver stoichiometric SiO_2 layers with low hydrogen and nitrogen content, high density, low etch rate and a refractive index of 1.46. Deposition conditions were optimised in order to obtain at near room temperature dielectrics similar to the thermally grown oxide.

Because these layers are intended for use as gate dielectrics in TFTs, the electrical properties of the films are very important. The ECR silicon oxides need to possess good dielectric strength in order to avoid short-circuiting between gate, source/drain and substrate, low leakage current [1], good interface with silicon to ensure high mobility carriers in the silicon bulk and very good reliability for a long-lifetime flat panel display.

Radio frequency plasma enhanced chemical vapour deposition is commonly used to obtain dielectrics at 300ºC. These layers incorporate significant concentrations of hydrogen (5-20 at.%) that may cause early breakdown. In addition these layers suffer from plasma damage due to high-energy ions (100-1000 eV) [2]. Previous attempts to develop SiO_2 at lower temperatures (70ºC) have included successful studies of ECR oxidation and plasma enhanced deposition [3-6]. A systematic study of electrical properties and dependencies on deposition conditions, however, was missing.

The influences of different deposition parameters upon the electrical behaviour of MOS capacitors realised with deposited ECR oxide deposited on monocrystalline silicon are investigated. The deposition temperature does not appear to have a significant impact upon the electrical film properties. By increasing the energy transfer from the plasma toward the substrate through increasing the microwave power or lowering the pressure, the high dielectric strength and low hydrogen content of the layers were preserved even for depositions at temperatures as low of 50ºC.

The interface and bulk properties have opposite dependencies on deposition conditions, due to ion bombardment, causing difficulties in selecting the optimal parameters. Correlations between the physical properties of the films, the plasma characteristics and the electrical properties have been made in order to explain the influence of the deposition conditions on the electrical quality of the layers.

Fowler-Nordheim tunnelling was found to be dominant at low pressure and low SiH_4 flow, while a trap-related mechanism is responsible for the conduction in the more leaky oxides. Both negative and positive charge were present in the SiO_2 layer when electric stress was applied, but the electron trapping was found to have the biggest influence upon the current saturation. Constant current stress measurements confirmed that low SiH_4 flow and low pressure are ideal deposition conditions for depositing a film comparable to thermally grown oxide from the reliability point of view.

4.2. Interface properties

High frequency and quasistatic capacitance-voltage (*C-V*) measurements have been performed on 0.05 mm^2 MOS capacitors, in order to determine the SiO_2/Si interface properties. The effective charge in the oxide, which includes the fixed charge and the trapped charge was calculated from the flatband voltage as mentioned in section 2.5.1. For these calculations, it was assumed that the oxide charge is localized at the silicon/oxide interface. The thickness of the films obtained with diluted SiH_4 was around 50 nm.

The interface trap density was derived by comparing the quasistatic and high frequency curves, using the Castagne method [7] (see section 2.5.1). Figure 4.1 shows typical *C-V* curves for the ECR deposited dielectrics, revealing the high-quality interface. There is no observable hysteresis effect in the high frequency *C-V* curves, upon sweeping from accumulation back to inversion, indicating a low density of mobile ionic charges [8].

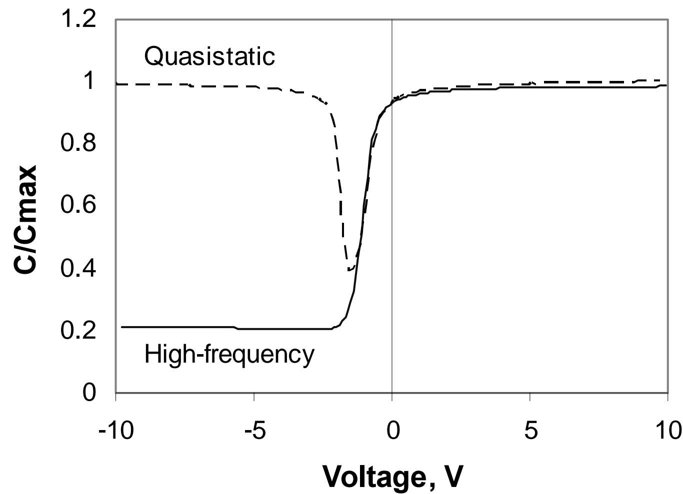

Figure 4.1. High-frequency and quasistatic *C-V* characteristics for an SiO_2 layer deposited by ECR PECVD, without substrate heating, with 5 sccm diluted SiH_4 and 20 sccm N_2O, at 400 W and 10 mTorr.

As in the case of physical properties, the influences of most of the important parameters upon the electrical properties were investigated. All wafers were subjected to post deposition anneal in a wet N_2 ambient (N_2 bubbled through DI water at room temperature) for 60 minutes, at a temperature of 500°C. The only exceptions were the layers described in sections 4.2.7 and 4.3.7, "Annealing role". Most of the *C-V* measurements were performed on MOS capacitors realised as described in section 2.5, with the exception of some measurements realised with a mercury probe. When the mercury probe is used instead of an aluminium gate, this is indicated in the figure captions.

4.2.1. SiH_4 flow role

Pure SiH_4 was used initially for deposition, but the electrical properties were poor, even with the lowest flow. Only a few results with pure SiH_4 will be presented here, due to the high leakage current and unstable *C-V* curves. Subsequently, the gas source was replaced with 2% SiH_4 diluted in helium,

and the interface trap density and the leakage current were reduced, due to a decrease in silicon dangling bonds density. Also the beneficial effects of helium in reducing the hydrogen incorporation in the layers [9-11] may have played an important role.

The flow of 2% diluted SiH_4 was varied from 5 to 15 sccm, thus the flow of pure SiH_4 in the reactor was very low, between 0.1 and 0.3 sccm. The oxide charge was not influenced by this variation in SiH_4 flow, as it can be seen in figure 4.2, despite small modifications in silicon content (section 3.4.1) and a considerable change in bulk electrical properties (see figure 4.16). The cause of positive charges in these ECR PECVD layers is attributed mainly to ion damage [12], which doesn't vary substantially with the SiH_4 flow.

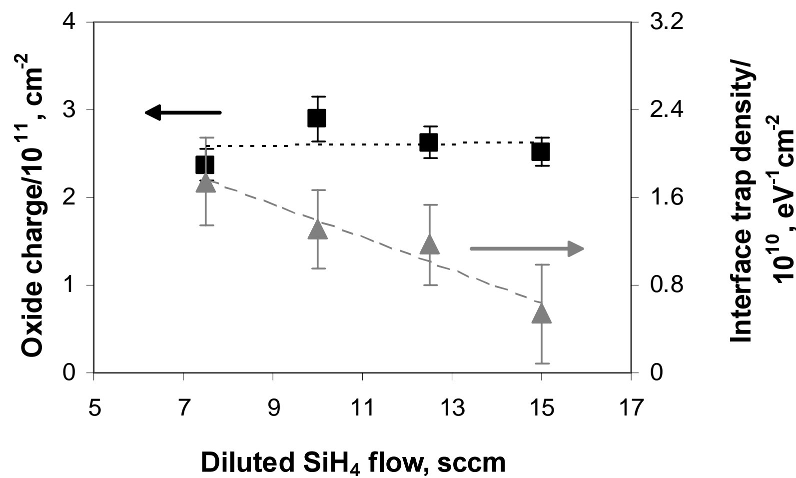

Figure 4.2. Net oxide charge and interface trap density versus diluted SiH_4 flow for films deposited without substrate heating, with 50 sccm N_2O, at 12 mTorr and 400 W.

Low interface trap densities between $6 \cdot 10^9$ and $1.7 \cdot 10^{10}$ $eV^{-1}cm^{-2}$ were obtained (figure 4.2). The slight decline with increasing the SiH_4 flow, is probably caused by higher concentration of hydrogen bonds at the interface, as it was measured by FTIR (table 3.1). It is known from several studies that hydrogen has a relaxing role upon the Si/SiO_2 interface [13].

4.2.2. Pressure role

The influence of total pressure on the interface properties is shown in figures 4.3, 4.4 and 4.5. Independent of the type of SiH_4 used (pure or diluted), of the microwave power and of the substrate temperature, the oxide charge decreases while the pressure rises from 5 to 25 mTorr. Apparently the interface is more damaged at low pressure due to higher-energy ion

bombardment. Also it is known from section 3.4.3 (figure 3.24) that the layers deposited at lower pressure contain less hydrogen, indicating that lower portion of the dangling bonds at the interface are saturated by hydrogen atoms.

The high-frequency *C-V* curves for the layers obtained with pure SiH_4 presented in figure 4.3. seem to be unstable at higher pressure, due to increased leakage, whereas for the oxides obtained at lower pressure, the *C-V* characteristics are more stable. However, a higher shift in the flatband voltage is observed for low pressures. It seems that the extra energy provided through ion-bombardment at low pressure while creating stronger chemical bonds [14] and inhibiting the leakage current, may also damage the film interface.

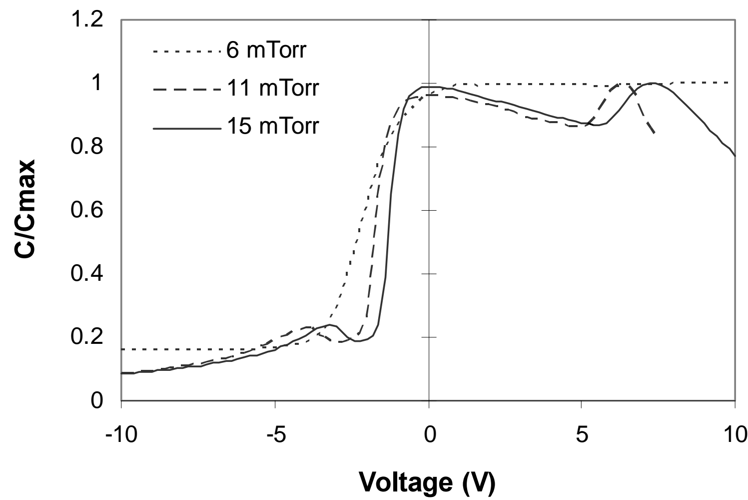

Figure 4.3. High-frequency *C-V* curves measured with the mercury probe for layers deposited at room temperature with 2 sccm pure SiH_4, 25 sccm N_2O, at 300 W and various pressures.

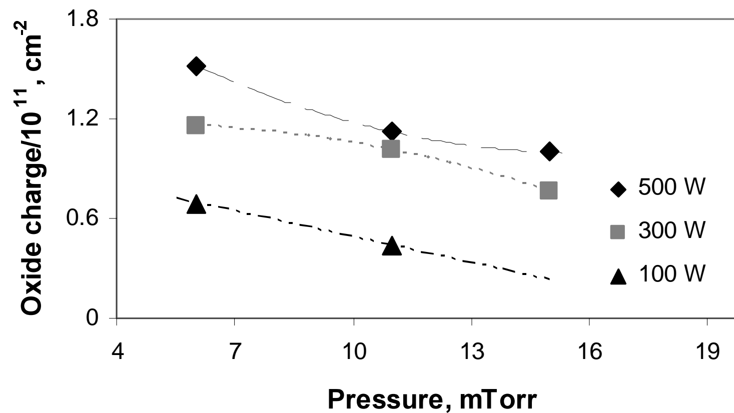

Figure 4.4. Net oxide charge versus pressure for films deposited without substrate heating, with 2 sccm pure SiH_4, 25 sccm N_2O, for various microwave powers. Measurements were done with the mercury probe.

Nevertheless, the oxide charge had low values (around $3\cdot10^{11}$ cm^{-2}) for a plasma deposited film even at low pressures (figure 4.5), for low-temperature dielectrics.

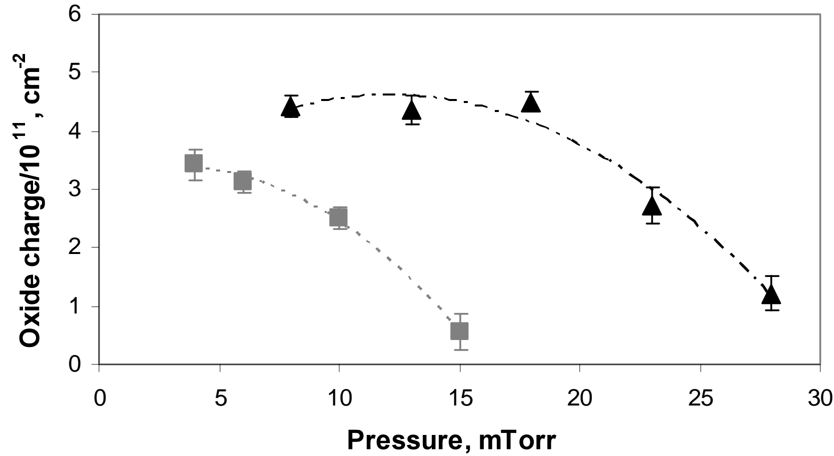

Figure 4.5. Net oxide charge versus pressure for films deposited with 5 sccm diluted SiH_4 and 20 sccm N_2O, (▲) at 500°C and 150 W, or (■) without substrate heating and 400 W.

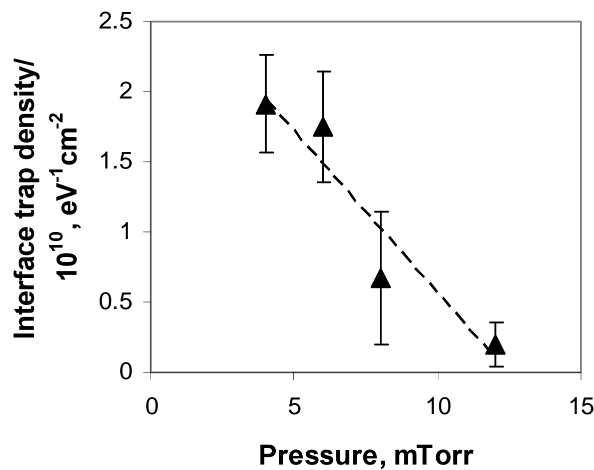

Fig. 4.6. Interface trap density versus pressure for films deposited without substrate heating, with 5 sccm diluted SiH_4 and 20 sccm N_2O, at a microwave power of 400 W.

Further analysis of the *C-V* curves revealed that the interface trap density declined with increasing pressure (figure 4.6), an effect that can be also associated with the higher density of N-H bonds measured in the infrared spectra of high pressure layers (figure 3.25).

4.2.3. Microwave power role

Figure 4.7 shows how the positive charge at the Si/SiO_2 interface, measured with a mercury probe, is modified as a function of the microwave power, for different pressures.

It is well known that at higher microwave power the plasma damage is enhanced. In addition, plasma measurements with a Langmuir probe in an ECR plasma reactor have proven that ion energy and density are increased with absorbing more power from the microwave source, intensifying the ion-bombardment upon the film surface [15]. Therefore, the oxide charge is increased at higher microwave power, as it can be seen in figure 4.7.

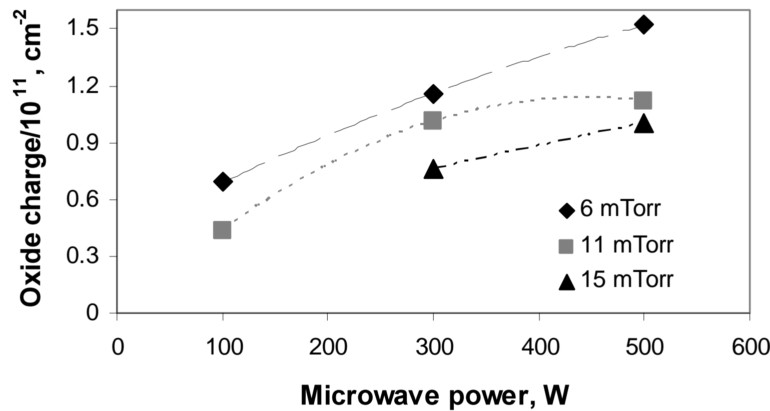

Figure 4.7. Net oxide charge versus microwave power for ECR films deposited without substrate heating, with 2 sccm pure SiH_4, 25 sccm N_2O, for various pressures; measurements were done with the mercury probe.

The trend of oxide charge versus microwave power was the same also for layers deposited with highly diluted SiH_4 and measured with the help of aluminium–gate capacitors (figure 4.8). It is important to notice that significant plasma damage occurs only for microwave powers closer to 500 W. In a similar manner as the net charge at the interface, the interface trap density is also affected by the intensified ion-bombardment at high microwave powers of 500 W, reaching values up to almost 10^{11} $eV^{-1}cm^{-2}$ (figure 4.8).

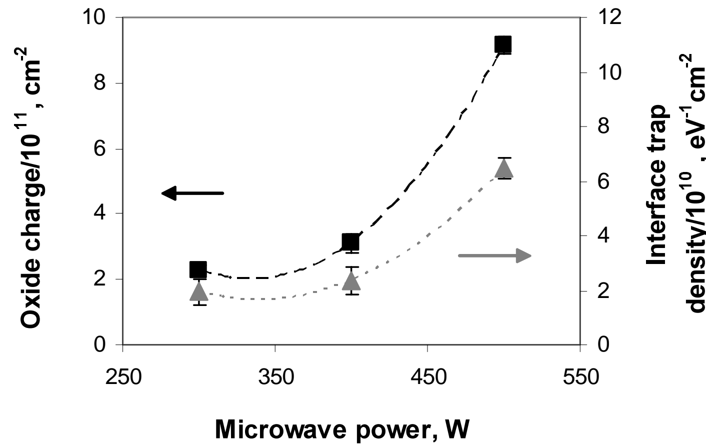

Figure 4.8. Net oxide charge and interface trap density versus microwave power for ECR films deposited without substrate heating, with 5 sccm diluted SiH_4, 20 sccm N_2O and 6 mTorr.

4.2.4. *N_2O flow role*

In figure 4.9 the influence of N_2O flow rate upon the interface is presented. As it can be seen, the oxide charge decreases with N_2O flow increasing from 3 sccm to 75 sccm, indicating that the interface is better for higher N_2O flows. An explanation may be given by the density and composition changes. It has been shown in sections 3.3.4 and 3.4.4 that high N_2O flow diminishes the film refractive index and density, due to lower energy transfer from the plasma toward the film. In conclusion, for less hydrogen desorption and lower ion bombardment, the layers exhibit smaller flatband voltage shifts and less positive charge at the interface.

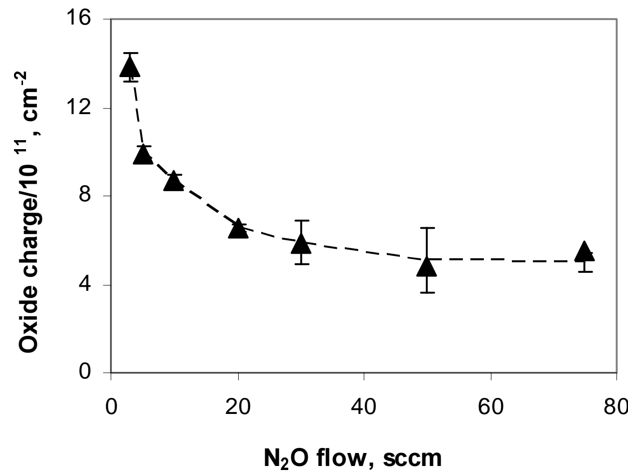

Figure 4.9. Net oxide charge versus N_2O flow rate for ECR films deposited at 500°C, with 5 sccm diluted SiH_4, 20 sccm N_2O and 6 mTorr; measured with mercury probe.

4.2.5. Temperature role

Surprisingly, more positive charge ($4.5\cdot10^{11}$ cm^{-2}) was measured at the interface of the dielectrics deposited at 500ºC (figure 4.5), compared with the ones obtained at floating temperature ($3\cdot10^{11}$ cm^{-2}), in contradiction with other works [13]. This can be explained based on the fact that usually layers obtained at near-room temperature contain a lot of hydrogen. The hydrogen content measured by FTIR had similar values for the two cases presented in figure 4.5, probably due to the fact that the differences in hydrogen content for layers obtained at low pressure are too small to be observed in the infrared spectra.

For the layers deposited at 500ºC, the decline of positive charge occurs at higher pressures than in the case of near-room temperature dielectrics. This can be attributed to the better desorption of hydrogen in the case of substrate temperature higher than 500ºC even for high pressures, while the hydrogen content increases considerably with pressure for room temperature layers (figure 3.25).

4.2.6. Thickness role

In figure 4.10 the film thickness and the oxide charge versus the distance from the edge of the wafer was plotted. It can be observed that the positive charge depends on the position of the MOS capacitor on the silicon wafer. There are two possible causes for the variation in positive charge throughout the wafer, the stress due to different film thickness and the different plasma damage. In order to make a distinction between these two causes, films with different thickness were deposited in the same conditions and the charge at the interface was measured and plotted in figure 4.11.

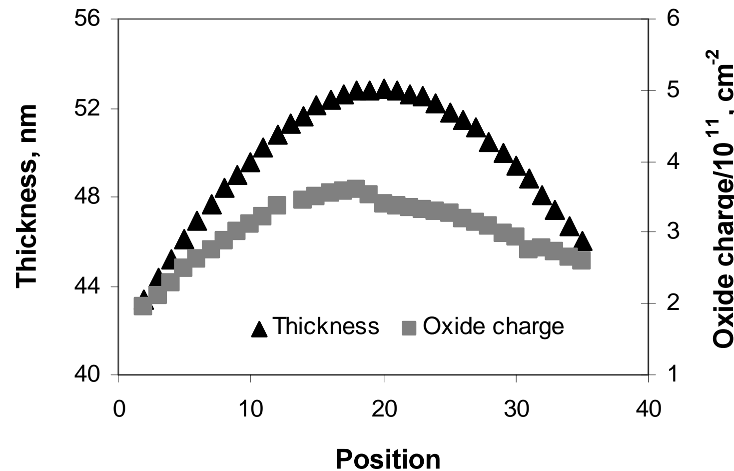

Figure 4.10. Net oxide charge and film thickness versus position on wafer for an ECR film deposited with 5 sccm diluted SiH_4, 20 sccm N_2O, at 10 mTorr and 400 W.

As one can see in figure 4.11, the charge increases slightly from $3.5 \cdot 10^{11}$ to $4.5 \cdot 10^{11}$ ions/cm^2, while the thickness triples from 30 to 90 nm. This modification in oxide charge is too small to explain how over the wafer surface (figure 4.10) the charge doubles, when the thickness increases only by 8 nm. Furthermore, the modification perceived in figure 4.11 is brought not only by the change of oxide thickness, but in addition there is more plasma damage in the thicker films due to a longer exposure to the plasma. Nevertheless, the combined effect of these two factors is much smaller than the change in oxide charge observed over the wafer surface in figure 4.10.

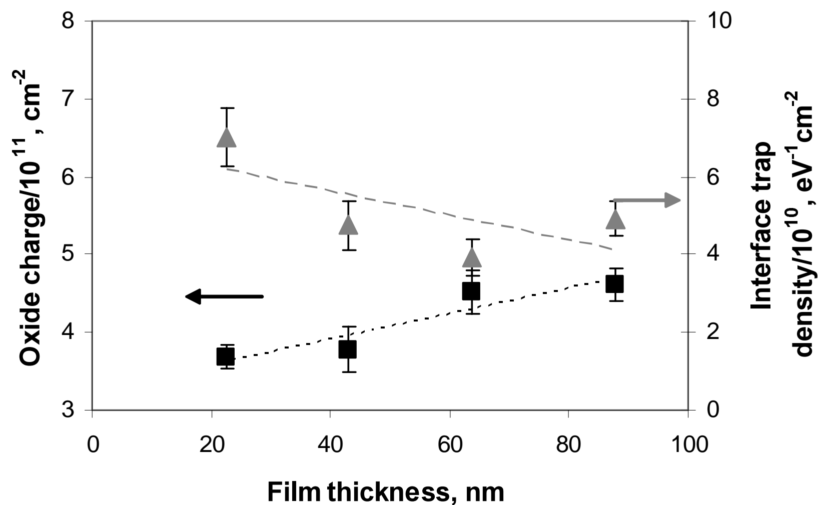

Figure 4.11. Net oxide charge and interface trap density versus average film thickness for ECR films deposited with 5 sccm diluted SiH_4, 20 sccm N_2O, at 6 mTorr and 400 W.

Therefore, we can conclude that the differences in oxide charge at different positions on the wafer (figure 4.10) are produced by non-

uniformities in plasma distribution. It is well known from measurements performed in the ECR reactor [16] that ions diffuse toward the substrate, mainly in the centre of the plasma dome, bombarding thus the centre of the wafer more than the edge. Thus, the increased charge in the middle of the wafer is caused by a higher concentration of energetic ions. Scanning the wafer under the microwave plasma can be a solution for improving the film uniformity.

The interface trap density was not significantly influenced by the film thickness, except for the thinner layer which possessed a larger interface trap density.

4.2.7. Annealing role

All the aluminium-gate MOS capacitors described above were annealed at 500°C after deposition (see section 2.5). The post-deposition annealing (PDA) effect was not crucial however for the interface. In figure 4.12, the *C-V* curves of two SiO_2 layers deposited at room temperature, one without PDA and the other with PDA are superposed. The modification in interface trap density was not significant and the flatband voltage shifted with less than 0.5 V, thus we can deduce that the ECR SiO_2 is not a porous film, and the wet annealing performed at 500°C is not essential for the film's electrical behaviour. Apparently, it would be possible to deposit high-quality silicon oxide on the cheap, flexible plastic substrates. Both layers were subjected to a post metallization annealing (section 2.5) that can be replaced by a treatment in hydrogen plasma.

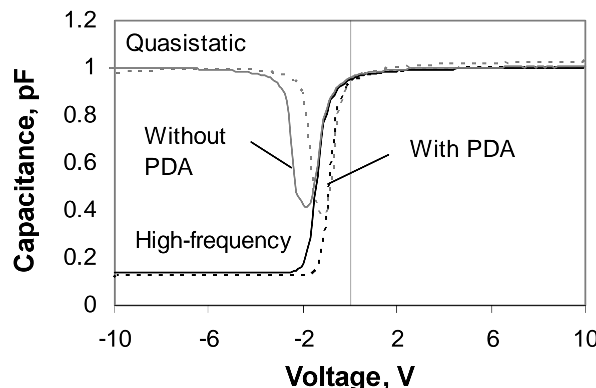

Figure 4.12. *C-V* characteristics before and after post deposition annealing of an ECR layer obtained at room temperature with 5 sccm diluted SiH_4, 20 sccm N_2O, at the pressure of 6 mTorr and microwave power of 400 W. Both layers suffered an aluminium sintering step of 5 minutes at 400°C.

4.2.7. Comparison between various dielectrics

The *C-V* characteristics of our near-room temperature SiO_2 with the rf-PECVD layer obtained at 300°C were compared. Both capacitors received a post-metallization annealing described in section 2.5. As it can be seen in figure 4.13, the quality of the interface between the ECR SiO_2 and silicon is much better. From the shape of the *C-V* curve we can notice that the ECR oxide exhibits less traps and a much less positive oxide charge.

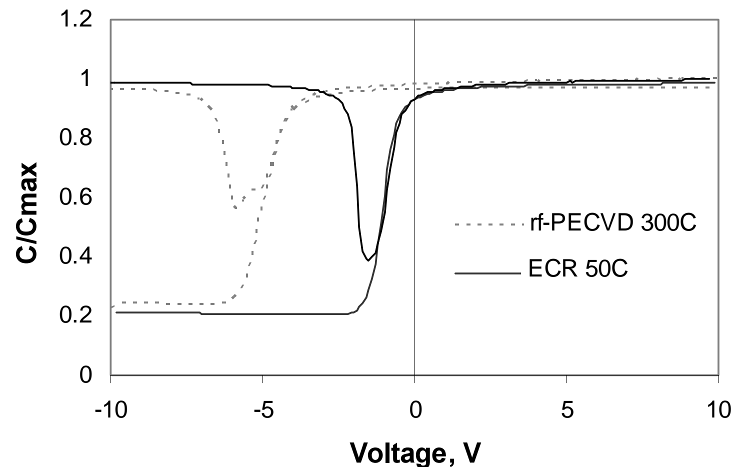

Figure 4.13. *C-V* characteristics of an ECR layer obtained at near-room temperature and a standard rf-PECVD layer of 60 nm obtained at 300°C.

In order to confirm furthermore the high quality of our layers, a comparison was drawn between several dielectrics obtained at various temperatures and by various deposition methods. The MOS capacitors were fabricated and measured at DIMES Research Institute, TU-Delft, Netherlands [17]. The ECR SiO_2 layer was deposited with our system. The devices were not subjected to any annealing process. The interface trap density, the fixed oxide charge and the mobile charge were extracted from the *C-V* curves by the researchers from DIMES and presented in table 4.1 for the three different oxide layers. It can be observed that the ECR layer is better than the LPCVD oxide obtained at a much higher temperature. The thermally grown oxide exhibits the best interface, which is expected, considering it is not deposited, but grown at a very high temperature.

This comparison has shown that ECR PECVD is a suitable method for obtaining layers at room temperature with good interface with silicon.

Table 4.1. The interface trap density (D_{it}), fixed oxide charge (N_{fix}), mobile charge (N_m) and thickness for a low pressure chemical vapor deposition (LPCVD) layer obtained at 600°C, an ECR layer obtained at room temperature and a thermally grown oxide.

SiO_2	Thickness (nm)	D_{it} (10^{10} $cm^{-2}eV^{-1}$)	N_{fix} (10^{10} cm^{-2})	N_m (10^9 cm^{-2})
LPCVD (600°C)	168.2	20	47	6.4
ECR (50°C)	53.7	9	5.3	1.6
Thermal (1100°C)	25	3.2	1.8	0

4.3. Dielectric strength

The high electrical quality of the ECR films was revealed also by comparing the current density - electric field (*J-E*) characteristics of a low-pressure ECR deposited SiO_2 film and a thermally grown oxide film (figure 4.14). One can observe the similarity of these curves. Moreover, the currents that pass through an rf-PECVD SiO_2 layer obtained at 300°C and an LPCVD SiO_2 layer prepared at 600°C where also compared to the room temperature ECR PECVD oxide current in figure 4.15. The superiority of the low-temperature dielectric in terms of leakage current and critical field is evident.

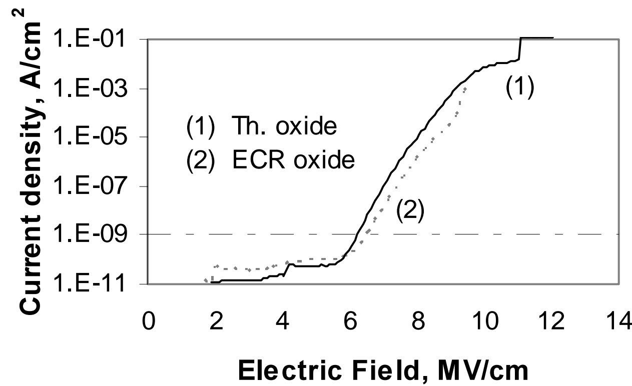

Figure 4.14. Current density versus electric field for a 25 nm thermal SiO_2 (1) and a 50 nm ECR oxide (2) deposited at near room temperature, with 5 sccm diluted SiH_4, 20 sccm N_2O, at 4 mTorr and 400 W.

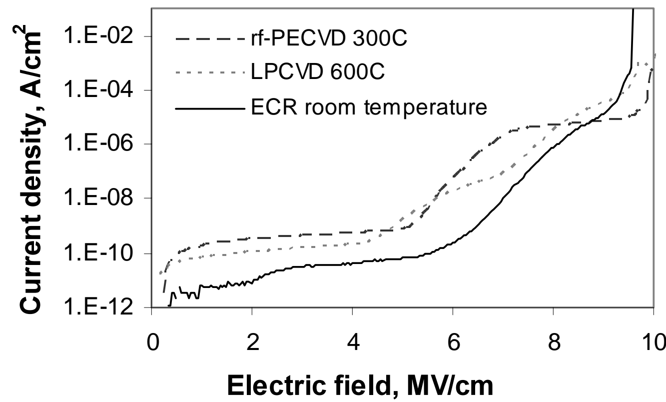

Figure 4.15. Current density - electric field characteristics of (1) rf-PECVD SiO_2 layer obtained at 300°C, (2) LPCVD SiO_2 layer prepared at 600°C and (3) ECR oxide deposited at room temperature, with 5 sccm diluted SiH_4, 20 sccm N_2O, at 4 mTorr and 400 W. All films have 50 nm thickness.

From such *J-E* curves, the critical electric field and the resistivity were calculated as indicated in section 2.5.2. Several parameters that influence the dielectric strength were investigated, in order to reach the optimal deposition conditions for layers with both good interface and bulk properties.

4.3.1. SiH_4 flow role

The influence of SiH_4 flow on the bulk electrical properties is shown in figure 4.16. Both critical field and resistivity decrease with increasing the SiH_4 flow. A possible cause is the higher silicon content in the film, which was measured by ERD and presented in section 3.4.1. Furthermore, the presence of silicon dangling bonds was confirmed by the lower frequency of the Si-O stretching mode (section 3.4.1), and higher refractive index (section 3.3.1). Excess silicon is known to have deleterious consequences such as increased trap concentration, high leakage current and low dielectric strength [18].

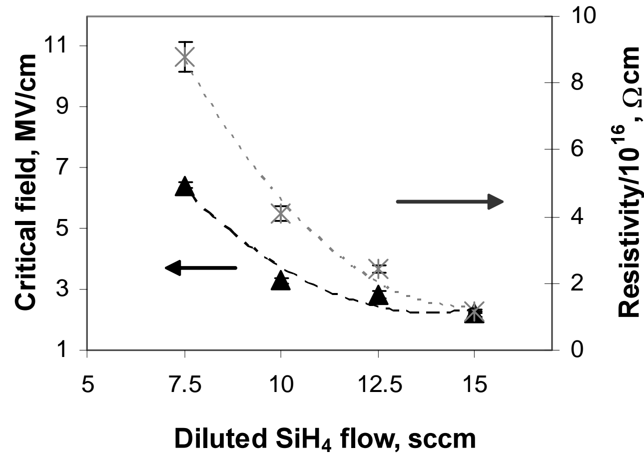

Figure 4.16. Critical field and resistivity versus diluted SiH_4 flow for films deposited without substrate heating, with 50 sccm N_2O, at 12 mTorr and 400 W.

4.3.2. Pressure role

From the critical field versus pressure plot presented in figure 4.17, we notice a deterioration of electrical properties at higher pressures, which can be attributed to the different surface ion-bombardment. It seems that at elevated pressures, the energy provided by the particles is not sufficient to densify the layer and eliminate hydrogen from the film bulk [19]. This is in agreement with the lower value of the refractive index (section 3.3.2) and the higher hydrogen content obtained at high pressures (section 3.4.3). It is well known that porous layers have lower breakdown field and higher leakage current, explaining thus the inferiority of high-pressure SiO_2 layers.

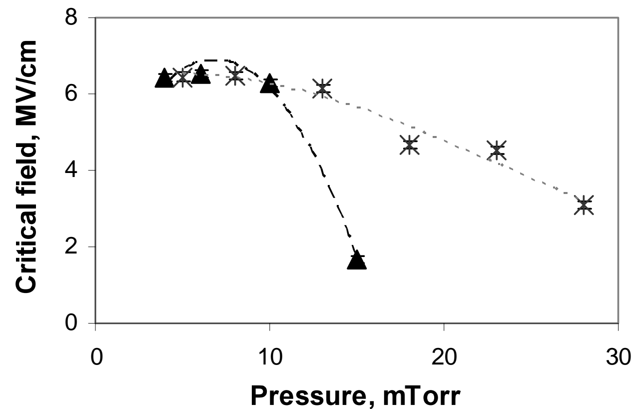

Figure 4.17. Critical field versus pressure for films deposited with 5 sccm diluted SiH_4 and 20 sccm N_2O, (✳) at 500°C and 150 W, or (▲) without substrate heating and 400 W.

The resistivity of the layers follows the same trend as the critical field, confirming the beneficial effect that low pressure has upon the ECR layers (figure 4.18).

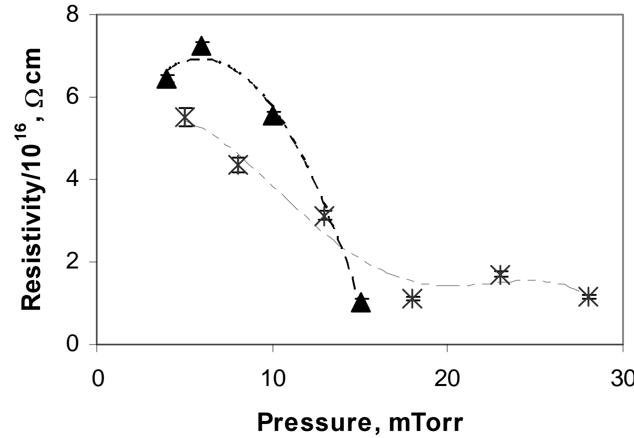

Figure 4.18. Film resistivity versus pressure for films deposited with 5 sccm diluted SiH_4 and 20 sccm N_2O (✳) at 500°C and 150 W or (▲) without substrate heating and 400 W.

4.3.3. Microwave power role

The critical field and film resistivity are improved by increasing the microwave power (figure 4.19). More energy is absorbed from the microwave source by the plasma at higher microwave powers, thus the film deposited will be denser, have stronger chemical bonds and lower hydrogen content. The hydrogen bonds are destroyed when the layers are subjected to electric stress, increasing the leakage current and lowering the critical field. The presence of more hydrogen in layers deposited at low microwave power was confirmed by the low values of refractive index and composition measurements (sections 3.3.3 and 3.4.2). Because the layers obtained at microwave powers of 400 W and 500 W are quite similar from the dielectric strength point of view, we can assume that 400 W is sufficient for obtaining a film with good bulk properties, avoiding the interface damage obtained at higher microwave powers (figure 4.8).

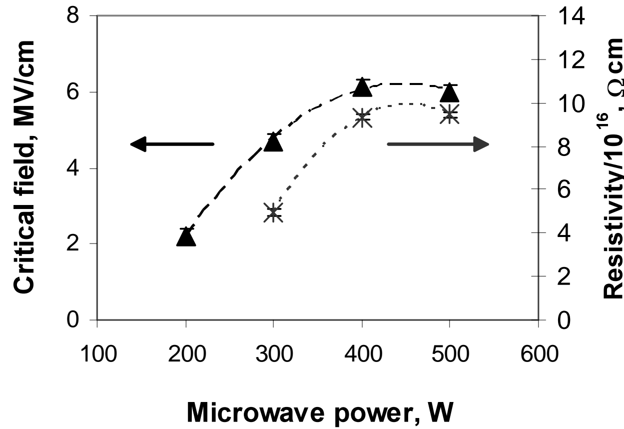

Figure 4.19. Critical field and resistivity versus microwave power for films deposited without substrate heating, with 5 sccm diluted SiH_4, 20 sccm N_2O and 6 mTorr.

4.3.4. N_2O flow role

The critical electric field film resistivity gradually decreases with increasing N_2O flow as it can be observed in figure 4.20. Because silicon and oxygen contents in the bulk of the films are not dependent on N_2O flow within the accuracy of Auger measurements, we have to attribute the changes of the dielectric strength to other matters.

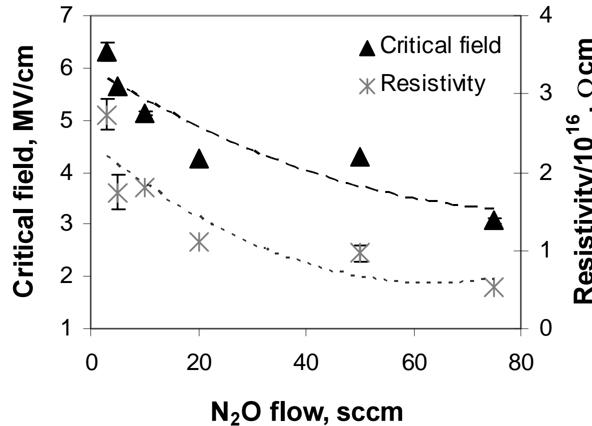

Figure 4.20. Critical field and resistivity versus N_2O flow rate for ECR films deposited at 500°C, with 5 sccm diluted SiH_4, 20 sccm N_2O and 6 mTorr.

The refractive index decreased with increasing the N_2O flow and the infrared measurements indicated a lower concentration of Si-O bonds, thus it can be assumed that film lower density is responsible for the deterioration of the bulk properties at high N_2O/SiH_4 ratios. The main cause for the film porosity is the lower energy transfer from the plasma at high flows due to a decreased concentration of ions at high flow (see section 3.3.4).

4.3.5. Temperature role

For the films deposited at various temperatures, the electrical properties were similar at low pressures (figure 4.17). However, they deteriorate much faster at near-room temperature with increasing the pressure. This occurs, probably because the room-temperature film properties are more influenced by the energy of the particles which arrive at the substrate, due to the lack of external heating. The resulting near-room-temperature layers obtained at low pressure and with higher microwave power, possess good electrical strength, proving that ECR PECVD is a good choice for low-temperature SiO_2 deposition.

4.3.6. Thickness role

The critical field and the film resistivity do not vary with the film thickness for films between 25 to 95 nm, as it can be seen in figure 4.21. Also the critical field is not influenced by the position of the measured capacitor on the wafer, except for the edge of the wafer, where due to increased contamination, the electric properties are degraded. Apparently the long exposure time to plasma damage does not deteriorate the film dielectric strength, as it does the film interface (section 4.2.6). On the contrary, it has been shown that high-energy bombardment at low pressure and high microwave power reduces the leakage current.

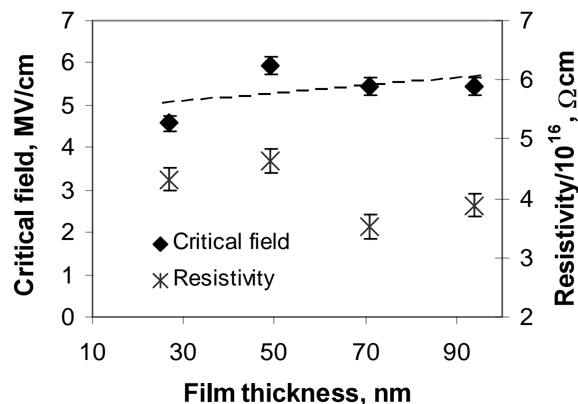

Figure 4.21. Critical field and resistivity versus average film thickness for ECR films deposited with 5 sccm diluted SiH_4, 20 sccm N_2O and 6 mTorr.

4.3.7. Annealing role

Neither the post-metal-annealing (PMA) nor the post-deposition-annealing (PDA) (section 2.5) have any effect upon the *J-E* curves of superior dielectrics, as it can be observed in figure 4.22. The shape of *J-E* curves is modified after PMA for the inferior dielectrics, due to trap charging phenomena, but the values of critical field and breakdown field are comparable.

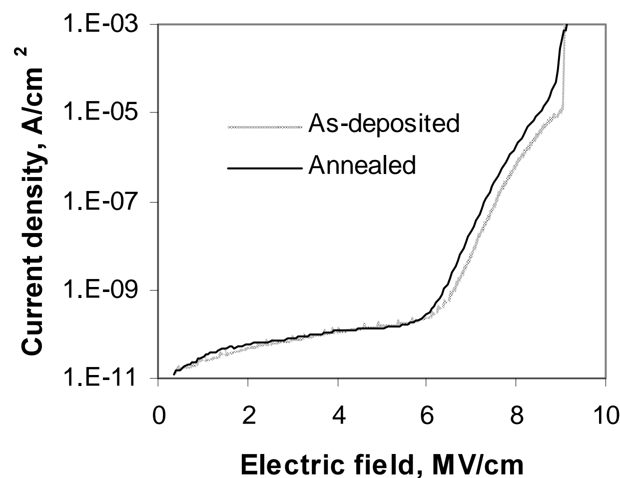

Figure 4.22. J-E curves of a high-quality ECR SiO_2 layer before and after post-metal-annealing at 400°C for 5 minutes, without any post-deposition anneal step.

4.4. Conduction mechanism

Because the critical field and film resistivity do not always give sufficient information about the bulk electrical properties, the conduction mechanism of the dielectric was investigated by studying the temperature dependence of *I-V* characteristics, first for superior layers with low leakage current and then for leaky dielectrics obtained at high pressure and high SiH_4 flow.

Figure 4.24 shows that *J-E* characteristics of the ECR SiO_2 layers are similar with that of thermally grown oxide presented in figure 4.14. However, it can be observed in figure 4.23 and figure 4.24 that only if the deposition pressure and SiH_4 flow are lower than 12 mTorr and 8 sccm respectively, the ECR layers possess low leakage current. It is also noticeable that for higher deposition pressures and flows the *J-E* curves have a different shape and the leakage current increases substantially, despite the constant breakdown field. This effect was explained based on composition departure from the stoichiometric SiO_2 due to hydrogen contamination in case of high pressure and silicon excess in case of high SiH_4 flow rate (sections 4.3.1 and 4.3.2) [20].

Because all the inferior dielectrics exhibited *J-E* curves with similar shape, but different slopes and magnitude, an investigation of the mechanisms of electrical transport in the layers was performed.

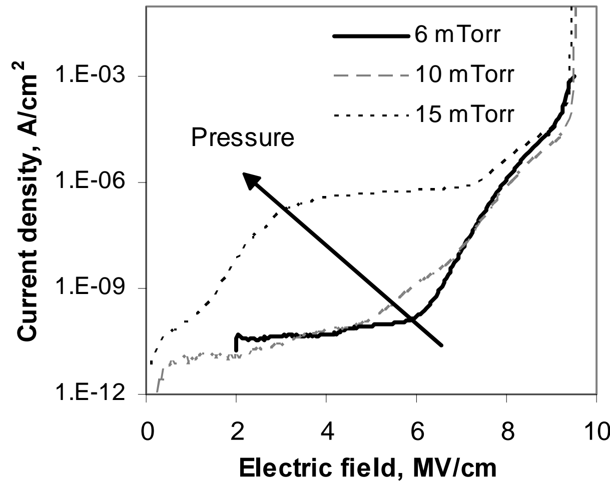

Figure 4.23. Current density versus electric field for films deposited at near room temperature, with 20 sccm N_2O and 5 sccm diluted SiH_4, at 400 W and various pressures.

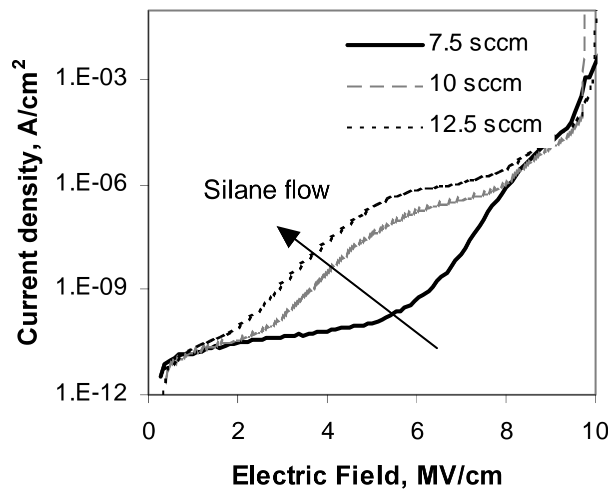

Figure 4.24. Current density versus electric field for films deposited at near room temperature, with 20 sccm N_2O, at 400 W, 12 mTorr and various SiH_4 flows.

4.4.1. Superior oxides conduction mechanism

First, the dependency of *J-E* curves on temperature was studied (fig. 4.25) for the high-quality sample formed at the lowest pressure (4 mTorr). The layer is characterised by low leakage current, high resistivity and high critical field.

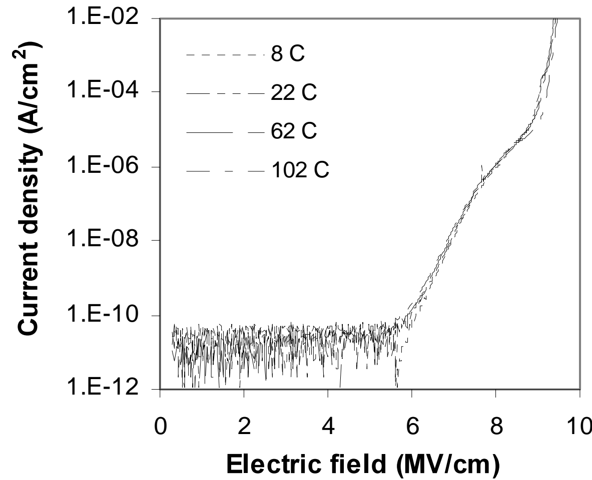

Figure 4.25. Current density versus electric field for a film deposited at near room temperature with 5 sccm diluted SiH_4 and 20 sccm N_2O, at 400 W and 4 mTorr, measured at several temperatures.

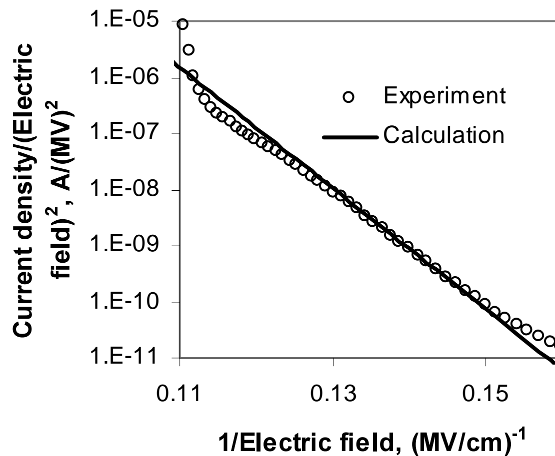

Figure 4.26. Fowler-Nordheim plot for a film deposited at near room temperature with 5 sccm diluted SiH_4 and 20 sccm N_2O, at 400 W and 4 mTorr.

It is noticeable that the current measured at electric fields higher than 6 MV/cm was practically independent of the chuck temperature. This indicates that the electrons are transported through the oxide layer by Fowler-Nordheim tunnelling (section 2.5.2). In order to confirm this hypothesis, the Fowler-Nordheim plot (ln (J/E^2) against E^{-1}) is shown in figure 4.26. The experimental data can be fitted with a straight line and from the slope, the energy barrier was extracted: $\phi = 3.11$ V. Similar values were obtained for the barrier height in thermally grown oxide [21]. From these results it can be concluded that the dominant conduction mechanism in the high-quality layers obtained at low pressure and low SiH_4 flow is Fowler-Nordheim tunnelling.

4.4.2. Non-stoichiometric oxides conduction mechanism

Next, the behaviour of an oxide deposited at near room temperature with a higher SiH_4 flow, and showing a higher leakage current was studied at different temperatures (figure 4.27) in order to determine the main conduction mechanism.

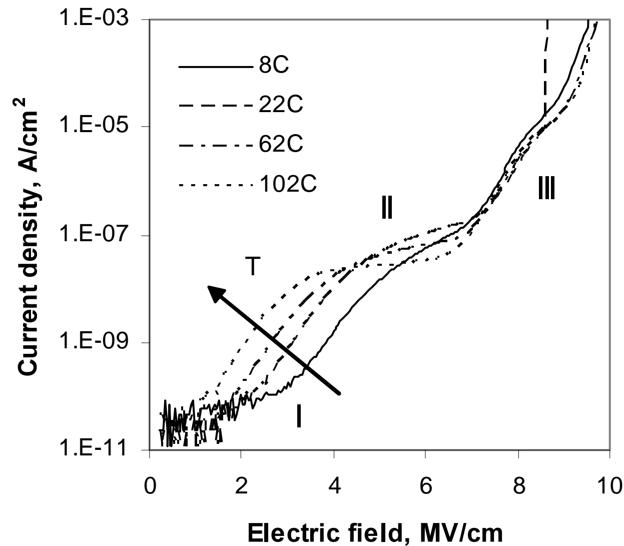

Figure 4.27. Current density versus electric field for a film deposited at near room temperature, with 12.5 sccm diluted SiH_4 and 20 sccm N_2O, at 400 W and 12 mTorr, measured at several temperatures.

Three different regions can be distinguished in the plot. In region I, at low biases the current depends highly on temperature, while in region III, at electric fields higher than 7 MV/cm, no dependency on temperature can be detected.

In region II the current increases very slowly with the applied voltage. This "quasi-saturation" of the current may be caused by charge trapping in the dielectric. As a result, an internal electric field, opposed to the external electric field is produced and the carrier flow is suppressed [22, 23].

To verify the trap-charging hypothesis, the *J-E* was measured twice without delay until 8.5 MV/cm (figure 4.28).

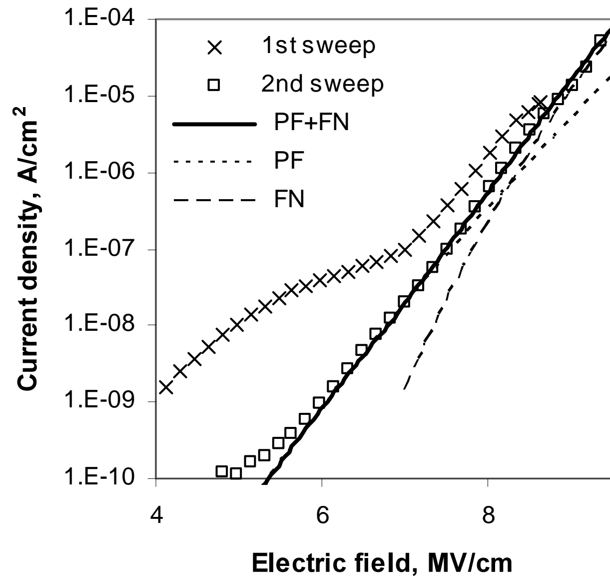

Figure 4.28. Two consecutive measurements of current density versus electric field for the same capacitor made with a film deposited at near room temperature, with 10 sccm diluted SiH_4 and 20 sccm N_2O, at 400 W and 12 mTorr; theoretical Poole-Frenkel (PF), Fowler-Nordheim (FN) currents and the sum of PF and FN currents.

The electric field is reduced due to charge trapping during the first sweep and consequently the current is lower for the second sweep in region I and II. Because the silicon wafer is n-doped and positive gate voltage is applied, it is assumed that substrate injection of electrons is mainly responsible for the conduction process [24]. Consequently, the charge stored in the oxide is also negative and impedes the subsequent electron movement from the silicon toward the gate. It cannot be excluded that trapped holes or fixed positive charge can also exist in the oxide provided that its density is lower than that of the negative charge.

In region I, until saturation occurs, the current for the first and second measurement can both be fitted with a straight line if represented in the Poole-Frenkel plot, therefore the main conduction mechanism in these layers at low biases is most probably the Poole-Frenkel effect, whose expression is written in section 2.5.2. Since the Poole-Frenkel effect is the thermal emission of charge carriers from traps [25], the high dependence of current on temperature in region I is hence explained. Also it is known that the probability of Poole-Frenkel emission is increased when a high density of shallow traps exists in the bandgap, which was confirmed by the remeasurement of the J-E characteristics.

Because the first measurement is transient, the conduction mechanism for the second sweep was determined. As it can be seen in figure 4.28, the shoulder in region II disappears in the second J-E measurement, thus regions I and II become one region, where the current is still dependent on

temperature (figure 4.29). In region III, no significant modification appears between the first and the second J-E curve, and temperature has no significant effect upon the current even for the second measurement (figure 4.29). Due to this dual temperature dependence, the current measured in the second sweep was written as a sum of Poole-Frenkel current (dominant at low voltages) and Fowler-Nordheim tunnelling current (dominating at high biases).

$$J = J_{Poole-Frenkel} + J_{Fowler-Nordheim} \tag{4.1}$$

As shown in fig. 4.28, the theoretical expression fits very well the measured current. In order to verify this model, the second sweep current was measured for four different temperatures: 8°C, 22°C, 62°C and 102°C and compared them with the current calculated with expression 4.1 for these temperatures. Figure 4.29 shows a good fit for all the temperatures for a trap energy (ϕ_T) of 0.87 eV and a barrier height (ϕ) of 3.0 eV.

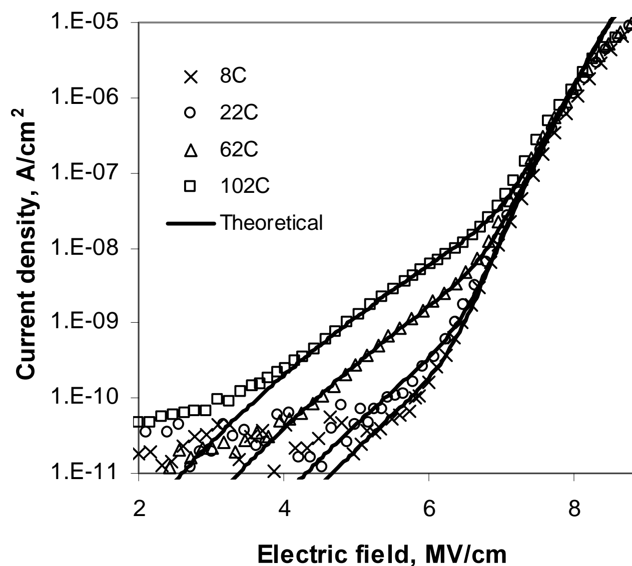

Figure 4.29. Current density versus electric field for a film deposited at near room temperature, with 7.5 sccm diluted SiH_4 and 20 sccm N_2O, at 400 W and 12 mTorr measured at 8°C, 22°C, 62°C and 102°C; theoretical current as a sum of Poole-Frenkel current and Fowler-Nordheim current, ϕ_T = 0.87 eV, ϕ = 3.0 eV.

The same conduction processes were found in all the films deposited at high pressure and high SiH_4 flow. Moreover, the leakage current and the electric field shift increased with both SiH_4 flow and pressure (figures 4.23 and 4.24), indicating an increase in trap density [26]. In the case of high SiH_4 flow, it is believed that the traps are a result of silicon dangling bonds of oxides deposited at high SiH_4 flow [27]. For high deposition pressure, the

efficiency of energy transfer from the plasma toward the depositing film is lower [28]. Consequently, there is less energy necessary for particles to migrate on the film surface, for hydrogen desorption and for creation of strong chemical bonds [29]. Therefore, the density of weak bonds, especially hydrogen bonds increases, as measured in the infrared spectra (section 3.4.3) and more traps participate in the low-field conduction process.

For either high total pressure or high SiH_4 flow, an increase in SiH_4 partial pressure occurs, and consequently the deposition rate is increased. The higher the growth rate, the smaller the probability of forming strong chemical bonds and of hydrogen desorption, therefore inferior dielectrics are produced.

In summary, it has been observed that ECR plasma enhanced deposition at pressures lower than 10 mTorr can provide SiO_2 layers with a Fowler-Nordheim tunnelling conduction mechanism, just like in the case of thermally grown oxide. With increasing either the pressure, or the SiH_4 flow, the conduction mechanism in the layer is modified, becoming Poole-Frenkel emission for low electric fields.

4.5. Charge trapping during electrical stress

For a better understanding of trapping phenomena at the Si/SiO_2 interface, electric fields of 5, 6, 7 and 8 MV/cm were applied to MOS capacitors of 0.1 mm^2 in the condition of substrate accumulation. The bias was applied for three periods of time of 36, 54 and 72 seconds. *C-V* measurements were performed after each stress period. Figure 4.30 shows the *C-V* curves before and after stressing the oxide with 6 and 8 MV/cm for 36 seconds.

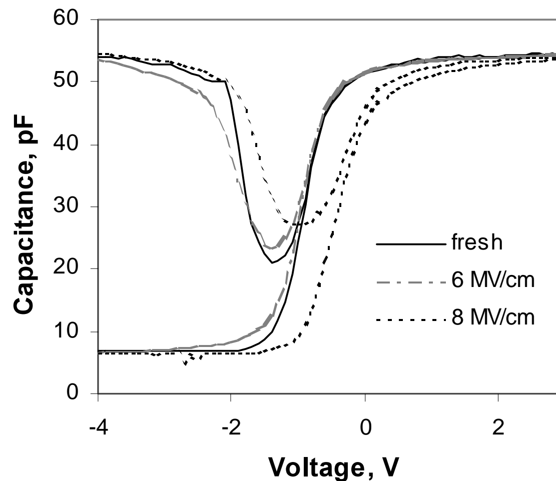

Figure 4.30. *C-V* curves for a film deposited with 7.5 sccm diluted SiH_4 and 20 sccm N_2O, at 400 W and 12 mTorr, before and after stressing with various biases for 36 s.

In figure 4.30, a small shift of the *C-V* curve toward negative voltages is observed for the low electric field stress (6 MV/cm), indicating an increase in positive charge. The curve shifts towards positive voltages for high fields of 8 MV/cm due to a raise in negative charge. The same effect was registered for all layers, dense or porous, only the magnitude of the shift in the flatband voltage varied on deposition parameters, as it can be observed in figure 4.31, where the trapped charge, extracted from the flatband voltage, is presented for various deposition conditions. The positive bias of 8 MV/cm can be identified as the onset of electron trap generation at the interface.

The differences in net oxide charge were presented also versus the stress time in figure 4.32 for layers obtained with various SiH_4 flows. The positive charge density created by applying an electric field of 6 MV/cm is much smaller than the negative charge trapped during an 8 MV/cm electrical stress.

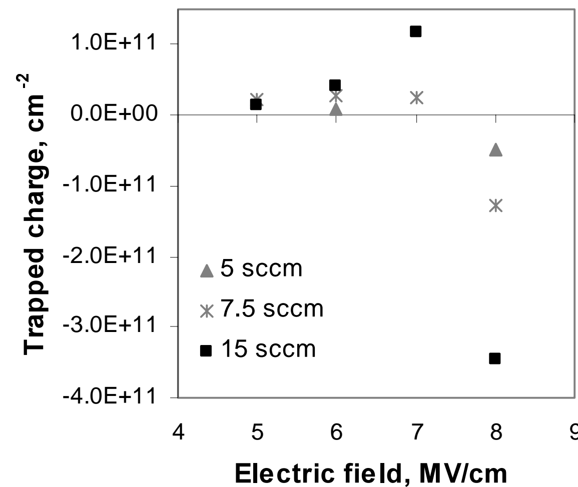

Figure 4.31. Variation in trapped charge versus electric field stress (during 36 s) for the films deposited with 20 sccm N_2O, at 400 W, 12 mTorr and various diluted SiH_4 flows (5, 7.5 and 15 sccm).

With increasing the SiH_4 flow, from both figure 4.31 and figure 4.32, it can be observed that the charge trapped during stress increases, which is an indication that the layers deposited at higher SiH_4 flow possess more dangling or weak bonds. A similar behaviour was observed for layers obtained at higher pressure.

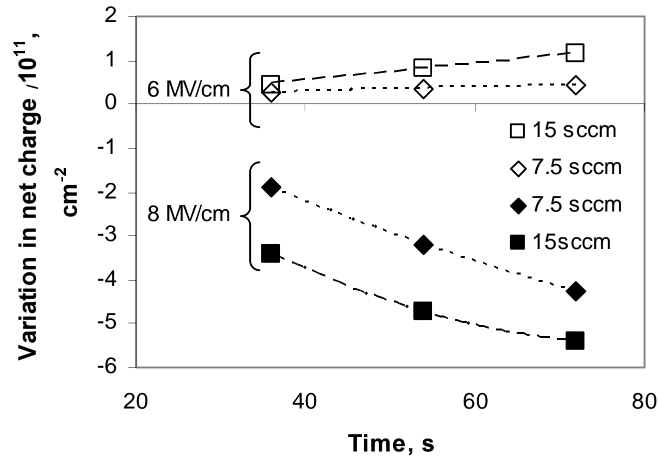

Figure 4.32. Variation in oxide charge versus stress time for two films deposited with 20 sccm N_2O, at 400 W, 12 mTorr, near room temperature and various SiH_4 flows (7.5 sccm and 15 sccm).

The sign of the trapping charge ("+" for low biases and "-" for high biases) could not be correlated with the conduction mechanism; all oxides began to trap electrons at the interface at 8 MV/cm. However, for poorer dielectrics the charge value and the ratio between the charge and the interface trap density (table 4.2) were higher. The oxide obtained at 4 mTorr and 5 sccm SiH_4 exhibited only $7 \cdot 10^9$ cm^{-2} positive charge trapped during the 36 seconds stress of 6 MV/cm, and $4 \cdot 10^{10}$ cm^{-2} electrons in case of an electric field of 8 MV/cm.

The changes in flatband voltage cannot be explained in terms of mobile ion drift, because the mobile ion density, measured by bias temperature stress (BTS) has very low values (~10^9 cm^{-2}), thus the oxide can be considered free of mobile ions.

Experiments performed with thermally grown oxide by DiMaria [30] have shown the same trend of capturing holes for low injected charge and trapping electrons at the interface for high injected charge. However, in the case of the referred experiment, the applied fields were higher than 8 MV/cm and the current increased during electrical stress, not decreased like in the ECR films (figure 4.32.). The phenomenon was explained by DiMaria in terms of trapped holes, which were created by hot electrons that arrive at the aluminium gate by Fowler-Nordheim tunnelling. However for superior ECR oxides, the Fowler-Nordheim tunnelling is quite small at 5-6 MV/cm.

The shoulder in the J-E curves presented in the previous section indicated that electrons are trapped in the dielectric bulk even at low electric fields of 5 MV/cm for the inferior oxides. Furthermore, the *I-t* curves measured during stressing for superior and inferior oxides and presented in figure 4.33 and 4.34 respectively, indicate also that negative charge is trapped in the oxide,

decreasing the total current. Nevertheless, the charge present at the interface calculated from *C-V* characteristics is positive for low biases and negative only for high biases of 8 MV/cm. Other experiments with plasma deposited SiO_2 layers [31, 32] have shown the same trapping characteristics during electric stress, i.e. positive charge shown by the *C-V* characteristics and negative charge revealed by the current behaviour. Because the flatband voltage is sensitive only to the charge trapped close to the Si/SiO_2 interface, the electrons can be trapped at the metal/SiO_2 interface, as shown in experiments performed with non-stoichiometric layers [32, 33], and their negative charges are not reflected in the *C-V* characteristics. For low electric fields the positive charge situated at the interface exceeds the charge of electrons trapped at the interface. With increasing the electric field, more electron traps are created at the Si/SiO_2 interface and the *C-V* curves shift towards positive voltage.

By applying a negative bias to the metal gate, a larger shift in the flatband voltage than in the case of positive bias stress was observed. This phenomenon is already known in literature [35], for lower biases (2-4 MV/cm) and higher temperatures (200°C) however, from comparing the damage caused by negative bias temperature stress (NBTS) with the effects of positive bias temperature stress (PBTS). The degradation process of thermally grown SiO_2 was described by a chemical reaction proposed by Jeppsen and Svensson [35] and applied also in the case of rf-PECVD layers [9]. The reaction takes place with destruction of silicon-hydrogen bonds and removal of electrons:

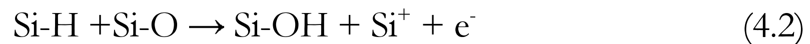

$$\text{Si-H} + \text{Si-O} \rightarrow \text{Si-OH} + \text{Si}^+ + e^- \tag{4.2}$$

This degradation process can be the source of positive charge that appears in the ECR layers at low biases. Furthermore, the destruction of Si-H bonds can explain the severe degradation in case of dielectrics obtained at high pressure and with high SiH_4 flow. The presence of high concentration of Si-H bonds in the inferior oxides, may lead to increased flux of electrons towards the metal gate, raising the value of current with the applied voltage as it can be seen in figures 4.23 and 4.24.

Furthermore, the interface trap density (D_{it}) was calculated after a stress of 6 MV/cm and the ratio between the additional oxide charge (N_{ss}) and D_{it} is presented in table 4.2 for three different periods of time. The N_{ss}/D_{it} ratios exhibit values around unity for the dense oxides and the thermally grown oxide, and ten to thirty times higher for the porous and non-stoichiometric layers deposited with high SiH_4 flow and at high pressure. This shows that there are not only differences in the magnitude of the charge measured at the interface between the layers. The mechanisms of charge creation and trap

filling are different for the leaky oxides and the superior dielectrics. Apparently at low electric fields the formation of positive charge at the interface is more significant that trap filling for the leaky oxides.

Table 4.2. The ratio between generated oxide charge and interface trap density after a positive electric stress of 6 MV/cm was applied for 36 s on the gate of MOS capacitors with oxides obtained with various SiH_4 flow and pressures.

N_{ss}/D_{it}	**36 s**	**54 s**	**72 s**
Thermal oxide	1.58	2.26	0.75
4 mTorr	0.35	0.6	0.88
10 mTorr	1.62	1.66	1.87
15 mTorr	*10.23*	*10.87*	*9.06*
7.5 sccm	0.57	1.12	1.03
15 sccm	*29.09*	*28.48*	*20.31*

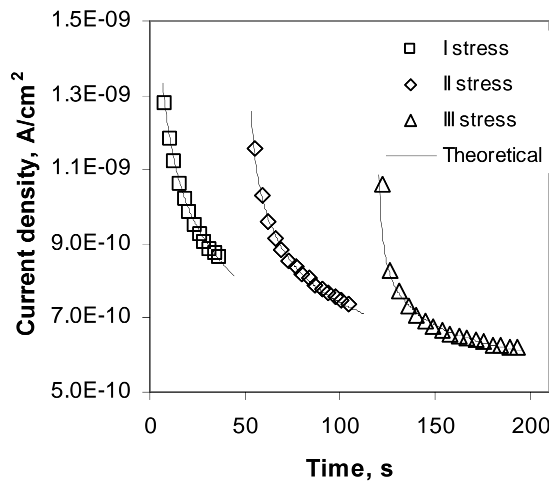

Fig. 4.33. Current density versus stress time for a film deposited with 5 sccm diluted SiH_4, 20 sccm N_2O, at 400 W, 4 mTorr and near room temperature, while stressed by 6 MV/cm.

The current passing through the oxide under stress decreases with increasing the stress time, as shown in figure 4.33, for all electric fields from 5 to 9 MV/cm. The current density recovers between the measurements, indicating that some of the trapped electrons were detrapped during the subsequent *C-V* measurement. The recovery of the current was also

dependent on deposition conditions. For inferior dielectrics obtained at high SiH_4 flow or high pressure, the traps were deeper and the current at the beginning of the second stress had values similar with the ones measured at the end of the first stress (figure 4.34).

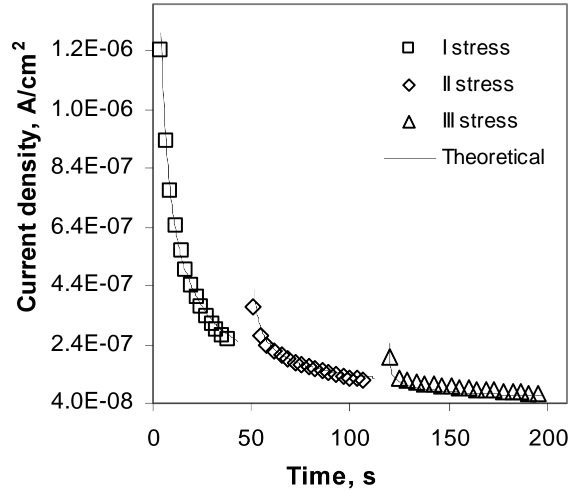

Figure 4.34. Current density versus stress time for a film deposited with 5 sccm diluted SiH_4, 20 sccm N_2O, at 400 W, 15 mTorr and near room temperature, while stressed by 6 MV/cm.

The transient current is well described by a power-law dependence on time similar to the one predicted by the trap-assisted tunnelling model [34]:

$$J = J_0 t^a, \quad a < 0 \tag{4.3}$$

where a was found to take values between –1 and –0.1. Apparently, a saturation of the trapped charges appears in time and only a higher field can induce more defects in the dielectric.

4.6. *Reliability*

For further understanding of the oxide integrity in case of strong electric stress, constant current measurements were performed as described in section 2.5.2. In figure 4.35, the charge-to-breakdown distributions (Weibull plots) for ECR oxides deposited at different pressures and for a thermally grown oxide are presented.

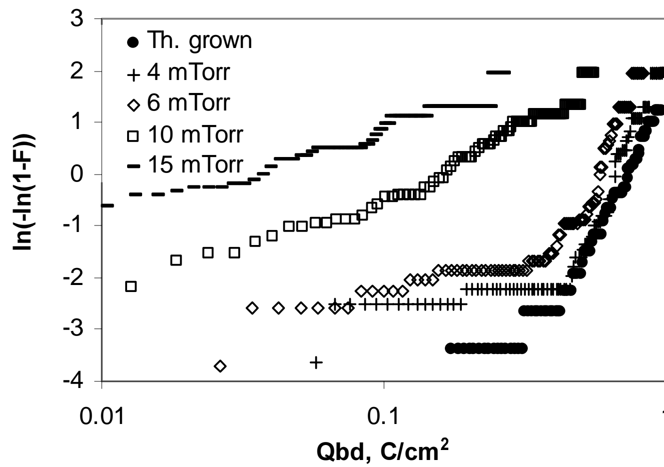

Figure 4.35. Weibull plot for films deposited with 5 sccm diluted SiH_4 and 20 sccm N_2O, at 400 W and various pressures and for a thermally grown oxide.

It is noticeable that the films deposited at lower pressure (4 and 6 mTorr) have high values for the maximum charge-to-breakdown (1 C/cm^2). The Weibull plot for the oxide deposited at 4 mTorr is similar to the one for the 25 nm reference SiO_2 film grown at 1000°C.

On the contrary, the layers deposited at higher pressure featured a smaller charge-to-breakdown and a larger distribution of extrinsic breakdowns. This indicates a higher density of defects in the bulk of dielectrics deposited at higher pressure. It is confirmed once again that multipolar ECR PECVD is a very good deposition system when used at very low pressures.

The effect of SiH_4 flow rate upon the oxide reliability was studied next (figure 4.36). Low values for the charge-to-breakdown and large distributions of defect-related breakdowns are observed for the films deposited with high SiH_4 flow, probably due to an increased number of silicon unsaturated bonds.

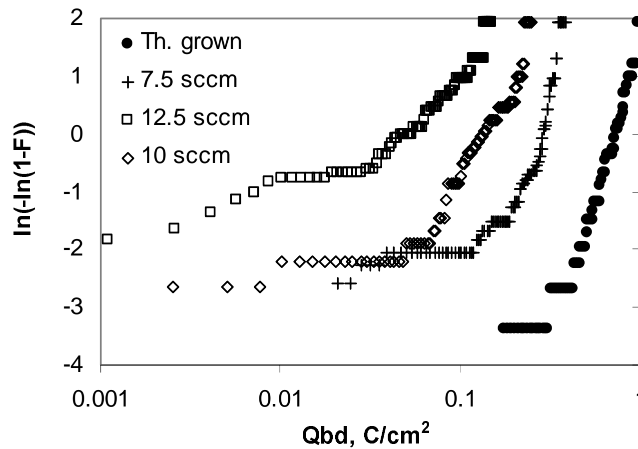

Figure 4.36. Weibull plot for films deposited with 20 sccm N_2O, at 400 W, 12 mTorr and with various diluted SiH_4 flows and for a thermally grown oxide.

While stressing the dielectrics with constant current, an increase in the required voltage was measured, caused by charge trapping and appearance of an internal electric field. From the voltage variation, the density of negative trapped charges was calculated after [26] to be around 10^{17} cm^{-3}. The experiments presented in this section demonstrate that oxides with good reliability can be deposited at near room temperature for optimal conditions.

4.7. *Summary*

SiO_2 films with critical field of 6 MV/cm, breakdown field of 10 MV/cm, resistivity of $10^{16}\Omega\cdot$cm, maximum charge-to-breakdown of 1 C/cm^2, net oxide charge density in the order of 10^{11} cm^{-2} and interface trap density of 10^{10} $eV^{-1}cm^{-2}$ have been deposited by a multipolar ECR plasma source at near-room temperature. These electrical properties are comparable with the ones of thermal oxide grown at 1000ºC, except for the positive charge, which is one order higher due to plasma damage. It is difficult to obtain dielectrics with both good interface and bulk electrical properties, due to their opposite dependencies on principal deposition parameters. Low pressure (4-6 mTorr), low diluted SiH_4 flow (5 sccm), average N_2O flow (20 sccm) and medium microwave power (400 W) were found to provide high-quality layers. The effects of different deposition conditions on electrical properties were explained by composition changes and surface bombardment. The layers which exhibited high density, stoichiometric composition and low hydrogen content possessed also the best electrical properties. The main conduction mechanisms in the ECR PECVD SiO_2 were identified. For the films obtained at relatively low pressure and low SiH_4 flow, the detected conduction mechanism was Fowler-Nordheim tunnelling. For films deposited at higher flows or higher total pressures, the conduction mechanism is trap related. Electrons were trapped in the oxide bulk during electric stress, while positive and negative charge was measured to be present at the interface, depending on the stressing electric field. The high quality of the ECR plasma deposited SiO_2 layers make them very attractive as gate dielectrics.

4.8. References

1. D.G. Farber, S. Bae, M. Okandan, D.M. Reber, T. Kuzma, S.J. Fonash, "Pathway to depositing device-quality 50 degrees C silicon nitride in a high-density plasma system", J. Electrochem. Soc. **146**, pp. 2254-2257 (1999).

2. T.V. Herak, T.T. Chau, D.J. Thomson, S.R. Mejia, D.A. Buchanan, K.C. Kao, "Low-temperature deposition of silicon dioxide films from electron cyclotron resonant microwave plasmas", J. Appl. Phys. **65**, pp. 2457-2463 (1989).
3. K. Kim, M.H. An, Y.G. Shin, M.S. Suh, C.J. Youn, Y.H. Lee, K.B. Lee, H.J. Lee, "Oxide growth on silicon (100) in the plasma phase of dry oxygen using an electron cyclotron resonance source", J. Vac. Sci. Technol. B **14,** pp. 2667-2673 (1996).
4. K.T Sung, S.W. Pang, "Oxidation of silicon in an oxygen plasma generated by a multipolar electron cyclotron resonance source", J. Vac. Sci. Technol. B **10,** pp. 2211-2216 (1992).
5. M. Firon, M. C. Hugon, B. Agius, Y. Z. Hu, Y. Wang, and E. A. Irene, "Comparison of the physical and electrical properties of electron cyclotron resonance and distributed electron cyclotron resonance SiO_2", J. Vac. Sci. Technol. B **14**, pp. 2543-2549 (1996).
6. D. Landheer, J.E. Hulse, T. Quance, "Formation of high-quality silicon dioxide films by electron cyclotron resonance plasma oxidation and plasma-enhanced chemical vapour deposition", Thin Solid Films **293**, pp. 52-62 (1997).
7. R. Castagne, A. Vapaille, "Description of the SiO_2-Si interface properties by means of very low frequency MOS capacitance measurements", Surface Science, **28**, pp. 157-193 (1971).
8. N. Jiang, M.C. Hugon, B. Agius, T. Kretz, F. Plais, D. Pribat, T. Carriere, M. Puech, "Device quality SiO_2 deposited by distributed electron cyclotron resonance plasma enhanced chemical vapor deposition without substrate heating", Jpn. J. Appl. Phys. **31**, pp. 1404-1407 (1992).
9. S.W. Hsieh, C.Y. Chang, S.C. Hsu, "Characteristics of low-temperature and low-energy plasma-enhanced chemical vapor deposited SiO_2", J. Appl. Phys. **74,** pp. 2638-2648 (1993).
10. P.G. Pai, S.S. Chao, Y. Takagi, G. Lucovsky, "Infrared spectroscopic study of SiO_x films produced by plasma enhanced chemical vapor deposition", J. Vac. Sci. Technol. A **4**, pp. 689-694 (1986).
11. G. Lucovsky, D.V. Tsu, S.S. Kim, R.J. Markunas, G.G. Fountain, "Formation of thin film dielectrics by remote plasma-enhanced chemical-vapor deposition (remote PECVD)", Appl. Surf. Sci. **39**, pp. 33-56 (1989).
12. S. Garcia, I. Martil, G. Gonzalez Diaz, E. Castan, S. Duenas, M. Fernandez, "Deposition of SiN_x:H thin films by the electron cyclotron resonance and its application to Al/SiN_x:H/Si structures", J. Appl. Phys. **83**, pp. 332-338 (1998).
13. D. Landheer, L.Å. Ragnarsson, S. Belkouch, "Physical and electrical analysis of silicon dioxide thin films produced by electron-cyclotron

resonance chemical-vapour deposition", Microelectronic Engineering, **36**, pp. 53-60 (1997).
14. O. Joubert, R. Burke, L. Vallier, and C. Martinet, R. A. B. Devine, "Influence of ion energy on the physical properties of plasma deposited SiO_2 films", Appl. Phys. Lett. **62**, pp. 228-230 (1993).
15. P. Mak, G. King, T.A. Grotjohn, J. Asmussen, "Investigation of the influence of electromagnetic excitation on electron cyclotron resonance discharge properties", J. Vac. Sci. Technol. A **10**, pp. 1281-1287 (1992).
16. J. Asmussen, "Electron cyclotron resonance microwave discharges for etching and thin-film deposition", J. Vac. Sci. Technol. A, **7,** pp. 883 (1989).
17. Barry van Dijk, "Transistors in excimer-laser formed monocrystalline silicon thin-film for large area electronics", Progress report, Delft, 31 January, 2002.
18. M.J. Hernandez, J. Garrido, J. Martinez, J. Piqueras, "Electrical properties of electron cyclotron resonance plasma-deposited silicon dioxide: effect of the oxygen to silane flow ratio", Semic. Sci. Technol. **11**, pp. 422-426 (1996).
19. F.S. Pool, "Nitrogen plasma instabilities and the growth of silicon nitride by electron cyclotron resonance microwave plasma chemical vapor deposition", J. Appl. Phys., **81**, pp. 2839-2846 (1997).
20. G. Isai, A. Kovalgin, J. Holleman, P. Woerlee, H. Wallinga, "High quality silicon oxide deposited with a multipolar electron cyclotron resonance plasma source", Electroch. Soc. Proc. **2000-31**, 169 (2001).
21. V. Houtsma, Ph. D. thesis, Twente University, The Netherlands, 1999, p. 23.
22. V. S. Lysenko, I. P. Tyagulski, Y. V. Gomeniuk, I. N. Osiyuk, "Effect of traps in the transition Si/SiO_2 layer on input characteristics of SOI transistors", Microelectronics reliability **40**, pp. 799-802 (2000).
23. B. L. Yang, H. Wong, Y. C. Cheng, "Study of process-dependent electron-trapping characteristics of thin nitrided oxides", Solid-St. Electron. **37**, pp. 481-486 (1994).
24. D.A. Buchanan, J.H. Stathis, P.R. Wagner, "Trapped positive charge in plasma-enhanced chemical vapor deposited silicon dioxide films", Appl. Phys. Lett. **56**, pp. 1037-1039 (1990).
25. W.R. Harrell, J. Frey, "Observation of Poole–Frenkel effect saturation in SiO_2 and other insulating films", Thin Solid Films **352**, 195 (1999).
26. Y.C. Jeon, H.Y. Lee, S.K. Joo, "I-V characteristics of electron-cyclotron-resonance plasma-enhanced chemical-vapor-deposition silicon nitride thin films", J. Appl. Phys. **75**, pp. 979-984 (1994).
27. A. Yokozawa, Y. Miyamoto, "First-principles exploration of possible trap terminators in SiO_2", Appl. Phys. Lett. **73**, pp. 1122-1124 (1998).

28. G. King, F.C. Sze, P.Mak, T.A. Grotjohn, J. Asmussen, "Ion and neutral energies in a multipolar electron cyclotron resonance plasma source", J. Vac. Sci. Technol. A **10**, pp. 1265-1269 (1992).
29. J.R. Flemish, R.L. Pfeffer, "Low hydrogen content silicon nitride films from electron cyclotron resonance plasmas", J. Appl. Phys. **74**, pp. 3277-3281 (1993).
30. D.J. DiMaria, E. Cartier, D. Arnold, "Impact ionization, trap creation, degradation, and breakdown in silicon dioxide films on silicon", J. Appl. Phys. **73**, pp. 3367-3384 (1993).
31. L.M. Landsberger, R. Ghayour, M. Sayedi, M. Kahrizi, D. Landheer, J.A. Bardwell, Y. Riopel, C. Jean, V. Logiuduce, "Electrical characterization of metal-oxide-semiconductor capacitors with anodic and plasma-nitrided oxides", J. Vac. Sci. Technol. A **18**, pp. 676-680 (2000).
32. F. Irrera, F. Russo, "Enhanced injection in n^{++}-poly/SiO_x/SiO_2/p-sub MOS capacitors for low-voltage nonvolatile memory applications: experiment", IEEE Trans. El. Dev. **46**, pp. 2315-2322 (1999).
33. T.T. Chau, S.R. Mejia, K.C. Kao, "Thickness dependence of the dielectric behavior of SiO_2 films fabricated by microwave electron cyclotron resonance plasmas", J. Vac. Sci. Technol. B **9**, pp. 50-57 (1991).
34. R. Rofan, C. Hu, "Stress-induced oxide leakage", IEEE El. Dev. Lett. **12**, pp. 632-636 (1991).
35. K.O. Jeppson, C.M. Svensson, "Negative bias stress of MOS devices at high electric fields and degradation of MNOS devices", J. Appl. Phys. **48**, pp. 2004-2014 (1977).

Chapter 5 ECR-PECVD Silicon Nitride

Abstract

In this chapter the investigation of silicon nitride deposited by multipolar Electron Cyclotron Resonance Plasma Enhanced Chemical Vapour Deposition (ECR-PECVD) from N_2 *and* SiH_4 *is presented. In order to optimise the deposition process, the influences of different parameters (nitrogen flow rate, total pressure, microwave power, annealing processes and film thickness) on physical and electrical properties have been investigated and explained. High quality silicon nitride films, with a refractive index of 1.9, dielectric constant of 7.2, Si/N ratio values around 0.78, and very low hydrogen content (under 1%) have been produced with relatively low pressure, high nitrogen flow and high microwave power. Also a low oxygen contamination of around 2% is obtained under these deposition conditions. The good dielectric strength of the layers was confirmed by large breakdown fields of 12 MV/cm, very high resistivity of* 10^{16} Ω*cm and maximum charge to breakdown of 90* C/cm^2*. The density of interface charge was estimated to be in the range of* $3\text{-}16\cdot10^{11}$ cm^{-2} *and it was improved with increasing the pressure and decreasing the nitrogen flow due to increased oxygen incorporation. The dominant conduction mechanism in the layers is the Poole-Frenkel effect; furthermore, the extracted trap energy and the critical field show the same dependency on deposition pressure. Fowler-Nordheim tunnelling dominates at high biases only for the layer deposited at the highest pressure of about 22 mTorr.*

5.1. Introduction

Silicon nitride is extensively used as gate dielectric in TFTs, in oxide-nitride-oxide (ONO) dielectrics for storage capacitors in dynamic random access memory (DRAM) circuits, and as passivation layer. It does not play a role as gate dielectric in standard CMOS, because the silicon oxide interface with silicon is much better than the Si_3N_4/Si interface. Although both SiO_2 and Si_3N_4 are amorphous materials, Si_3N_4 has a much more rigid structure than the oxide due to the necessity of nitrogen forming three and not two

bonds like oxygen atoms [1]. Consequently, Si_3N_4 is denser, harder, has a higher stress level, more dangling bonds and its interface with crystalline silicon is more strained, with increased interface trap density.

On the contrary, experiments have shown that the interface between amorphous silicon and nitride is better in terms of threshold voltage than the α-Si/SiO_2 interface. An explanation arises from the fact that the nitride used in TFTs contains a lot of hydrogen (10-20%) [2], terminating the dangling bonds produced by the inflexible structure. Since the hydrogen content in amorphous silicon is also 10-20%, it is plausible that the interface with SiN_xH_y is favoured.

Si_3N_4 layers were deposited from SiH_4 (pure or diluted to 2% in helium) and N_2. N_2 was chosen as gas precursor because it was reported that layers obtained from N_2 are denser and contain less hydrogen, compared to Si_3N_4 deposited from NH_3 [3]. In addition, it is known from literature that ECR plasma has a higher electron density [4] and therefore can dissociate N_2 much easier than rf-PECVD, thus there is no need to use NH_3 to obtain stoichiometric films. N_2 is dissociated in the plasma by collisions with high-energy electrons, as follows:

$$e + N_2 \rightarrow N^+ + N^* + 2e \qquad (5.1)$$

SiH_4 is dissociated either by electrons inside the plasma or by collisions with nitrogen molecules and radicals. In this case, SiH_x^* radicals are formed [5]:

$$e + SiH_4 \rightarrow SiH_3 + H \qquad (5.2)$$

$$SiH_4 + N_2^* \rightarrow SiH_3 + NH \qquad (5.3)$$

Reaction (5.1) needs 12.25 eV in order to occur, whereas reaction (5.2) requires only 6.5 eV [6]. This is the reason why SiH_4 is introduced downstream, in order to avoid deposition of silicon-rich films. In addition, it has been noticed that if SiH_4 is introduced directly into the plasma, the hydrogen content in the deposited film increases [7]. The reaction between SiH_x^* radicals and nitrogen radicals continues on the wafer surface with hydrogen desorption, until Si_3N_4 is formed.

Hydrogen may also be incorporated in the layer, either in Si-H or N-H bonding configurations. Because hydrogen desorption takes place usually at substrate temperatures above 350ºC, Si_3N_4 obtained at room temperature by rf-PECVD can contain 10-20% hydrogen. Higher density plasmas at low pressures like ECR PECVD can be a solution for hydrogen minimisation. Although very good Si_3N_4 films have been deposited at room temperature

with divergent ECR plasma sources and distributed ECR plasma sources [8-10], the level of hydrogen contamination could not be reduced under 5 at.%. Our aim is to obtain layers with less than 1 at.% hydrogen contamination at room temperature by multipolar ECR PECVD, without any annealing process.

Some studies have shown the presence of oxygen contamination in ECR nitrides [3, 10, 11-15] and the efforts to minimise it by reducing the sputtering phenomena through decreasing the microwave power [15]. However, the reduction of oxygen content by modifying the deposition pressure and by improving the dissociation of N_2 was not investigated in detail.

Several papers have shown that it is difficult to obtain layers at room temperature with concomitant good stoichiometry, good interface trap densities, low trapped charge density and high breakdown field [16-18]. In order to obtain an optimised film, the influence of different deposition parameters on deposition kinetics, film composition, *C-V* and *I-V* characteristics were studied in this chapter. The film reliability and conduction mechanism were also investigated. Correlations between the total pressure, the oxygen content in the layers and the electrical behaviour of the films have been made.

5.2. Deposition kinetics

5.2.1. Pressure role

Pressure has a significant influence on the rate at which molecules are integrated in the film (see fig 5.1). The deposition rate depends on the radicals' concentration as in the case of SiO_2 deposition (see expression 3.3). With increasing the total pressure, the SiH_4 partial pressure increases, therefore the films are deposited faster, an observation confirmed also by other authors [11, 19].

Diluted SiH_4 was also employed in fabrication of silicon nitride layers, and a huge decrease in deposition rates from 15-30 nm/min to less than 1 nm/min, due to a lower SiH_4 flow was observed. However the trend in the growth rate with pressure for layers deposited with diluted SiH_4 is the same as for the ones obtained with pure SiH_4 , as it can be seen in figure 5.2 for two different series of experiments. The slope in figure 5.2 depends on other parameters; in this case the microwave power is the significant influencing factor.

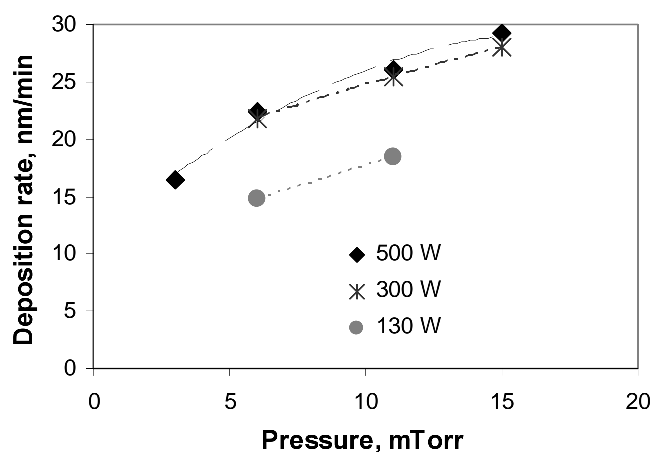

Figure 5.1. Deposition rate versus pressure for nitrides obtained with 2 sccm SiH_4, 30 sccm N_2, without substrate heating and at various microwave powers.

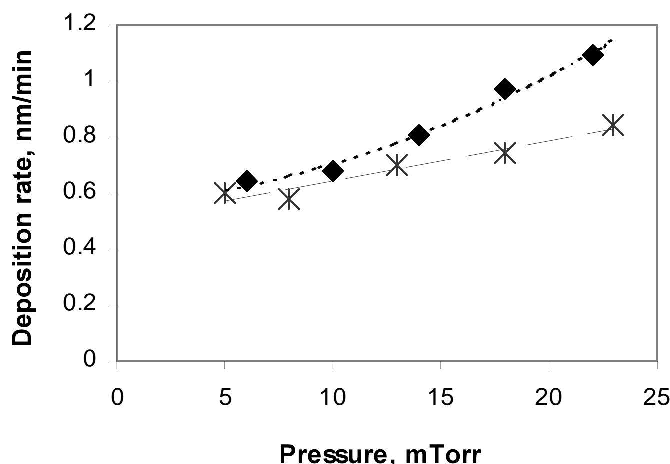

Figure 5.2. Deposition rate versus pressure for nitrides (✳) obtained with 5 sccm diluted SiH_4 and 18 sccm N_2, at 500°C and 150 W; and nitrides (◆) obtained with 5 sccm diluted SiH_4 and 30 sccm N_2, at 400 W and without substrate heating.

5.2.2. Microwave power role

The microwave power effect upon deposition kinetics is presented in figure 5.3 for various pressures. There is a significant rise in deposition rate with increasing the power for the first part of the graph, between 100 and 300 W. As shown in chapter 2, the electron density and temperature rise with increasing the total power absorbed from the microwave source [21] (see section 2.1.1). Consequently, the increase in power can be translated in an increased radical concentration and a higher deposition rate. The microwave power has a much smaller effect upon the deposition rate between 300 W and 500 W. This effect was encountered also for SiO_2 deposition (section

3.2.3). Also the refractive index increases slower for microwave powers between 300 and 500 W (see figure 5.8), thus apparently the nitrogen radical formation is limited in this region.

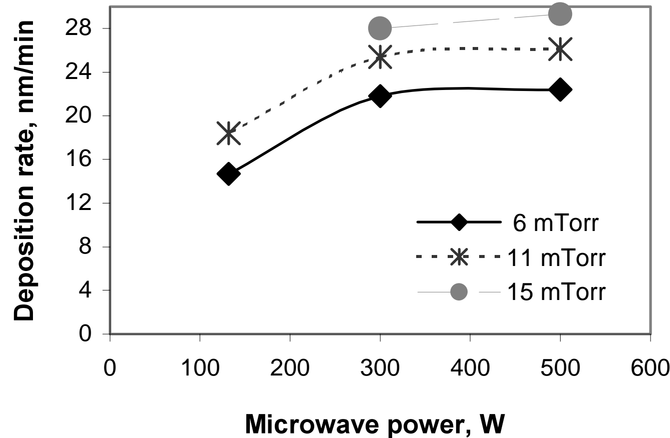

Figure 5.3. Deposition rate versus microwave power for nitrides obtained with 2 sccm SiH_4 and 30 sccm N_2, without substrate heating and for several pressures.

5.2.3. N_2 flow role

In figure 5.4, two series of experiments realised at various deposition conditions, show the effect that N_2 flow rate has upon the deposition kinetics. For films obtained at 500ºC and only 150 W, the deposition rate decreases with increasing N_2 flow, due to a decline in SiH_4 partial pressure. The evidence suggests that the deposition rate is limited by the SiH_4 radicals flux at the substrate, in agreement with other work [17].

At a higher power of 400 W, however, the deposition rate is maintained constant, in spite of the fact that the SiH_4 partial pressure becomes three times smaller at high N_2 flows, while the N_2 partial pressure increases only from 12 to 13.4 mTorr. Due to a higher concentration of nitrogen radicals and ions arriving from the plasma, at higher N_2 flow and higher microwave power apparently all the SiH_4 molecules react, therefore maintaining the deposition rate constant. Another possibility is that diffusion of SiH_4 molecules into the plasma and deposition of SiO_2 in the plasma is suppressed at high N_2 flows. Consequently the concentration of SiH_4 in the vicinity of the wafer does not decrease considerably with increasing the N_2 flow (see section 3.2.4).

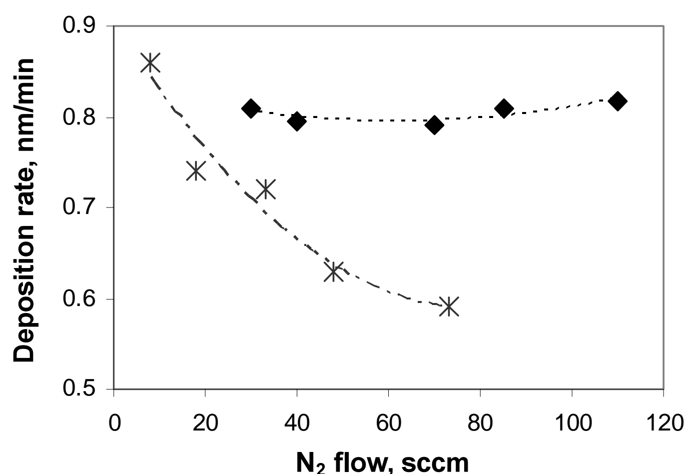

Figure 5.4. Deposition rate versus N_2 flow rate for nitrides (✳) obtained with 5 sccm diluted SiH_4, at 18 mTorr, 500°C and 150 W; and nitrides (◆) obtained with 5 sccm diluted SiH_4, at 14 mTorr, 400 W and without substrate heating.

5.2.4. The effect of consecutive depositions

In order to verify the reproducibility of the layers, the same experiment was repeated four times, keeping the entire parameters constant, including the deposition time. A small change in the deposition rate can be observed in figure 5.5. The first layer was deposited faster, and a possible explanation is the oxygen contamination. It is known that SiO_2 has a higher deposition rate compared to Si_3N_4, due to its less dense structure. The system was not flushed with N_2 before experiments, thus it is possible that background O_2/H_2O concentration in the system or gas lines can contaminate the first deposited films of the day, increasing the film thickness. This explanation was confirmed in section 5.3.4 by the variation in refractive index. The oxygen incorporation decreases for the next films, due to continuous N_2 flow inside the deposition chamber during the experiments.

The observed variation in deposition rate and composition was not large enough to influence the electrical film properties. The effect can be avoided by flushing the system and the gas lines before starting the deposition process.

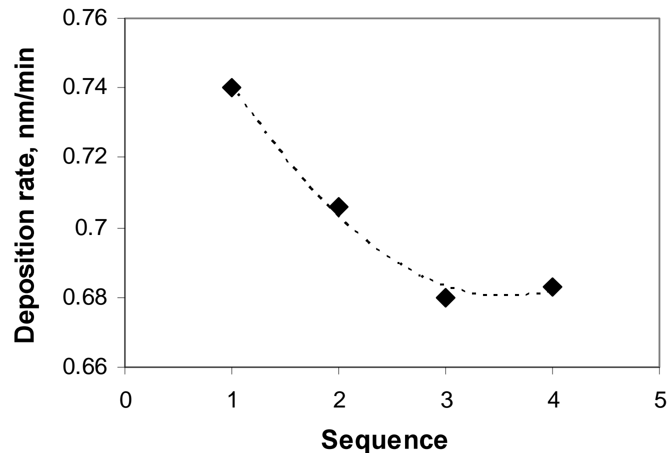

Figure 5.5. Deposition rate versus the deposition sequence for nitrides obtained with 5 sccm diluted SiH_4 and 40 sccm N_2, at 14 mTorr, 400 W and without substrate heating.

5.3. Refractive index

One can find a large variety of values for the refractive index of silicon nitride in literature. Stoichiometric silicon nitride deposited in our Clean Room with LPCVD at 800°C exhibited a refractive index of 1.98, while rf-PECVD Si_3N_4 has a refractive index of only 1.9 [22]. The difference between the two values is probably caused by the high hydrogen content in the rf-PECVD nitride. A refractive index over 2 usually indicates excess silicon in the layers, while a refractive index smaller than 1.95 is usually caused by oxygen or hydrogen contamination and density diminution.

5.3.1. Pressure role

As in the case of SiO_2 obtained with pure SiH_4, the refractive index of the silicon nitride decreases with increasing the pressure (figure 5.6). The very low values of the refractive index (1.7) at high pressure are caused by a raise in the oxygen content of the layers. This hypothesis was confirmed by Auger measurements, as it is described later (section 5.4.1).

Several studies have indicated the presence of oxygen contamination (1-20 at.%) in silicon nitride layers deposited with an ECR plasma [8, 10, 11-16]. The oxygen presence was attributed to either the sputtering of the quartz dome [8, 16], insufficient vacuum conditions [11, 12] or oxidation of highly porous films after deposition in the ambient [13, 15].

In our case the increase of oxygen content with pressure can be explained either by a higher porosity at higher pressure due to less ion bombardment

[23] or by a stronger deexcitation of nitrogen radicals at high pressure [11]. The first hypothesis was not confirmed by composition measurements done at different periods after deposition. In addition, the lack of hydrogen atoms observed in ERD measurements (section 5.3.1) indicates that the layers are very dense, thus the conclusion is that incorporation of oxygen took place during deposition.

Because the energy absorbed by the electrons from the electric field in ECR microwave plasma is proportional with the length of their trajectory, at low pressure, when the mean free path is large [24] (see expression 2.5), the electrons will possess high energy. In contrast, at high pressures, the electrons don't have enough energy (more than 10 eV) to dissociate the inert N_2 molecules, but the energy is high enough for dissociating the O_2/H_2O present in the chamber. As a consequence, more oxygen is incorporated in the growing film, decreasing the refractive index.

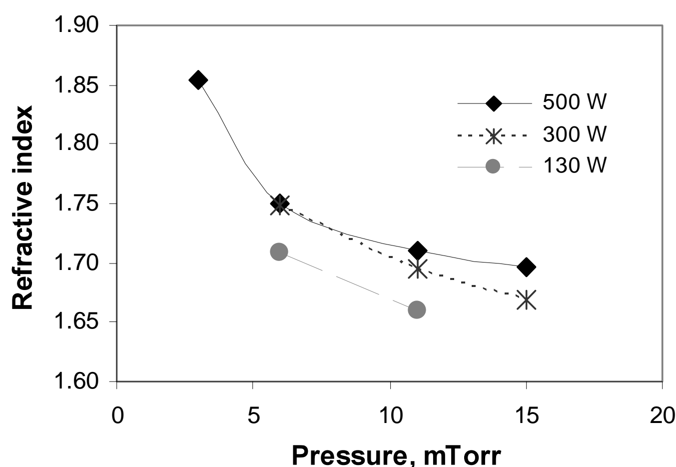

Figure 5.6. Refractive index versus pressure for nitrides obtained with 2 sccm SiH_4, 30 sccm N_2, without substrate heating and at various microwave powers.

The same trend appears for the refractive index versus pressure in the case of nitrides deposited with diluted SiH_4. For these films the deposition rate is much lower, thus the molecules have much more time to migrate on the surface and desorb the hydrogen, resulting in denser films with higher refractive indexes. Also the N_2/SiH_4 ratio is considerably larger, therefore there are fewer oxygen atoms incorporated in the film (section 5.3.1) and the refractive index is higher.

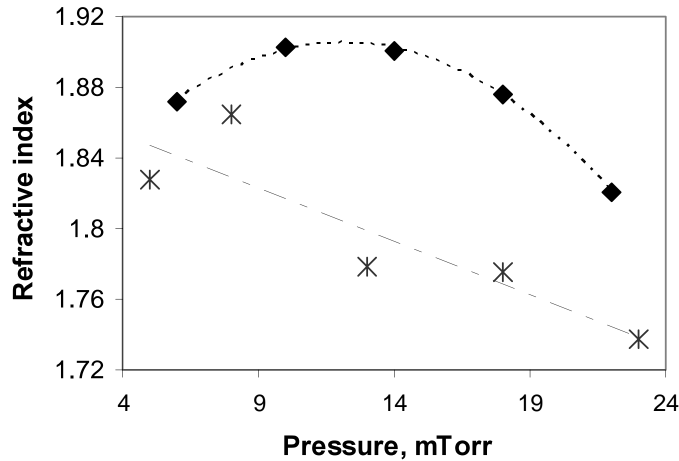

Figure 5.7. Refractive index versus pressure for nitrides obtained with (✳) 5 sccm diluted SiH_4 and 18 sccm N_2, at 150 W and 500ºC; and (◆) 5 sccm diluted SiH_4 and 30 sccm N_2, at 400 W and without substrate heating.

At very low pressures (5 mTorr), appears a small decrease in the refractive index of layers deposited with diluted SiH_4, which can be attributed to the sputtering of the quartz dome by high-energy particles. SiN_xO_y layers obtained with pure SiH_4 possessed high oxygen content and the sputtering contribution to oxygen content could not be observed at low pressures. Because the refractive index has a peak at around 10 mTorr, this can be considered to be the optimal deposition pressure.

5.3.2. Microwave power role

The influence of microwave power upon the refractive index of the layers was studied for films deposited with pure SiH_4 at different pressures (figure 5.8). With increasing the microwave power, the plasma becomes more energetic and more effective in dissociating N_2, which is then embedded in the film structure. Consequently lower oxygen contamination occurs and the refractive index increases for higher microwave power. For the lowest pressure, the microwave power increase between 100 and 300 W has an important effect upon the refractive index, but between 300 and 500 W, the effect is insignificant, as it was also the case of deposition rate (figure 5.3). For high pressures however, when the ECR plasma is less efficient, the additional energy brought to electrons by the modification of microwave power from 300 to 500 W is important for dissociating the N_2 molecules.

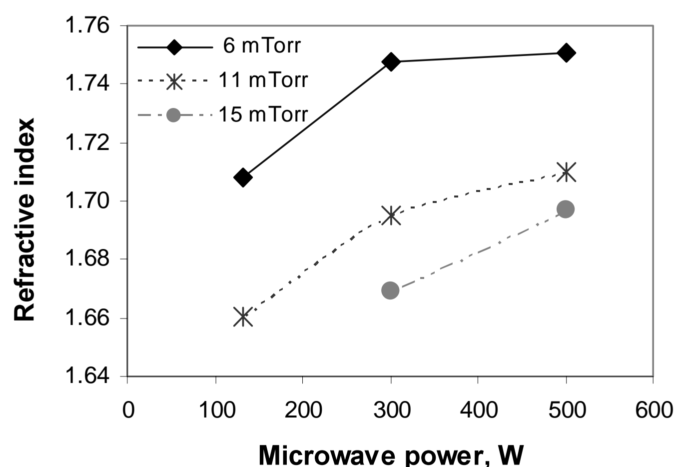

Figure 5.8. Refractive index versus microwave power for nitrides obtained with 2 sccm SiH_4 and 30 sccm N_2, without substrate heating and at various pressures.

5.3.3. N_2 flow rate

As expected, the refractive index is higher for the films deposited with higher N_2 flow (figure 5.9), due to an elevated concentration of nitrogen radicals in the plasma, and more nitrogen incorporated in the layers. This tendency shows that the source of O_2 in the system cannot be the impurities in the N_2 bottle, because an increase in N_2 flow would increase also the oxygen contamination, but rather the background O_2/H_2O concentration in the reactor and gas lines. The layers obtained with 400 W exhibited a higher refractive index (1.95) than the rf-PECVD layers, indicating a much lower hydrogen concentration in the ECR films.

Because it is difficult to measure accurately the refractive index of so thin layers with a constant wavelength, a thicker layer of 85 nm was grown at the same deposition conditions and the measured value of the refractive index increased from 1.95 to 1.98, a value comparable with the 800ºC LPCVD silicon nitride refractive index.

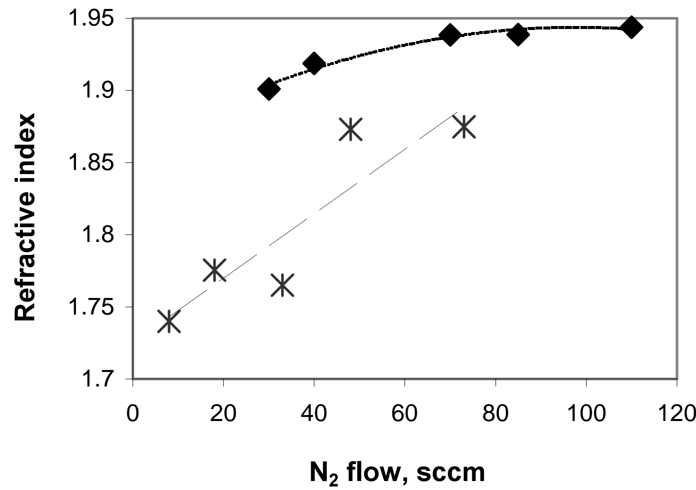

Figure 5.9. Refractive index versus N_2 flow rate for nitrides obtained with (✳) 5 sccm diluted SiH_4, at 18 mTorr, 500°C and 150 W; (◆) 5 sccm diluted SiH_4, at 14 mTorr, 400 W and without substrate heating.

5.3.4. The effect of consecutive depositions

The refractive index of layers deposited at the same deposition parameters, in successive order is shown in fig. 5.10. It can be noticed that the refractive index increases from the first until the last experiment, due to lower oxygen contamination. This proves that there is more O_2/H_2O present in the chamber during the first experiments of the day and after a few depositions it gradually diminishes, due to continuous flow of N_2 in the chamber and gas lines.

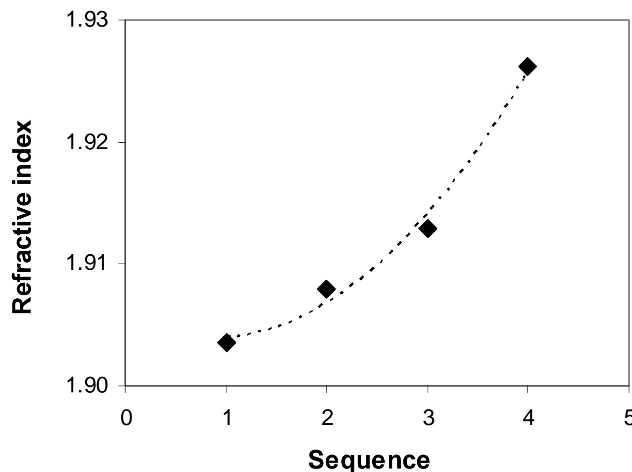

Figure 5.10. Refractive index versus the deposition sequence for nitrides obtained with 5 sccm diluted SiH_4 and 40 sccm N_2, at 14 mTorr, 400 W and without substrate heating.

5.4. Atomic composition

The atomic composition was investigated by infrared spectra, auger sputter profiles and X-ray spectroscopy photoemission (see section 2.4).

5.4.1. Pressure role

From Fourier transformed infrared spectra of nitrides deposited at different pressure, the absorption coefficient, the frequency and the mean peak width (FWHM) of Si-N stretching mode situated around 835 cm^{-1} [17] and the intensity of the N-H stretching bond at 3350 cm^{-1} were extracted and presented in table 5.1. One can notice that the layers deposited at lower pressure are characterised by a higher intensity Si-N absorption peak and a lower N-H absorption peak, indicating a denser film with less hydrogen content, due to a more intense ion bombardment.

Table 5.1. The absorption coefficient, the Si-N stretching frequency and the mean peak width (FWHM) for the Si-N stretching mode situated at 835 cm^{-1} and the intensity of the N-H bonds.

Pressure, mTorr	Si-N frequency cm^{-1}	Si-N absorption coefficient	Si-N FWHM	N-H absorption coefficient
0.7	853	30560	182	2210
1	856	28400	186	2240
2	872	23600	197	2690
3	876	21250	206	2970

The parameters shown in table 5.1 are also presented in figures 5.11 and 5.12 versus the deposition pressure. As one can observe, there is a rise in the mean peak width and a decline in the Si-N stretching frequency with increasing the pressure. This is an indication of higher oxygen contamination. The oxygen presence can be noticed also in a small Si-O absorption peak situated around 1100 cm^{-1}.

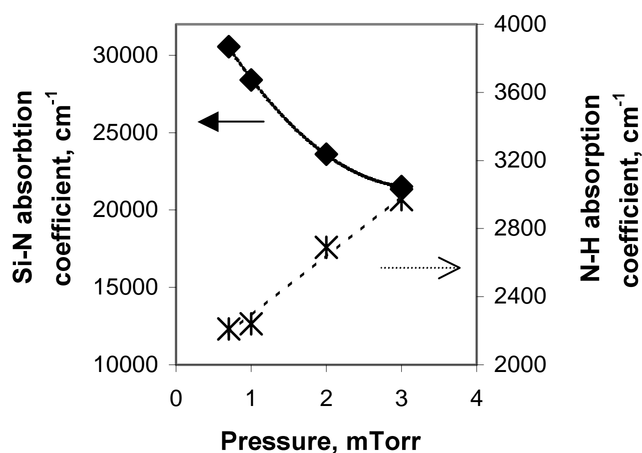

Figure 5.11. Absorption coefficients for Si-N and N-H bonds versus deposition pressure for nitrides obtained with 2 sccm SiH_4 and 10 sccm N_2, with 500 W and without substrate heating.

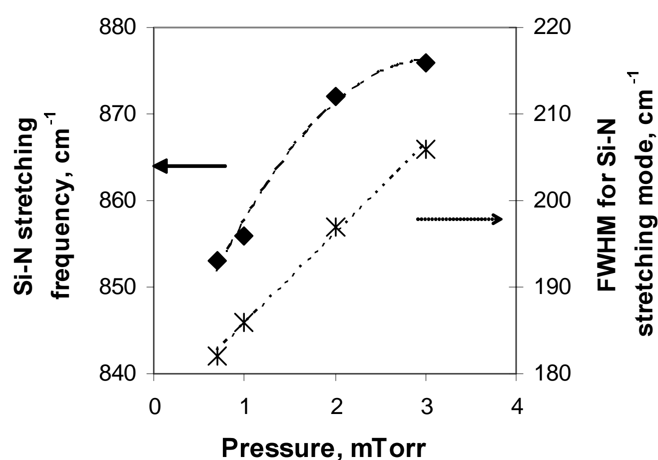

Figure 5.12. The frequency and mean peak width for the Si-N stretching mode versus deposition pressure for nitrides obtained with 2 sccm SiH_4 and 10 sccm N_2, with 500 W and without substrate heating.

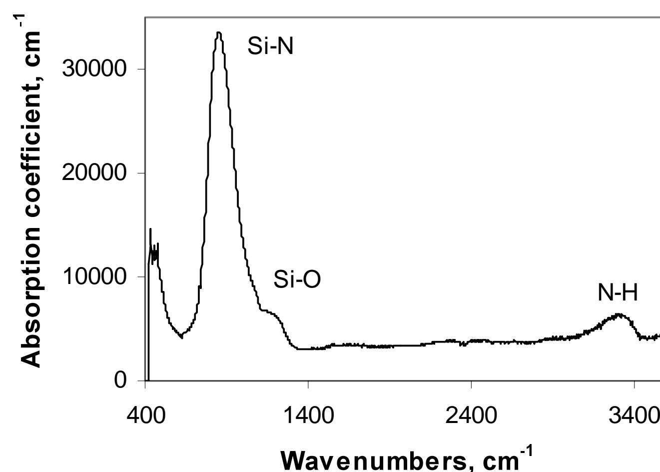

Figure 5.13. FTIR spectra for a silicon nitride layer obtained with 2 sccm SiH_4 and 10 sccm N_2, at 0.7 mTorr, 500 W and without substrate heating.

The pressure effect upon the layer structure was studied also for nitrides deposited with diluted SiH_4 at a lower microwave plasma of 150 W and higher pressures of 8-18 mTorr, where the ECR plasma source is not as efficient. It can be clearly seen that the concentration of Si-O bonds present around 1100 cm^{-1} increases, while the concentration of Si-N bonds situated between 800 and 900 cm^{-1} decreases with increasing the total pressure (figure 5.14). Obviously insufficient amount of N radicals are present at high pressure, due to a lack of efficiency in dissociating the gas molecules.

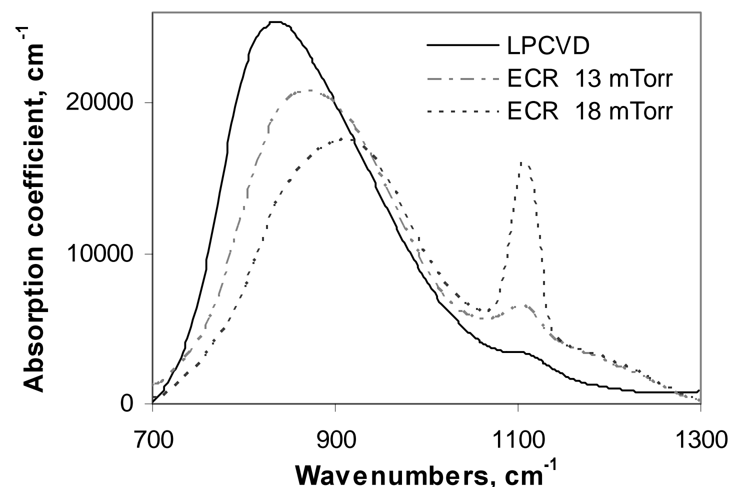

Figure 5.14. FTIR spectra for an LPCVD silicon nitride obtained at 800°C and for ECR nitrides deposited with 5 sccm diluted SiH_4 and 18 sccm N_2, at 500°C, 150 W and various pressures.

Auger measurements confirmed that pressure is an important factor in minimising the oxygen contamination in the ECR deposited silicon nitride (figure 5.15). In order to diminish the oxygen content even less than 10% in

this pressure range, other deposition parameters like microwave power should be tuned.

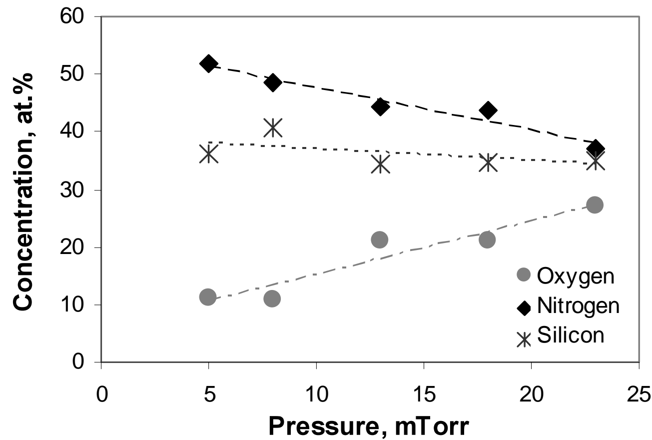

Figure 5.15. Film composition measurements versus pressure for ECR nitrides deposited with 5 sccm diluted SiH_4, 18 sccm N_2, at 500°C and 150 W.

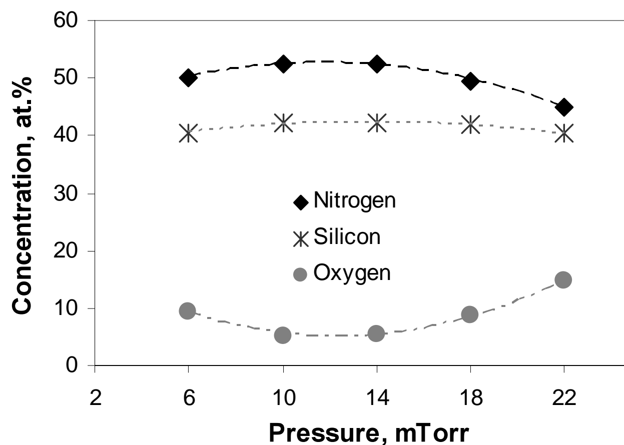

Figure 5.16. XPS measurements versus pressure for near room temperature ECR nitrides deposited with 5 sccm diluted SiH_4 and 30 sccm N_2, and 400 W.

Experiments were performed also with diluted SiH_4 at room temperature and the oxygen concentration also increased with increasing the total pressure (figure 5.16), due to insufficient energy for dissociating the N_2 molecules. The minimum oxygen content was obtained for pressures around 10 mTorr and had the value of 5 at.%. The reduction in oxygen contamination in the case of these films compared with the ones deposited at 500°C (figure 5.15) may be explained by a higher microwave power and higher N_2 flow. One can observe that the layer deposited at the lowest pressure possesses more oxygen, confirming the cause for a lower refractive index at 6 mTorr (figure 5.10) is the oxygen.

The drastic decrease in the SiH_4 flow following the shift from pure SiH_4 to diluted has a beneficial effect upon the hydrogen concentration, which decreased considerably until around 4 at.% for the nitrides deposited at 500°C

and 150 W. A possible cause is the lower deposition rate, which allowed more time for desorbing the hydrogen. The concentration of N-H bonds (3350 cm^{-1}) diminished with decreasing the pressure (figure 5.17), as in the case of the layers obtained with pure SiH_4. The highly energetic particles at low pressure and bombarded the wafer, breaking the undesirable hydrogen bonds.

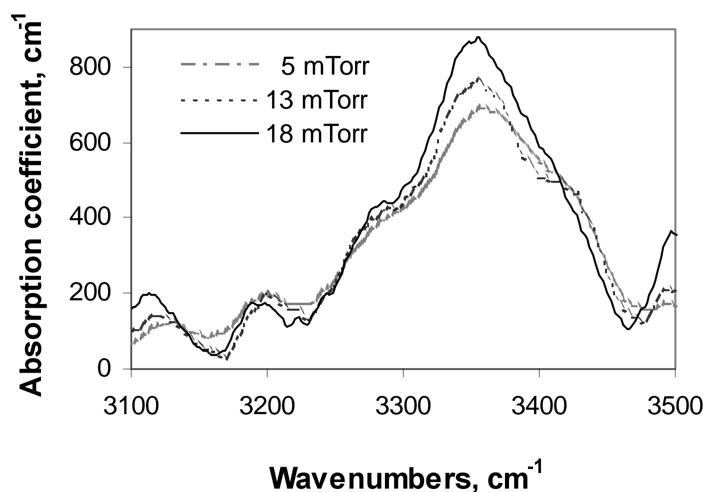

Figure 5.17. Hydrogen bonds in silicon nitrides deposited with 5 sccm diluted SiH_4 and 18 sccm N_2, at 500°C, 150 W and at various pressures.

For the layers deposited at room temperature, the hydrogen content was measured by ERD. The total hydrogen contamination was between 0.6 at.% and 1%, independent of deposition conditions. These silicon nitride layers were deposited at room temperature, with diluted SiH_4 and 400 W microwave power and did not experience any annealing process, however they exhibited the lowest hydrogen content measured until now. This proves that multipolar ECR PECVD is a very good method for obtaining films with a low thermal budget and good properties. For comparison, the hydrogen content of a standard LPCVD silicon nitride obtained at 800°C measured with the same ERD equipment was 3.3% [26].

5.4.2. Microwave power role

The films deposited without substrate heating with diluted SiH_4, have shown that in spite of the low deposition temperature (around 50°C), their hydrogen content extracted from ERD measurements is very low (< 1 at.%). The reason for this decrease in the hydrogen content compared with the layers deposited at 500°C is the increase of power from 150 W to 400 W. These results prove that nitrides can be deposited at room temperature with

very low concentration of hydrogen bonds, if the optimal conditions are found. There were no comparable results in terms of hydrogen content of room temperature silicon nitride found in literature.

The fact that the oxygen contamination was lower for layers deposited at 400 W than for the ones at 150 W proves that sputtering of the quartz dome is not the main cause of the oxygen presence.

5.4.3. N_2 flow role

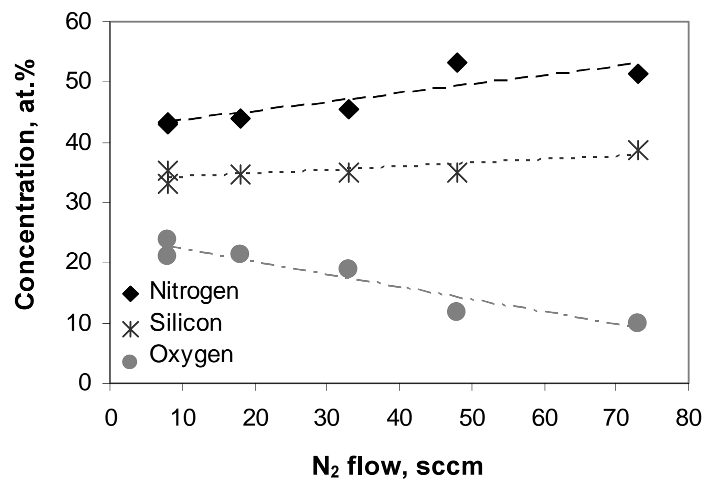

Figure 5.18. Auger spectroscopy measurements versus N_2 flow rate for ECR nitrides deposited with 5 sccm diluted SiH_4 and 18 mTorr, at 500°C and 150 W.

The composition of the layers as determined from Auger Spectroscopy varied with the N_2 flow used for deposition (figure 5.18). At high N_2 flow rates, the nitrogen content increased until 53%, while the oxygen contamination decreased until 10%. This confirms that the O_2 contamination source does not originate from the N_2 gas, but rather is caused by the O_2 background pressure in the system or gas lines. With increasing the N_2 flow, the partial pressure of the O_2/H_2O is decreased, and more nitrogen radicals reach the wafer surface.

The influence of N_2 flow rate on the composition of nitrides deposited at room temperature was also studied and the results of the XPS measurements are represented in fig 5.19. It confirmed that less oxygen is integrated in the layers at high N_2 flows, due to a smaller partial pressure of O_2/H_2O in the chamber. The oxygen contamination was minimized at 2 at.% for a deposition pressure of 14 mTorr and a N_2 flow rate of more than 55 sccm, while the hydrogen content was 0.5 at.%. Improving the vacuum conditions

by installing a new pump has been shown in the literature to eliminate completely the oxygen from the layers [12].

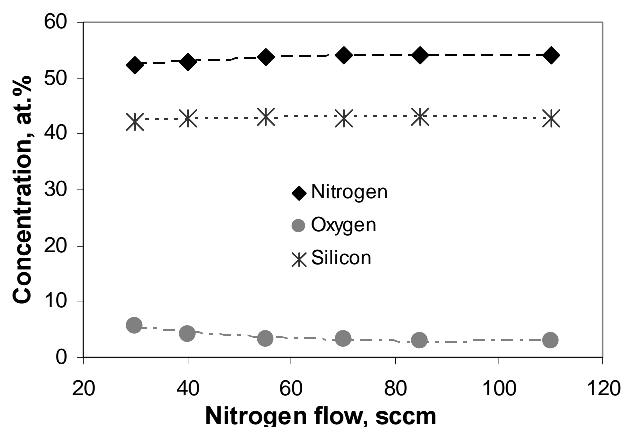

Figure 5.19. XPS measurements versus N_2 flow rate for ECR nitrides deposited with 5 sccm diluted SiH_4 at 14 mTorr, 400 W and near room temperature.

5.4.4. *The effect of consecutive depositions*

The oxygen content in the layers deposited at several moments in time was almost constant, except for the first experiment. In this case the oxygen contamination was higher (4.5 at.% compared to 2.5 at.%). Apparently before starting the experiments there is O_2/H_2O present in the chamber, which is incorporated in the first layer. After the first experiment most of the O_2/H_2O is eliminated from the chamber, and the layers have a more stoichiometric and constant composition.

5.5. *C-V characteristics*

MIS capacitors with aluminium gate electrodes were manufactured as described in section 2.5 in order to measure the electrical properties of the silicon nitride layers. All samples were subjected to an aluminium-sintering step for 5 minutes, at 400ºC in wet N_2 ambient, but no annealing after deposition of dielectric was performed.

Capacitance-Voltage (*C-V*) measurements were measured for the extraction of the interface trap density and the total net charge. Their evolution with the principal deposition factors was followed for two cases: layers deposited at 500ºC and films obtained at room temperature. A typical *C-V* curve for a nitride obtained at room temperature is represented in figure 5.20.

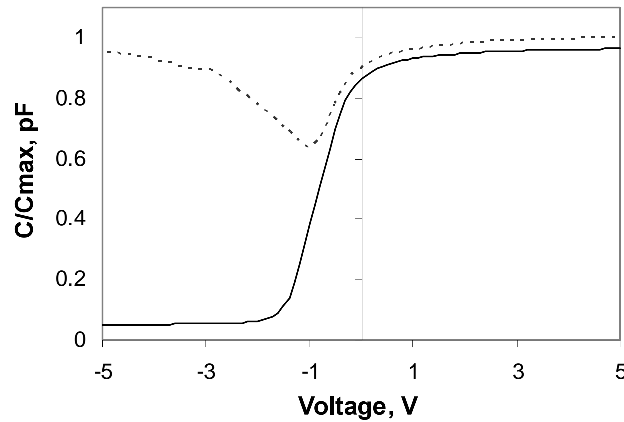

Figure 5.20. *C-V* measurement for an ECR nitride deposited with 5 sccm diluted SiH_4 and 30 sccm N_2, at 400 W and 18 mTorr without substrate heating.

5.5.1. Pressure role

The dependencies on deposition parameters of interface trap density, positive charge and refractive index appear to be very well correlated (see figure 5.15 and figure 5.21; figure 5.16 and figure 5.22). Because Si_3N_4 has a more rigid structure than SiO_2, it is also characterized by a higher concentration of silicon dangling bonds and a more strained interface with the silicon. A raise in oxygen concentration at the interface and in the bulk, as was noticed in the case of nitrides deposited at high pressure, can relax the stressed interface, limit the number of silicon dangling bonds, decrease the effective charge and interface trap density (fig. 5.21).

Another possibility is that the kinetic energy of the particles arriving from the plasma is lower at higher pressures and fewer defects are created due to bombardment. However, in the case of ECR oxides, the difference in the net charge was not very large when pressure was varied. Therefore, the large decrease in the positive charge and interface trap density observed in figure 5.21 and figure 5.22 can only be explained by the change in composition.

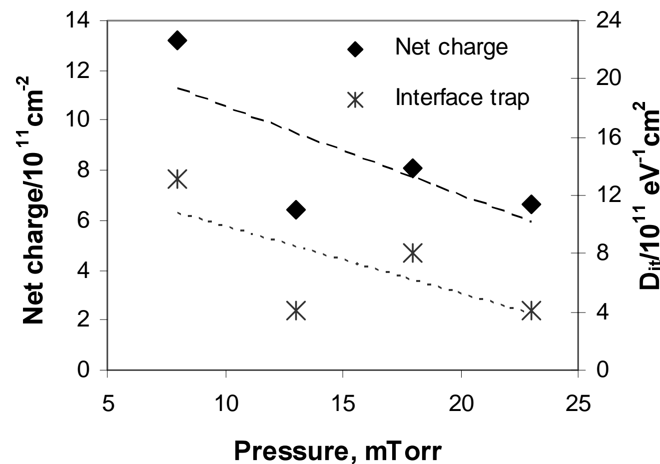

Figure 5.21. Total charge and interface trap density vs. pressure for ECR nitrides deposited with 5 sccm diluted SiH_4 and 18 sccm N_2, at 500ºC and 150 W.

Compared to LPCVD Si_3N_4 layers deposited at 800ºC and other layers obtained by ECR at room temperature [9], ECR dielectrics have lower effective charge. However the interface trap density is higher, probably due to the absence of hydrogen, which is known to saturate the dangling bonds existing at the interface [9]. The hysteresis shown in the high-frequency *C-V* measurements was only 0.01 MV/cm for the layers obtained at high pressure, and 0.085 MV/cm for the films obtained at high pressure and high N_2 flow. These values are much lower than the ones obtained for rf-PECVD nitrides or other ECR nitrides [27].

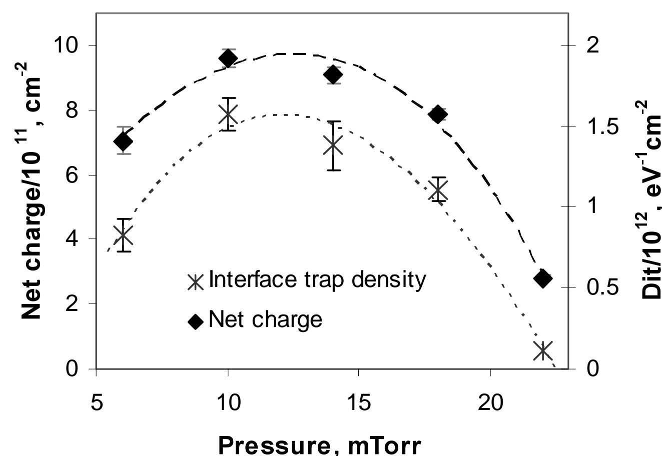

Figure 5.22. Total charge and interface trap density versus pressure for ECR nitrides deposited with 5 sccm diluted SiH_4 and 30 sccm N_2, at 400 W and without substrate heating.

5.5.2. N_2 flow role

The role of N_2 flow upon the net charge and interface trap density (figures 5.23 and 5.24) can also be explained by the oxygen atoms. At lower N_2 flows, the oxygen content in the film increases, reducing the number of defects and improving the interface. As a result, a reduction in oxide charge and interface trap density is detected at low N_2 flows (figure 5.23 and 5.24).

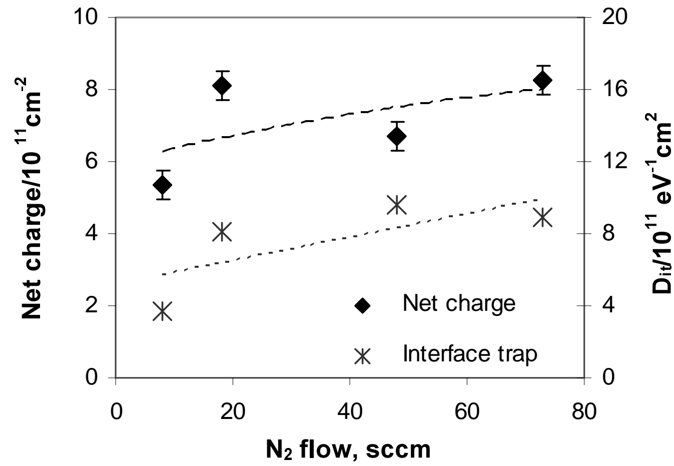

Figure 5.23. Total charge and interface trap density versus N_2 flow rate for ECR nitrides deposited with 5 sccm diluted SiH_4, at 500°C, 18 mTorr and 150 W.

The fact that layers deposited at room temperature and 400 W exhibit increased interface trap density (fig. 5.23 and fig. 5.24) is caused by the lower oxygen concentration (2 at.% in comparison with 10 at.%).

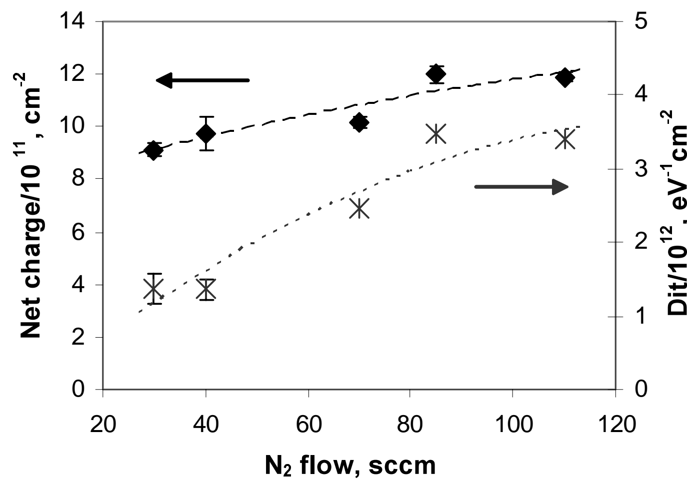

Figure 5.24. Total charge and interface trap density versus N_2 flow rate for ECR nitrides deposited with 5 sccm diluted SiH_4, at 14 mTorr, 400 W and without substrate heating.

5.5.3. Microwave power role

An increase in the net charge was observed also with increasing the microwave power as it can be observed in figure 5.25. There are two factors that can cause this behaviour: the decrease of oxygen content at high powers, due to a higher dissociation degree for N_2; and the increased plasma damage.

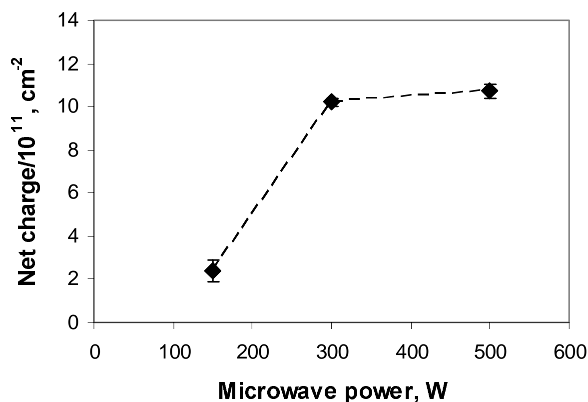

Figure 5.25. Total positive charge vs. microwave power for ECR nitrides deposited with 2 sccm SiH_4, 25 sccm N_2, 500°C and 6 mTorr.

5.5.4. Thickness role

Four films were deposited under the same conditions, but for different deposition time, thus possessing different thickness. Apparently there is not a significant difference in the positive charge and interface trap density measured in the layers, even if they were exposed different times to the plasma radiation (figure 5.26). Only the thinner film showed a worse interface.

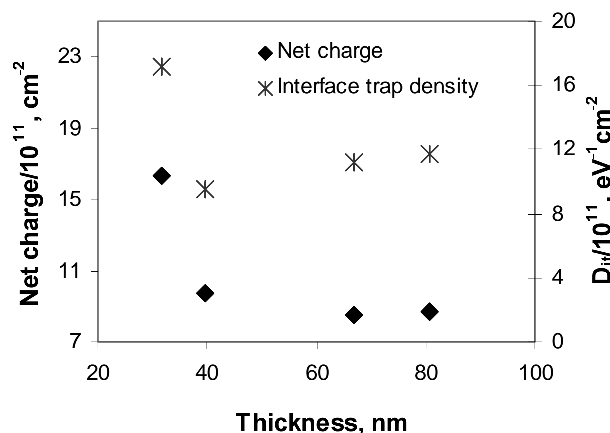

Figure 5.26. Total positive charge and interface trap density versus film thickness for ECR nitrides deposited with 5 sccm diluted SiH_4 and 40 sccm N_2, at 14 mTorr, 400 W and without substrate heating.

5.6. *J-E characteristics*

For the nitride layers, the critical field is defined as the electric field for which the current that passes through the nitride layer is higher than 10^{-8} A/cm^2, while breakdown is reached for currents higher than 10 A/cm^2. As it can be seen in fig. 5.27, the critical field marks the point where the current starts to increase. The maximum breakdown field was reached around 12 MV/cm, which is much higher than for the 300ºC rf-PECVD layers [13] and for other Si_3N_4 obtained by ECR [9, 14], probably due to the lack of hydrogen in the ECR layers.

The current that passes through the nitride can be represented as a straight line in the Poole-Frenkel graph (ln(J/E) vs. $E^{1/2}$). Therefore the measured current was fitted in figure 5.27 with a Poole-Frenkel current (section 2.5.2).

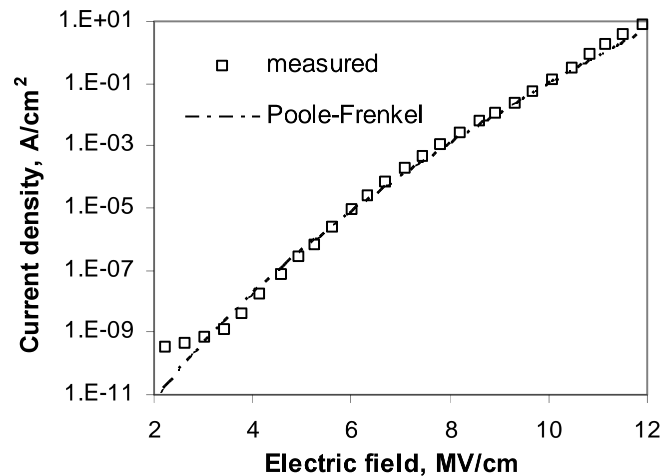

Figure 5.27. Measured current density versus electric field for a nitride deposited with 5 sccm diluted SiH_4 and 30 sccm N_2, at 14 mTorr and 400 W; and the Poole-Frenkel current fitted.

In order to verify the conduction mechanism, the current was measured for four different substrate temperatures (22ºC, 62ºC, 102ºC and 142ºC), and an almost perfect fitting was revealed in figure 5.28 for each temperature with the barrier height of the trap ϕ_T =0.94 V, the dielectric constant ε_R = 7 and the constant r =1 (see section 2.6.2). Hence, the current is described very well by the Poole-Frenkel effect.

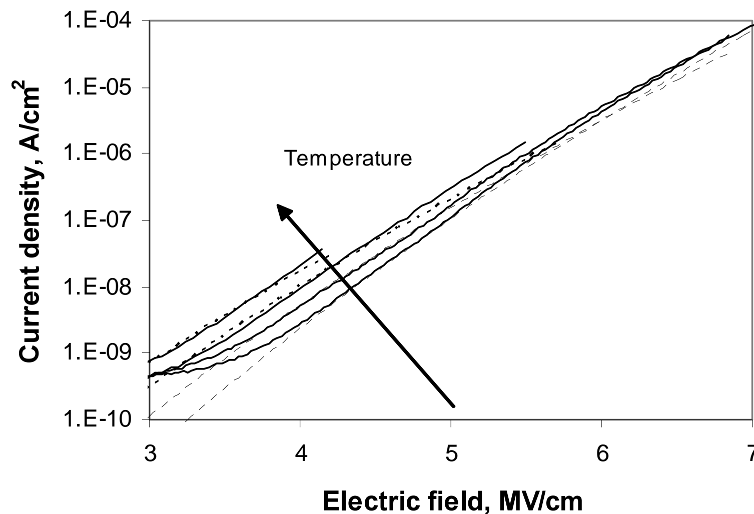

Figure 5.28. Current density measured for various substrate temperatures (22°C, 62°C, 102°C and 142°C) versus electric field for an ECR nitride deposited with 5 sccm diluted SiH_4 and 30 sccm N_2, at 18 mTorr and 400 W; and the Poole-Frenkel current fitted, ϕ_T =0.94 V.

5.6.1. Pressure role

The influence of pressure upon the breakdown field and critical field are presented in figures 5.29 and 5.30 for layers deposited at room temperature and at 500°C. Lower values of breakdown field for the films deposited at high pressure may be caused by lower efficiency in energy transfer from the plasma toward the substrate [4, 8, 11]. It is well known that the ions kinetic energy, which is responsible for densifying the layer and creating stronger bonds between the atoms, declines with pressure due to more collisions (see section 2.1.1).

Thus, the layers obtained at higher pressure suffer from earlier breakdown. The critical field increases with increasing the pressure (figures 5.29 and 5.30) most likely because of higher oxygen concentration. Because SiO_2 films exhibit critical fields of 6.5 MV/cm [28], while Si_3N_4 displays usually lower critical fields of 4 MV/cm [27] due to different conduction and trapping mechanisms. Therefore, the oxy-nitrides obtained at high pressure will have larger critical fields. This explains also, why the films deposited at 500°C, which possess 10-25 at% oxygen exhibit critical fields between 4.7 and 5.1 (figure 5.30), while the conduction process starts for room-temperature layers at much lower biases.

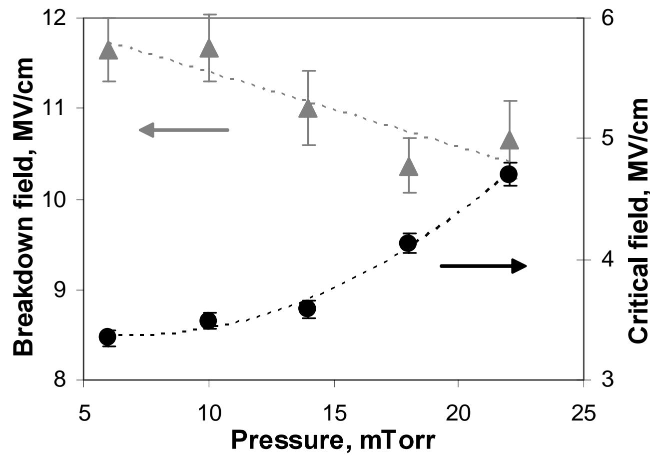

Figure 5.29. Breakdown and critical field versus pressure for nitrides deposited with 5 sccm diluted SiH_4, 30 sccm N_2 and 400 W.

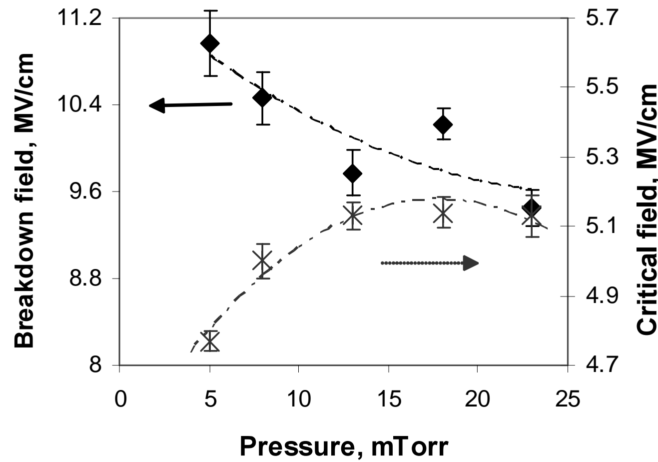

Figure 5.30. Breakdown field and critical field versus pressure for ECR nitrides deposited with 5 sccm diluted SiH_4 and 18 sccm N_2, at 500°C and 150 W.

The trap energy $q\phi_T$ and constant r were extracted from the fitted *J-E* curves and plotted versus pressure in figure 5.31. One can observe that r which takes values between 1 and 1.5 is related to the film stoichiometry, following the same trend as the oxygen content in the layers (see figure 5.16). $q\phi_T$ indicates the height of the traps in the forbidden bandgap of the dielectric. It increased from 0.67 eV to 0.94 eV with raising the pressure, suggesting that the traps are less shallow in case of oxygen contamination. Therefore, it is expected that in the case of low-pressure films, the Poole-Frenkel conduction mechanism to dominate and higher leakage currents to appear.

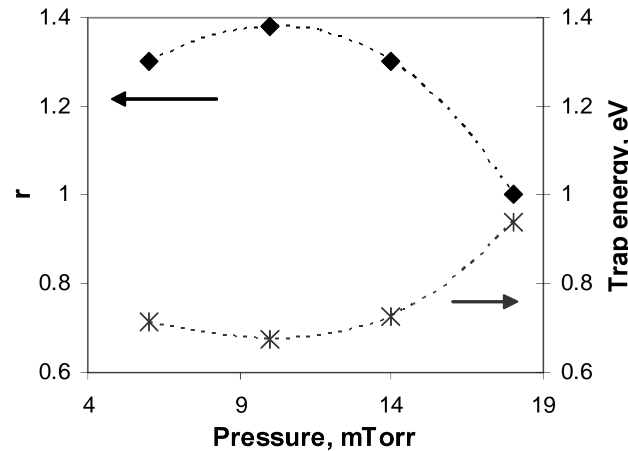

Figure 5.31. The constants r and ϕ_T versus pressure for nitrides deposited at near room temperature, with 5 sccm diluted SiH_4, 30 sccm N_2 and 400 W.

The current passing through the nitride deposited at the highest pressure of 22 mTorr, containing 15 at.% oxygen could not be fitted at high biases with the Poole-Frenkel effect, but instead exhibited Fowler-Nordheim (FN) tunnelling with a barrier energy of 2 eV (fig. 5.32). It seems that at high biases the probability of FN tunnelling becomes larger than the probability of emission from the deep traps situated in the dielectric bandgap.

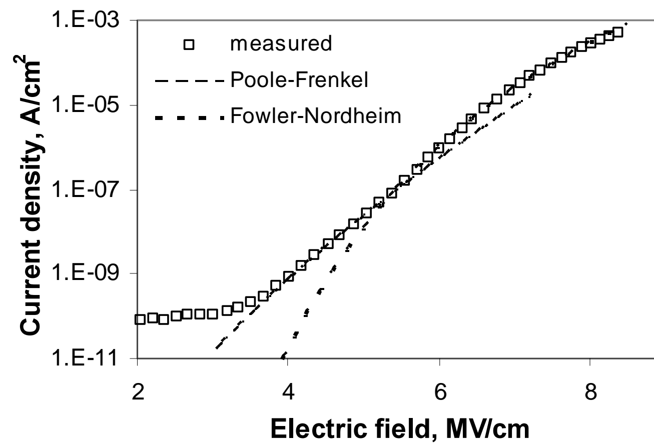

Figure 5.32. Measured current density versus electric field for a nitride deposited with 5 sccm diluted SiH_4 and 30 sccm N_2, at 22 mTorr and 400 W; the Poole-Frenkel and Fowler-Nordheim currents fitted.

5.6.2. N_2 flow role

One can observe in fig. 5.33 that the N_2 flow has insignificant influence upon the dielectric strength of films obtained at room temperature. Both critical and breakdown field have small variations within the statistical errors,

probably due to the fact that the oxygen content does not vary very much in these experiment series (fig. 5.19).

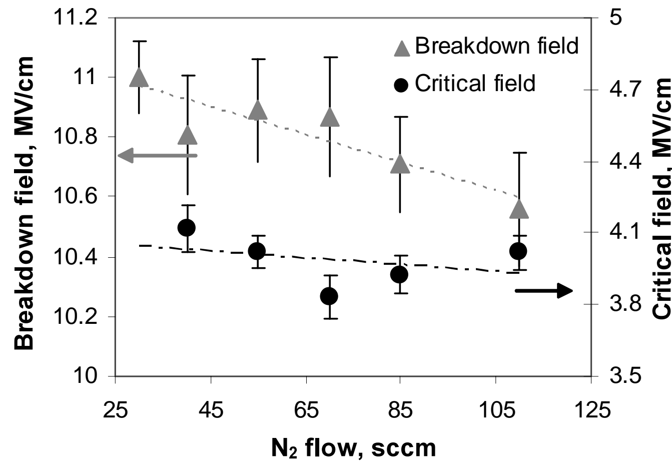

Figure 5.33 Breakdown field and critical field versus N_2 flow rate for ECR nitrides deposited with 5 sccm diluted SiH_4, at 14 mTorr, 400 W and without substrate heating.

For the layers deposited at 500°C (figure 5.34), the differences in dielectric strength are larger, due to a bigger difference in oxygen content (figure 5.18). A less efficient transfer of energy may cause the small decrease in the breakdown field at high N_2 flows from the plasma toward the substrate. The Poole-Frenkel conduction process appears for higher electric fields in case of silicon nitride layers obtained with low N_2 flow, confirming the hypothesis that in case of oxygen contamination the traps are less shallow.

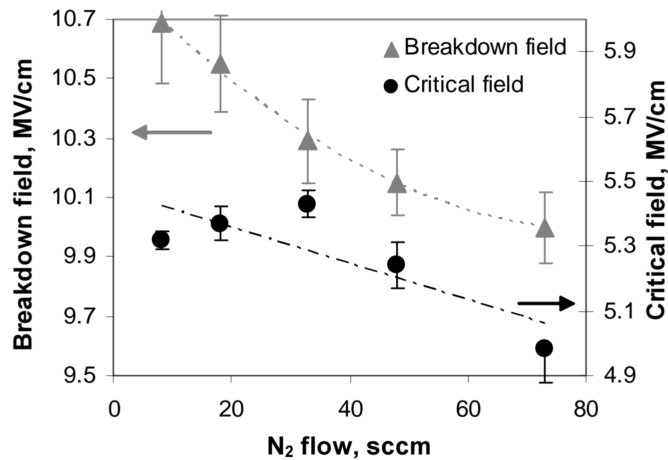

Figure 5.34. Breakdown field and critical field vs. N_2 flow rate for ECR nitrides deposited with 5 sccm diluted SiH_4 and 18 mTorr, at 500°C and 150 W.

The nitride integrity was tested by constant current stress measurements, as described in section 2.5.2. To our knowledge, the reliability of silicon nitride layers deposited by ECR PECVD was not tested until now. In fig. 5.35, the charge-to-breakdown distribution (Weibull plot) for two silicon nitride films deposited with different N_2 flow shows large maximum charge-

to-breakdown values of 90 C/cm^2. It is noticeable that the layer deposited with lower N_2 flow had improved reliability, contrary to the fact that nitrides possess higher charge-to-breakdown than oxides. It is possible that higher energy transfer from the plasma at low flows is responsible for this effect, but more research should be done for substantiation of this hypothesis.

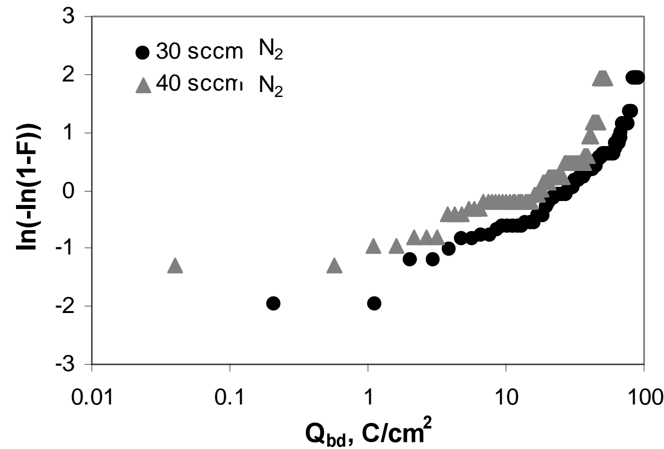

Figure 5.35. Weibull plot for nitrides deposited at near room temperature, with 5 sccm diluted SiH_4, at 14mTorr, 400 W microwave power and different N_2 flow.

5.6.3. Thickness role

While the critical field does not depend on film thickness, the breakdown field is considerably higher for thinner layers (figure 5.36). The same tendency exists also for SiO_2 films; the thinner layers possess higher breakdown field [29].

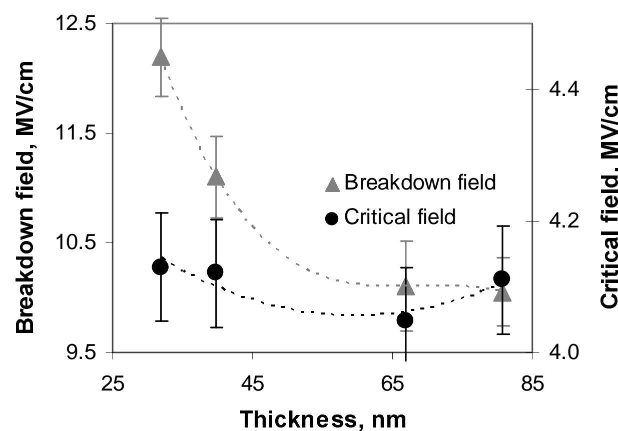

Figure 5.36. Breakdown and critical field for nitrides deposited with 5 sccm diluted SiH_4, 40 sccm N_2, at 14 mTorr, 400 W and various thicknesses.

5.7. Summary

The dependences of total pressure, N_2 flow, microwave power, SiH_4 dilution, temperature, film thickness and other deposition parameters on film properties were studied. Si_3N_4 films with a refractive index of 1.98, relative dielectric constant of 7.2, 2 at% oxygen content and 0.6 at.% hydrogen content were deposited by a multipolar ECR plasma source at near room temperature in order to determine optimal deposition conditions. Pure SiH_4 produced films with high hydrogen contamination, while diluting the SiH_4 with helium improves the film quality, diminishing the hydrogen contamination due to lower deposition rates. The oxygen contamination was minimised by decreasing the pressure and increasing the microwave power. In this way, the N_2 dissociation in plasma was improved due to a more efficient transfer of energy from the microwave source to the gas. The Si_3N_4 layers exhibited a breakdown field of 12 MV/cm, resistivity of 10^{16} Ωcm, maximum charge-to-breakdown of 90 C/cm^2 and net charge density less than 10^{12} cm^{-2}. At lower pressure and higher N_2/SiH_4 ratio films similar to LPCVD nitrides obtained at 800ºC were obtained. The extremely low hydrogen contamination was responsible for very good electric strength and film reliability, but also caused a sub-optimal interface quality. The effective charge and interface trap density, as well as the trap energy were very well correlated with the oxygen concentration. The decrease in substrate temperature from 500ºC to 60ºC did not degrade the electrical film properties. High quality Si_3N_4 layers can be deposited at near room temperature with ECR PECVD technology for 5 sccm diluted SiH_4, 55 sccm N_2, 400 W and 10 mTorr.

5.8. References

1. D.V. Tsu, G. Lucovsky, M.J. Martini, "Local atomic structure in thin films of silicon nitride and silicon diimide produced by remote plasma-enhanced chemical-vapor deposition", Phys. Rev. B **33**, pp. 7069-7076 (1986).
2. A. Sherman, Chemical Vapor Deposition for Microelectronics, Noyes Publications, 1988, p. 120.
3. F. Delmotte, M.C. Hugon, B. Agius, J.L. Courant, "Low temperature deposition of SiN_x:H using SiH_4-N_2 or SiH_4-NH_3 distributed electron cyclotron resonance microwave plasma", J. Vac. Sci. Technol. B, **15,** pp. 1919-1926 (1996).

4. S. Garcia, I. Martil, G. Gonzalez Diaz, E. Castan, S. Duenas, M. Fernandez, "Deposition of SiN_x:H thin films by the electron cyclotron resonance and its application to Al/SiN_x:H/Si structures", J. Appl. Phys. **83**, pp. 332-338 (1998).
5. D.L. Smith, A.S. Alimonda, F.J. von Preissig, "Mechanism of SiN_xH_y deposition from N_2-SiH_4 plasma", J. Vac. Sci. Technol. B, **8,** pp. 551-557 (1990).
6. Computational Optical and Discharge Physics, University of Illinois, http://uigelz.ece.uiuc.edu/data.html.
7. G. Lucovsky, T. Yasuda, Y. Ma, S. Habermehl, S.S. He, D.J. Stephens, "Low temperature plasma-assisted oxidation and thin-film deposition processes for forming device-quality SiO_2/Si and composite dielectric-SiO_2/Si heterostructures", Thin Solid Films **220**, pp. 38-44 (1992).
8. F.S. Pool, "Nitrogen plasma instabilities and the growth of silicon nitride by electron cyclotron resonance microwave plasma chemical vapor deposition", J. Appl. Phys., **81**, pp. 2839-2846 (1997).
9. D. Landheer, K. Rajesh, D. Masson, J.E. Hulse, G.I. Sproule, T. Quance, "Factors affecting interface-state density and stress of silicon nitride films deposited on Si by electron-cyclotron resonance chemical vapor deposition", J. Vac. Sci. Technol. A, **16**, pp. 2931-2944 (1998).
10. S. Garcia, J.M. Martin, I. Martil, G. Gonzalez-Diaz, "Dependence of the physical properties of SiN_x:H films deposited by the ECR plasma method on the discharge size", Thin Solid Films, **315**, pp. 22-28 (1998).
11. J.R. Flemish, R.L. Pfeffer, "Low hydrogen content silicon nitride films from electron cyclotron resonance plasmas", J. Appl. Phys. **74**, pp. 3277-3281 (1993).
12. J.C. Barbour, H.J. Stein. O.A. Popov, M. Yoder, C.A. Outten, "Silicon nitride formation from a silane-nitrogen electron cyclotron resonance plasma", J. Vac. Sci. Technol. A, **9**, pp. 480-484 (1991).
13. A.J. Flewitt, A.P. Dyson, J. Robertson, W.I. Milne, "Low temperature growth of silicon nitride by electron cyclotron resonance plasma enhanced chemical vapour deposition", Thin Solid Films **383**, pp. 172-177 (2001).
14. M. Lapeyrade, M.P. Besland, C. Meva'a, A. Sibai, G. Hollinger, "Silicon nitride thin films deposited by electron cyclotron resonance plasma-enhanced chemical vapor deposition", J. Vac. Sci. Techol. A, **17**, pp. 433-444 (1999).
15. S. Garcia, J.M. Martin, M. Fernandez, I. Martil, G. Gonzalez-Diaz, "Analysis of the oxygen contamination present in SiN_x films deposited by electron cyclotron resonance", J. Vac. Sci. Technol. A, **13**, pp. 826-830 (1995).

16. I.G. Isai, A.Y Kovalgin, J. Holleman, H. Wallinga, P.H. Woerlee, & C. Cobianu, "Electrical Characterisation of Gate Dielectrics Deposited with Multipolar Electron Cyclotron Resonance Plasma Source", Proceedings of the 30th European Solid State Device Research Conference, ESSDERC 2000, pp. 424-427.
17. S. Sitbon, M.C. Hugon, B. Agius, F. Abel, J.L. Courant, M. Puech, "Low temperature deposition of silicon nitride films by distributed electron cyclotron resonance plasma-enhanced chemical vapor deposition", J. Vac. Sci. Technol. A **13** pp. 2900-2907 (1995).
18. J.A. Theil, S.V. Hattangady, G. Lucovsky, "Effects of NH_3 and N_2 source gases and plasma excitation frequencies on the reaction chemistry for Si_3N_4 thin-film growth by remote plasma-enhanced chemical-vapor deposition", J. Vac. Sci. Technol. A, **10**, pp. 719-727 (1992).
19. K. Saito, N. Chiba, T. Fukuda, K. Suzuki, M. Ohue, "Effects of excited species in electron cyclotron resonance plasma on SiN film resistivity", Jpn. J. Appl. Phys., **31**, pp. 1102-1106 (1992).
20. G. King, F.C. Sze, P.Mak, T.A. Grotjohn, J. Asmussen, "Ion and neutral energies in a multipolar electron cyclotron resonance plasma source", J. Vac. Sci. Technol. A **10**, pp. 1265-1269 (1992).
21. P. Mak, G. King, T.A. Grotjohn, J. Asmussen, "Investigation of the influence of electromagnetic excitation on electron cyclotron resonance discharge properties", J. Vac. Sci. Technol. A **10**, pp. 1281-1287 (1992).
22. A. Sherman, Chemical Vapor Deposition for Microelectronics, Noyes Publications, 1988, p. 121.
23. S.A. Moshkalyov, J.A. Diniz, J.W. Swart, P.J. Tasch, M. Machida, "Deposition of silicon nitride by low-pressure electron cyclotron resonance plasma enhanced chemical vapor deposition in $N_2/Ar/SiH_4$", J. Vac. Sci. Technol. B, **15**, pp. 2682-2687 (1997).
24. A. Sherman, Chemical Vapor Deposition for Microelectronics, Noyes Publications, 1988, p. 45.
25. I. Jonack-Auer, R. Meisels, F. Kuchar, "Determination of the hydrogen concentration of silicon nitride layers by Fourier transform infrared spectroscopy", Infrared Physics & Technology **38**, 223 (1997).
26. B. Stannowski, J.K. Rath, R.E.I. Schropp, "Hot-wire silicon nitride for thin-film transistors", Thin Solid Films, **395**, pp. 339-342 (2001).
27. D.G. Farber, S. Bae, M. Okandan, D.M. Reber, T. Kuzma, S.J. Fonash, "Pathway to depositing device-quality 50 degrees C silicon nitride in a high-density plasma system", J. Electrochem. Soc., **146,** pp. 2254-2257 (1999).
28. G. Isai, A. Kovalgin, J. Holleman, P.W. Woerlee, H. Wallinga, "Room temperature SiO_2 films deposited by multipolar ECR PECVD", J. Phys. IV, **11**, 747 (2001).

29. A. Aassime, "High field electron trap generation and oxide breakdown in thin silicon dioxide layers", Thin Solid Films, **385**, pp. 252-254 (2001).

Chapter 6 Jet Vapour Deposition of SiO_2

Abstract

A novel deposition method, Jet Vapour Deposition has been explored. SiO_2 films have been deposited at room temperature, with a multipolar electron cyclotron resonance (ECR) plasma source and a modified manner of introducing the silane (SiH_4) gas. SiH_4 was highly diluted in a light carrier gas, helium and transported efficiently to the wafer as a supersonic jet. A convergent-divergent nozzle ensured a high velocity. The effects of SiH_4, N_2O and He flow rate, total pressure and annealing conditions on physical properties and electrical properties were studied. Increasing the helium flow, i.e. the pressure in the nozzle had beneficial effects upon the bulk properties. High-density SiO_2 films of 10-20 nm with a refractive index of 1.45, 1% voids and Si/O ratio of 1/2, an interface trap density of 10^{11} $eV^{-1}cm^{-2}$, an oxide charge concentration in the order of 10^{10}-10^{11} cm^{-2} and a breakdown field of 12 MV/cm were obtained at room temperature, low pressure, low SiH_4 flow and high helium flow.

6.1. Introduction

In order to improve furthermore the SiO_2 properties, we have explored Jet Vapour Deposition (JVD), a very good technique for obtaining silicon nitride films [1]. It is based on a high-speed jet of helium transporting the reactive gases such as SiH_4 to the wafer. N_2O is dissociated by the multipolar ECR plasma source. The deposition is fast [2], therefore the probability of gas-phase reactions is small. This technique was explored because of its advantage of ensuring extra kinetic energy for the impinging particles, therefore eliminating the need to heat the wafer in order to achieve good dielectric strength. A convergent-divergent nozzle with a large pressure difference (see section 1.3) was employed in order to obtain supersonic speeds [3].

The main disadvantage of this deposition technique is its localised nature [2]. Basically only a spot of a few cm^2, with a large nonuniformity is obtained under the nozzle. The wafer was scanned underneath the nozzle in order to ensure a good uniformity in film thickness within 5%. However, the

microwave influence upon the holder bearings seemed to interfere with the holder's movements and its lifetime.

A detailed description of the deposition system is made in section 2.2. Due to the fact that ECR is most efficient at low pressures [4] and N_2O is dissociated by ECR plasma, the pressure range for JVD was kept as in the case of ECR, at 1-25 mTorr. Other authors have shown the benefits of JVD at high pressure, but higher pressures could not be investigated with our plasma source.

The variation of gas velocity, pressure and temperature in a convergent-divergent nozzle was calculated based on the principles of fluid mechanics [3].

SiO_2 films with thickness between 10 and 20 nm were deposited at 400 W microwave power and floating temperature, without external heating. Due to plasma heating, the temperature of the substrate measured by a thermocouple bonded inside the sample holder reached a maximum of 30°C.

In this work, several deposition parameters such as pressure, film thickness, annealing processes, SiH_4, N_2O and helium flow rates were varied, while monitoring the film composition, refractive index, *C-V* and *I-V* characteristics. Correlations between the physical and the electrical properties were made, in order to detect the optimal deposition conditions. The effect of increased pressure in the SiH_4/He gas line was studied in order to show the influence of high-speed jet upon film properties. Also comparisons have been made between the ECR films and the layers obtained by JVD.

There was no data found in literature about properties of SiO_2 obtained by JVD.

6.2. Nozzle design

The nozzle has the role of accelerating the gas by converting its static enthalpy to kinetic energy. The nozzle presented in literature as the manner of obtaining supersonic jets is a convergent nozzle of 1-2 mm [2], which handles a few thousands of sccm. However it is impossible to obtain a supersonic jet with a convergent nozzle. The maximum velocity obtained in this case is the sonic speed at the exit of the nozzle [3]. The dimensions and shape of the nozzle were calculated (L and D in figure 6.1) in order to obtain a sonic speed at the nozzle throttle. The expansion of helium inside the nozzle was considered isentropic, therefore the evolution of temperature with pressure can be written:

$$T = T_0 \left(\frac{P}{P_0} \right)^{\frac{\kappa}{\kappa - 1}} \qquad (6.1)$$

where T_0 and P_0 are the temperature and pressure at the nozzle inlet, T, P the gas temperature and pressure inside the nozzle and κ the specific heat ratio for helium. By setting the nozzle angle to 12 degrees, we can calculate from the nozzle area the values for the nozzle diameter and length. The gas velocity and nozzle area can both be written as functions of temperature:

$$V = \sqrt{2c_p(T_0 - T)} = \sqrt{2c_p T_0\left[1 - \left(\frac{P}{P_0}\right)^{\frac{\kappa}{\kappa-1}}\right]} \tag{6.2}$$

$$A = \frac{\rho_0 QRT}{VPM} \tag{6.3}$$

where V is the jet velocity, A is the nozzle area, ρ_0 the gas density for standard atmospheric conditions, R the gas constant, c_p the constant pressure specific heat for helium, M the mole weight for helium and Q the helium flow rate. The inlet and outlet pressures were set to 175 Torr and 20 mTorr respectively. The pressure inside the nozzle was modified with small pressure steps, while keeping the flow constant and calculating for each pressure step the temperature, the gas velocity and the nozzle diameter and length, according to equations 6.1-6.3. The obtained nozzle shape is shown in figure 6.1.

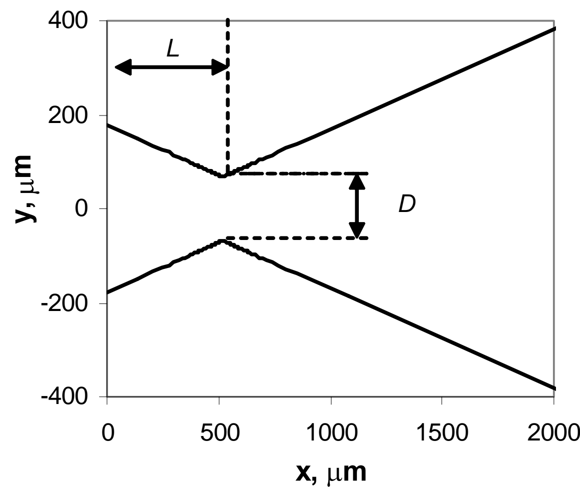

Figure 6.1. Longitudinal cross-section of the nozzle, showing shape and dimensions. L is the length of the convergent nozzle and D the diameter of the throttle.

According to the simulation results, the throat nozzle is situated at 0.5 mm from the entrance of the nozzle. In this first area, the gas is accelerated to sonic speed, as it can be seen in figure 6.2. For a flow of 20 sccm, the nozzle throat must have a diameter of 150 µm in order to reach sonic speed. The

second part of the nozzle is important for increasing the speed of the jet to supersonic speeds. A nozzle with the total length of 2 mm and the shape presented in figure 6.1 was manufactured from quartz and bonded to the gas line in the deposition chamber, as shown in section 2.2.

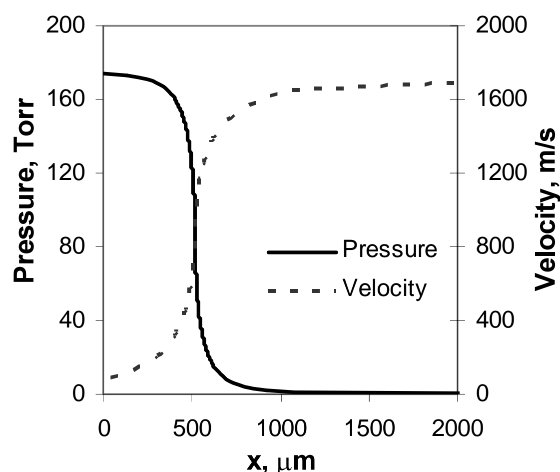

Figure 6.2. Pressure and gas velocity inside the nozzle.

Figure 6.2 shows the calculated gas pressure and velocity versus the nozzle length. As one can see, the simulation confirms the theory [3], the gas reaches sonic speeds at the throat of the nozzle, and it rises over the sonic limit in the divergent part of the nozzle. Because the process is an isentropic expansion, the gas acceleration is associated with a huge drop in gas pressure and temperature. The temperature at the nozzle exit is around 50 K.

6.3. Film composition and refractive index

SiO_2 layers of 20 nm have been deposited at rates of 0.5-1 nm/min with the system described in section 2.2. The effects of total pressure, gas flows, film thickness and other parameters on the refractive index and chemical composition have been investigated in order to find the optimal deposition conditions. The voids concentration in the layers was calculated from the refractive index value (see section 2.4). The film was modeled as a mixture of stoichiometric SiO_2 and voids. The microwave power used was set at 400 W. The substrate was not intentionally heated and the thermocouple inside the holder indicated a temperature of 30°C.

The deposition rate was lower than in the case of ECR plasma, due to the fact that the deposition is localised at the nozzle outlet. A scanning substrate holder was required in order to ensure good film uniformity and the film deposition rate was decreased due to the scanning process.

The pressure at the entrance of the nozzle during the experiments was between 5 and 175 Torr, depending on the diluted SiH_4 flow.

6.3.1. Pressure influence

From the spectroscopic ellipsometry (SE) measurements, it can be observed that the refractive index decreases with increasing the total pressure in the deposition chamber (figure 6.3). This was interpreted as an increase in the concentration of voids, which were calculated from the SE measurements as described in section 2.4. As in the case of ECR films obtained at different pressure, the explanation of lower density at higher pressure lies in the lower surface bombardment (Section 3.3.2 and 3.4.3) [5].

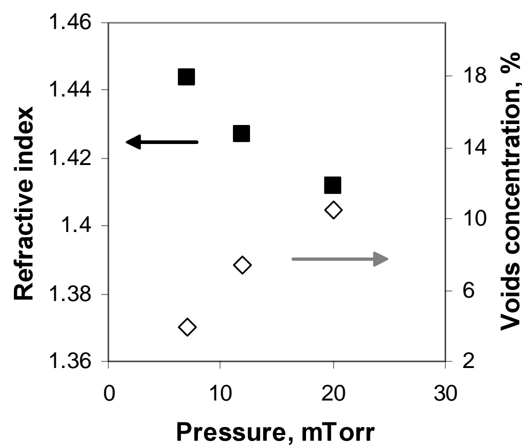

Figure 6.3. Refractive index and voids concentration for layers deposited with 20 sccm N_2O and 5 sccm diluted SiH_4 flow.

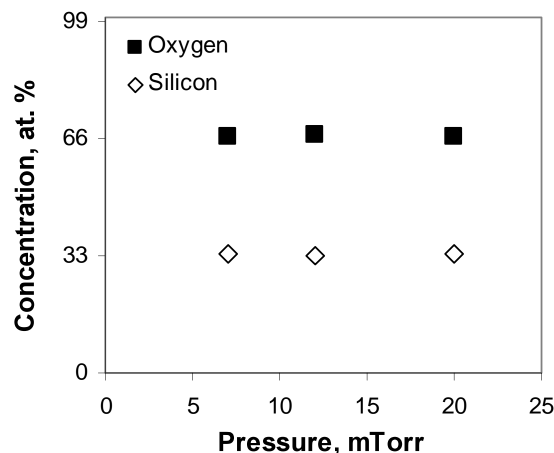

Figure 6.4. Chemical composition of layers deposited with 20 sccm N_2O and 5 sccm diluted SiH_4 flow.

In calculating the voids concentration, it was assumed that the layers composition is stoichiometric. The variation in silicon concentration observed in figure 6.4 is within the error margin of the measurement. Thus, our assumption is correct, and the decrease in refractive index with pressure is caused not by a change in composition, but by lower film density i.e. increased voids incorporation. All the layers had thickness between 18 and 20 nm.

6.3.2. SiH_4 flow influence

The composition of the film is homogeneous and very close to the one of thermally grown oxide, as it can be seen in figure 6.5. The atomic concentration was calculated by averaging the concentration at various depths into the bulk film and presented in table 6.1. A higher SiH_4 flow increases slightly the silicon concentration in the layers, decreasing the O/Si ratio from 1.996 to 1.964 (Table 6.1).

Table 6.1. Refractive index, voids concentration and composition for layers of 27 nm, deposited at 20 mTorr, with 100 sccm N_2O and different diluted SiH_4 flow.

Diluted SiH_4 flow, sccm	Refractive index	Voids conc., %	O, at.%	Si, at.%	O/Si ratio
5	1.448	1.9	66.62	33.37	1.996
10	1.450	2.6	66.35	33.78	1.964

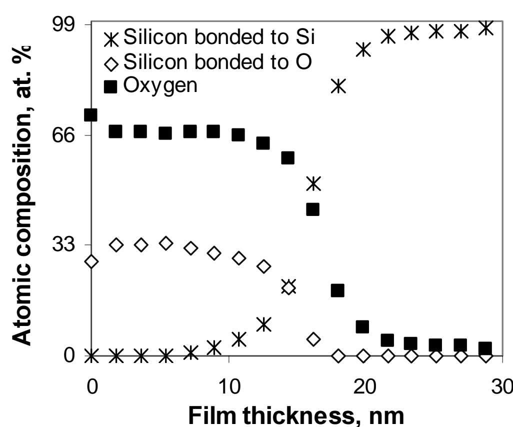

Figure 6.5. XPS depth profile for a layer deposited at 20 mTorr, with 5 sccm diluted SiH_4, and 20 sccm N_2O.

The refractive index increased, slightly (table 6.1), from 1.448 to 1.450, probably due to the small increase in silicon content. The voids concentration

increased with increasing SiH_4 flow rate, most likely because of the fact that the deposition rate doubled.

The differences in the film composition and density with modifying the SiH_4 flow are very small, within the measurement error. However these small changes causes considerable deterioration of the electrical bulk properties (see figure 6.7).

6.3.3. N_2O flow rate influence

The O/Si ratio does not change significantly, with increasing the N_2O flow from 20 sccm to 100 sccm. N_2O flow has no significant influence upon the film composition, due to the fact that there are sufficient oxygen radicals created in the plasma to oxidise completely all the SiH_4 molecules in the chamber.

Table 6.2. Refractive index, voids concentration and composition for layers deposited with 5 sccm diluted SiH_4 flow, at 20 mTorr and various N_2O flow.

N_2O flow sccm	Thickness nm	Refractive index	Voids conc., %	O at.%	Si at.%	O/Si ratio
20	20	1.412	10.5	66.55	33.44	1.990
100	27	1.448	1.9	66.62	33.37	1.996

Although the composition is similar, a large decrease in the refractive index (from 1.46 to 1.427) and a huge increase in the voids concentration (from 0.4% to 7.4%) were observed for the layers obtained at different N_2O flow rates (table 6.2). Apparently the layer deposited with lower flow was more porous. However the electrical properties of the layer deposited with lower N_2O flow, i.e. high void concentration were much better (figure 6.11). In addition, the refractive index and density of the ECR oxides exhibited an opposite tendency with the N_2O flow, due to a lower energy transfer from the plasma (figure 3.14). Because the layer obtained with 20 sccm N_2O is 8 nm thinner than the one obtained with higher flow, the effect of thickness upon the ellipsometry measurements was studied in the next section (see section 6.3.4).

6.3.4. Thickness influence

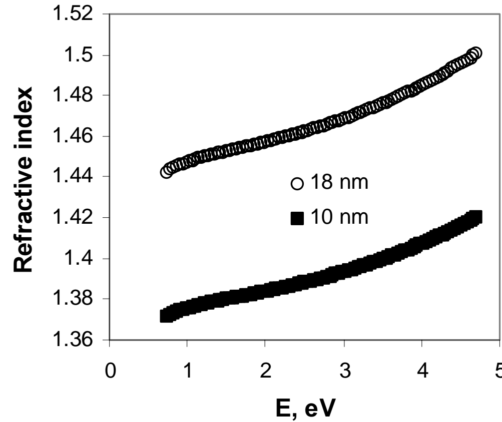

Figure 6.6. Refractive index as a function of the spectral energy for two layers deposited at 12 mTorr, with 5 sccm diluted SiH_4 flow and 20 sccm N_2O flow.

Thinner films contained much more oxygen than the thicker ones, though only the bulk composition was taken in consideration. A layer of 18 nm contained 66.67 at.% oxygen, while a thinner layer of only 10 nm deposited in the same conditions shows 68.2 at.% oxygen. The cause of excess oxygen in thinner layers was not yet clarified and it is still under investigation. The value of the measured refractive index was considerably lower for the thinner film (figure 6.6). The cause cannot be only the lower silicon incorporation, but is probably the large increase in the error of spectroscopic ellipsometry measurements for very thin layers. In the calculation of refractive index, the interface layer was not considered, and it is known that the interface plays a more important role in the thinner films.

6.4. J-E characteristics

In order to investigate also the electrical properties of the layers, MOS capacitors with an area of 0.01 mm^2 were made as described in section 2.5 and *J-E* (current density – electric field) curves were measured (Section 2.5.2) after a post-metallization-anneal (PMA) step at 400°C for 5 min in wet N_2 ambient.

The effects of different deposition parameters on the film electrical properties were investigated in order to find the optimal deposition conditions. The influences of helium flow and gas line pressure have been investigated in order to determine the importance of the high-speed jet upon the film properties.

As observed earlier for the oxides deposited by ECR PECVD (Section 4.3.1), the layer deposited with 20 sccm SiH_4 flows exhibits a much higher leakage current than the one obtained with 5 sccm diluted SiH_4 (Figure 6.7). The small excess of silicon and the higher presence of voids shown in Section 6.3.2 degrade the dielectric strength quite drastically, increasing the current by four orders of magnitude. The current shown in figure 6.7 reaches a saturation region whose extent is also an indication of the trap concentration caused by silicon dangling bonds [7].

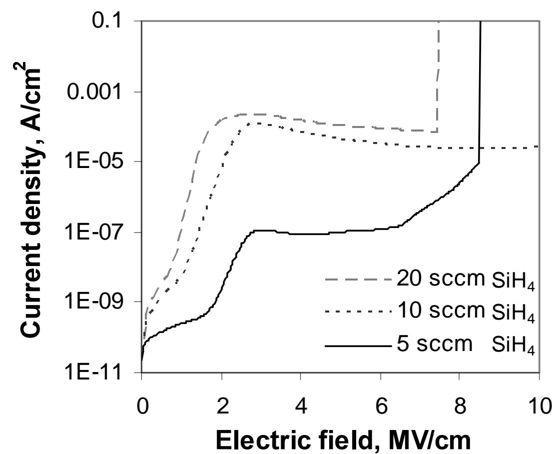

Fig. 6.7. *J-E* characteristics for layers deposited at 20 mTorr, with 100 sccm N_2O and different diluted SiH_4 flow.

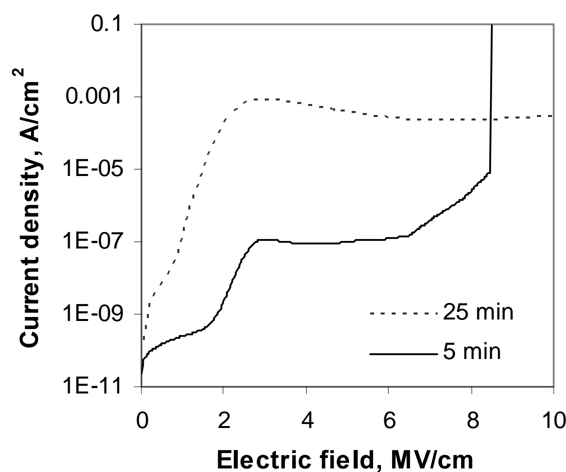

Figure 6.8. *J-E* characteristics for layers deposited at 20 mTorr, with 100 sccm N_2O, 5 sccm diluted SiH_4 flow and various delay time between introducing the gas flow and plasma ignition.

The current is influenced by the delay time between the introduction of gases into the reaction chamber and plasma ignition. As one can see in figure 6.8, the current increases by four orders of magnitude when the delay time

changes from 5 to 25 minutes. A possible explanation is the deposition of amorphous silicon at the interface due to the high-energy jet of SiH_4 impinging on the wafer, in the absence of plasma. In order to avoid these detrimental effects, the layers described below were deposited with minimum delay time.

The influences of the total pressure in the chamber and the pressure in the SiH_4/helium gas line upon the *J-E* characteristics have been investigated next. By comparing the *J-E* characteristics of two SiO_2 films deposited at various chamber pressures (figure 6.9), it can be observed that the current passing through the low-pressure oxide is dominated by the Fowler-Nordheim tunnelling [8], while the current for the high-pressure oxide exhibits a shoulder due to a higher density of traps [9]. It seems that due to a lower density (see section 6.3.1) at elevated pressures, more bulk traps are created during electric stress and the leakage current is increased. Therefore, the main conduction mechanism is trap-related (see section 4.4.2) [10] for electric fields around 5 MV/cm (figure 6.9).

In order to verify the beneficial role of the nozzle, an experiment with extra helium flow was carried out. Namely, 20 sccm of pure helium was added in the SiH_4/He gas line. The pressure in the gas line, measured with a barometer, increased from 5 Torr for 5 sccm of diluted SiH_4 flow to 35 Torr for 5 sccm diluted SiH_4 flow and 20 sccm He. One can observe in figure 6.10 that adding the helium flow has a beneficial role upon the deposited layer, decreasing the leakage current, although the total pressure in the gas chamber was kept constant at 20 mTorr. By this approach, high quality layers, similar to the films deposited at a low pressure of 7 mTorr can be deposited at a much higher pressure. This proves the importance of the high pressure at the entrance of the nozzle, which is responsible for the high speed of the jet.

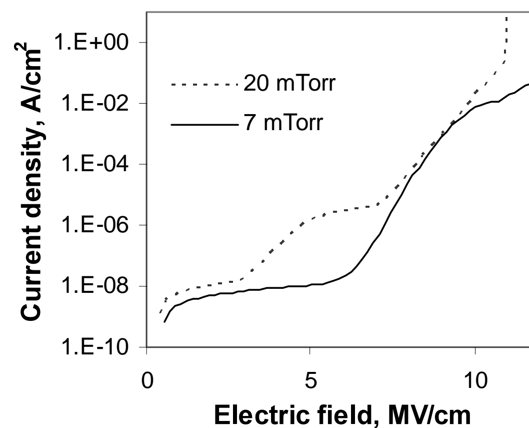

Figure 6.9. *J-E* characteristics for layers deposited with 5 sccm diluted SiH_4 and 20 sccm N_2O, at 7 and 20 mTorr.

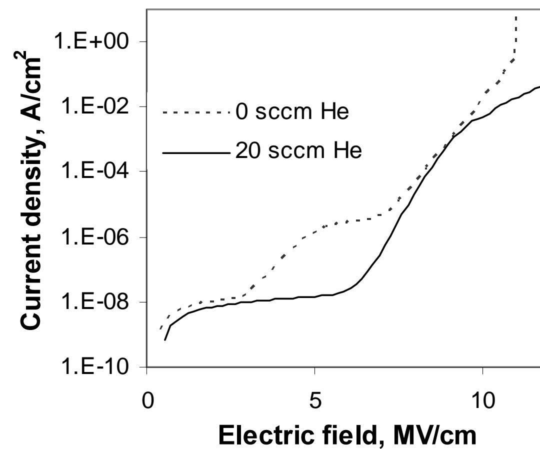

Figure 6.10. *J-E* characteristics for layers deposited at 20 mTorr, with 5 sccm diluted SiH_4, 20 sccm N_2O and various He flows.

The electrical properties are better for films obtained with low N_2O flows in terms of leakage current and breakdown field, as it can be seen in figure 6.11, despite the larger departure from thermally grown oxide for the layer obtained at lower N_2O flow (Section 6.3.3).

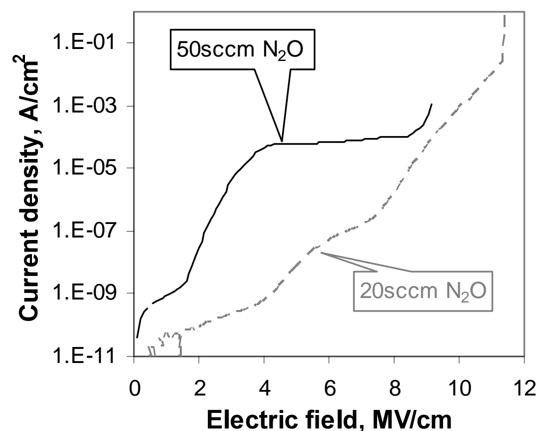

Figure 6.11. Current density versus electric field for a layer deposited at 12 mTorr, with 5 sccm diluted SiH_4 flow and various N_2O flows.

The *J-E* characteristics were not influenced by the film thickness, despite the difference in refractive index and interface role. The best JVD dielectrics exhibit *J-E* characteristics similar to the ones of thermally grown oxide.

6.5. C-V characteristics

High frequency and quasistatic *C-V* measurements of the SiO_2 layers have been carried out on MOS capacitors prepared as described in section 2.5. The high-quality interface is revealed by the *C-V* curves shown in figure 6.12, for

dielectrics deposited at various pressure. With decreasing the pressure, the shift in the flatband voltage increases, while the interface trap density is reduced. It seems that at lower pressures, due to the high-energy bombardment, there is more positive oxide charge accumulated in the layer. Nevertheless, the bombardment has a beneficial effect in terms of migration of radicals on the film surface, creating stronger bonds and diminishing the interface trap density [5]. The net oxide charge was calculated from the flatband voltage to be in the order of 10^{10} cm^{-2} for the best films, while the interface trap density was 10^{11} $eV^{-1}cm^{-2}$. The dielectric deposited at near room temperature with our deposition system has proven to have a better interface than the reference layer obtained at 300ºC by rf-PECVD.

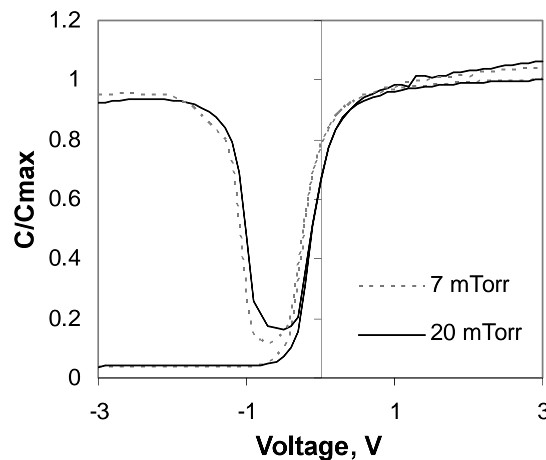

Figure 6.12. *C-V* characteristics for layers deposited with 5 sccm diluted SiH_4, 20 sccm N_2O and at various pressures (7 and 20 mTorr).

6.6. Annealing effect

Because the films described above were annealed, the influences of various annealing processes upon the bulk and interface properties were investigated. It is observed in figure 6.13 that the bulk properties are not significantly influenced by either the post-deposition-anneal (PDA) or by the post-metallization anneal (PMA) described in section 2.5.

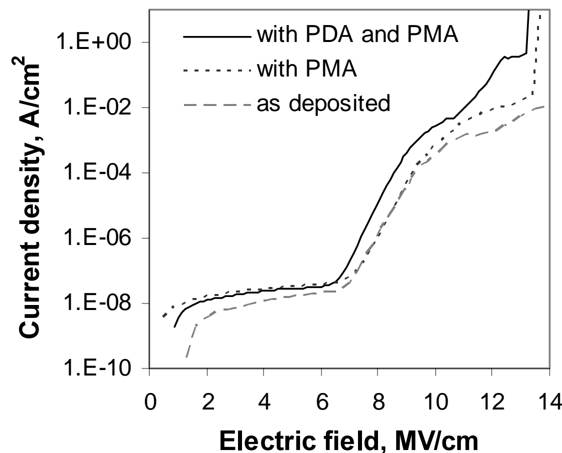

Figure 6.13. *J-E* characteristics for layers deposited at the same conditions, with various annealing processes.

The film deposited at near-room temperature exhibited the same resistivity, leakage current, breakdown field and conduction mechanism as the ones that received annealing processes at 400°C or 500°C. This confirms the high quality of the dielectrics obtained by ECR plasma and a jet of SiH_4/helium.

The *J-E* curves presented in fig. 6.13 belong to layers obtained with high helium flow. The films obtained without helium, thus with low pressure in the SiH_4/He line were not influenced by the PDA whereas the 5 minute post-metallization step had a small influence upon the *J-E* characteristics (figure 6.14).

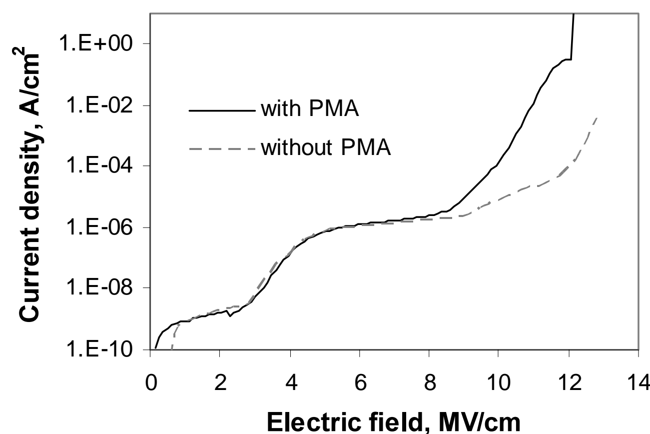

Figure 6.14. The effect of post-metallization anneal upon the *J-E* characteristics of layers deposited without helium flow.

From figure 6.14 it is concluded that the layer obtained without helium flow possesses more bulk traps and does not exhibit Fowler-Nordheim tunnelling before annealing. This shows once more the beneficial role of the high-speed jet.

The significance of annealing processes upon the interface properties was also studied. In figure 6.15, the *C-V* curves of two layers deposited at the same parameters are presented. Both layers have been subjected to post-metallization-annealing, but only one had post-deposition annealing. As one can see, the differences in terms of interface trap density and oxide charge are very small. The interface trap density is slightly lower after annealing, probably due to saturation of dangling bonds at the interface.

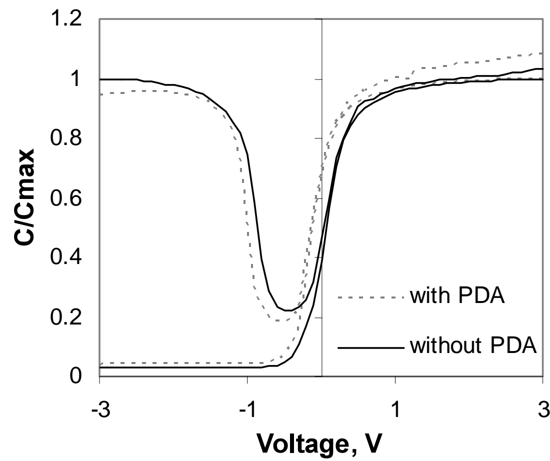

Figure 6.15. *C-V* characteristics for layers deposited at the same conditions and subjected to various annealing processes.

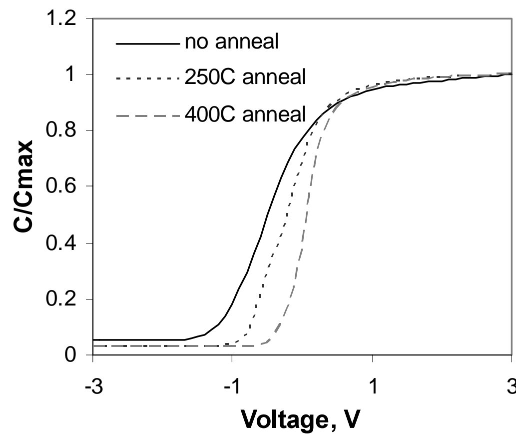

Figure 6.16. The effect of post-deposition annealing (PDA) upon the interface.

Next, the effect of post metallization anneal (PMA) upon the high-frequency C-V curves of deposited films is shown in figure 6.16. None of the layers were subjected to PDA, and after the aluminium gates were formed, one layer was annealed in a wet ambient for 5 minutes at 250°C, while another was annealed at 400°C for the same period of time. From the *C-V* curves in figure 6.16, it is concluded that both the oxide charge and interface

trap density decrease after each of the annealing processes, and that the improvement of the interface was better for elevated annealing temperatures. The elimination of traps and positive charge was not encountered during the post-deposition anneal process, in the absence or presence of PMA. Therefore, it seems that this effect is caused by reactions of aluminium with vapour molecules and release of hydrogen atoms that saturate the dangling bonds at the Si/SiO_2 interface.

6.7. Summary

It has been shown that the novel deposition method is promising for deposition of high-quality dielectrics with very low thermal budget. SiO_2 layers with a refractive index around 1.46 and stoichiometric O/Si ratio of 1.95 and less than 1% voids were deposited at room temperature by a multipolar ECR plasma source and a high-speed jet of SiH_4/helium. The layers exhibited very good electrical quality: breakdown field of 12 MV/cm, net oxide charge density in the order of 10^{10} cm^{-2} and interface trap density of 10^{11} $eV^{-1}cm^{-2}$. In order to optimise the deposition process, the effects of total pressure and gas flows on film properties were studied. At lower pressure and higher helium flow, due to increased energy transfer to the substrate, denser films with higher refractive index, less voids, stoichiometric composition and lower leakage current were deposited. Post-deposition anneal had no significant effect upon the film properties, while the post-metallization anneal step improved only the interface. The layers obtained with increased pressure in the SiH_4/He gas line possessed the best quality. Optimised layers can be obtained with 5 sccm SiH_4 flow, 20 sccm He, 20 sccm N_2O, 10 – 15 mTorr and 400 W.

6.8. References

1. T.P. Ma, "Making silicon nitride film a viable gate dielectric", IEEE Trans. El. Dev. **45**, pp. 680-690 (1998).
2. B.L. Halpern, J.J. Schmitt, "Multiple jets and moving substrates: Jet Vapor Deposition of multicomponent thin films", J. Vac. Sci. Technol. A, **12,** pp. 1623-1627 (1994).
3. R.W. Fox and A.T. McDonald, Introduction to Fluid Mechanics, Wiley, John & Sons, Incorporated, 1998, pp. 614.
4. S. Sitbon, M.C. Hugon, B. Agius, F. Abel, J.L. Courant, M. Puech, "Low temperature deposition of silicon nitride films by distributed electron

cyclotron resonance plasma-enhanced chemical vapor deposition", J. Vac. Sci. Technol. A **13** pp. 2900-2907 (1995).

5. J.R. Flemish, R.L. Pfeffer, "Low hydrogen content silicon nitride films from electron cyclotron resonance plasmas", J. Appl. Phys. **74**, pp. 3277-3281 (1993).
6. F. J. Kampas, Semiconductors and Semimetals, **21** A 153 (1984).
7. V. S. Lysenko, I. P. Tyagulski, Y. V. Gomeniuk, I. N. Osiyuk, "Effect of traps in the transition Si/SiO_2 layer on input characteristics of SOI transistors", Microelectronics reliability **40**, pp. 799-802 (2000).
8. E. Kameda, T. Matsuda, Y. Emura, T. Ohzone, "Study of the current-voltage characteristics in MOS capacitors with Si-implanted gate oxide", Solid-St. Electron., **42** 2105 (1998). 43, pp. 555-563 (1999).
9. B. L. Yang, H. Wong, Y. C. Cheng, "Study of process-dependent electron-trapping characteristics of thin nitrided oxides", Solid-St. Electron. **37**, pp. 481-486 (1994).
10. G. Isai, J. Holleman, H. Wallinga, P. Woerlee, "Electrical conduction processes in silicon oxide films obtained by ECR PECVD", Proceedings of SAFE2001, The Netherlands, p. 76.

Chapter 7 Transistors with low temperature gate dielectric

Abstract

In order to confirm the quality of ECR deposited dielectrics, p-channel metal-oxide-semiconductor-field-effect-transistors (PMOSFETs) and n-channel thin-film-transistor (TFTs) with low-temperature silicon oxide and silicon nitride gate dielectrics have been made. Simple process flows with only three or four masks were chosen for testing the dielectrics. The transistors exhibited low off-currents in the range of $10^{-12}A$*, low subthreshold slopes of 0.26-0.35 V/dec. and 1/2 of the mobility of the reference transistors with thermally grown* SiO_2*. The threshold voltage for different low-temperature gate dielectrics varied between 1.25 V and 2.5 V, similar values with the ones obtained for the reference transistors. Thin film transistors with large grain silicon and low temperature dielectric have been fabricated and measured. High electron mobilities (300-400* cm^2/Vs*) and low threshold voltage of -1 V were obtained for these TFTs.*

7.1. Introduction

One of the main applications for low temperature dielectrics is development of TFTs with high-mobility carriers for circuits on glass. Because a-Si:H TFTs and poly-Si TFTs have low mobility, it is difficult to investigate the influence of the gate dielectric on the carrier mobility with such devices. Therefore the multipolar ECR insulators were tested as gate dielectrics for PMOSFETs and large grain n-channel TFTs [1].

A simple process flow for MOSFETs was developed in order to demonstrate the feasibility of low-temperature insulators as gate dielectrics. Although the dopant diffusion was performed at high temperature there were no high-temperature steps after the low-temperature deposition of the dielectric. Therefore, the device properties were improved only by the aluminum-sintering step described in section 2.5.

ECR Plasma deposited SiO_2 was used for the fabrication of high mobility thin film transistors in cooperation with Delft Institute of Microelectronics and Submicron Technology (DIMES) in Netherlands.

The influence of the deposition temperature of the gate oxide and annealing processes on the transistor parameters were monitored. The devices have been compared with reference transistors realised with SiO_2 grown at 1050°C.

7.2. MOSFET fabrication

PMOSFETs have been fabricated on n-type crystalline silicon (Si). Because all the MOS and MNS capacitors, described in the previous chapters were fabricated on n-type Si, the same substrate was used for transistor fabrication. Two different types of dielectrics have been tested: ECR SiO_2 and Si_3N_4 obtained at 500°C and ECR SiO_2 deposited without external heating. The PMOSFET process flows are presented in paragraph 7.2.1 for gate dielectrics deposited at 500°C and in paragraph 7.2.2 for near room temperature gate dielectrics.

7.2.1. Transistors with low temperature gate dielectric

A simple fabrication process requiring only 3 masks was used in order to minimise the processing time. In figure 7.1 the process flow of PMOSFETs is presented. The complete process flowchart is presented in annex A.1.

Source and drain regions were formed by diffusion of boron (B) into the substrate at temperatures of 1050°C. The source of boron was a B-doped SiO_2 layer of 100 nm deposited by silox. During diffusion and activation of boron at 1050°C, a layer of SiO_2 was grown. It was subsequently etched and the gate dielectric of 60 nm was deposited by ECR PECVD at 500°C. Transistors with both SiO_2 and Si_3N_4 as gate dielectrics have been made. Aluminium (Al) was used as gate material and for connecting the source and drain. A titanium-tungsten (TiW) barrier of 70 nm was sputtered before depositing the Al layer. On the backside of the wafer Al was also sputtered in order to insure a good bulk contact. An annealing process in N_2 wet ambient, at 400°C was performed for 30 min.

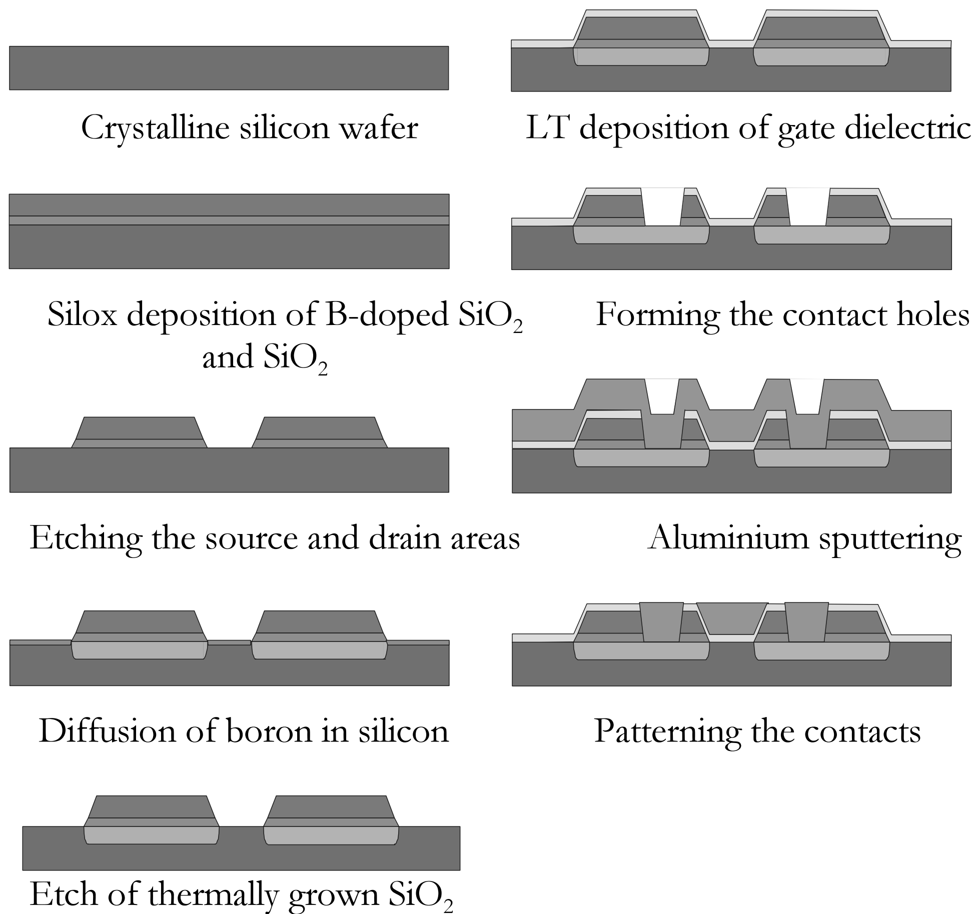

Figure 7.1. Process flow of PMOSFETs with low temperature gate dielectric.

7.2.2. Transistors with near room temperature gate dielectric

The SiO_2 layers obtained with the ECR plasma source, without intentional heating of the substrate have been also tested as gate dielectrics. The process flow was slightly modified [2] in order to isolate the active areas better than for the transistors described in the previous paragraph. The initial Si wafers were n-type with a low phosphorous (P) doping of around 10^{15} cm^{-3}. Due to the existent positive oxide charge at the Si/SiO_2 interface and the low doping, the Si substrate is in inversion even without applying a bias on the gate. In order to prevent the charges to flow from a transistor to another, a field stopper was realised by increasing the doping of the Si substrate outside the active areas. A P-doped SiO_2 layer of 100 nm was deposited by silox and the Si layer was doped by thermal diffusion with a calculated dopant concentration of 10^{19}cm^{-3}. A mask was added in the previous process flow in order to define the active area (figure 7.2).

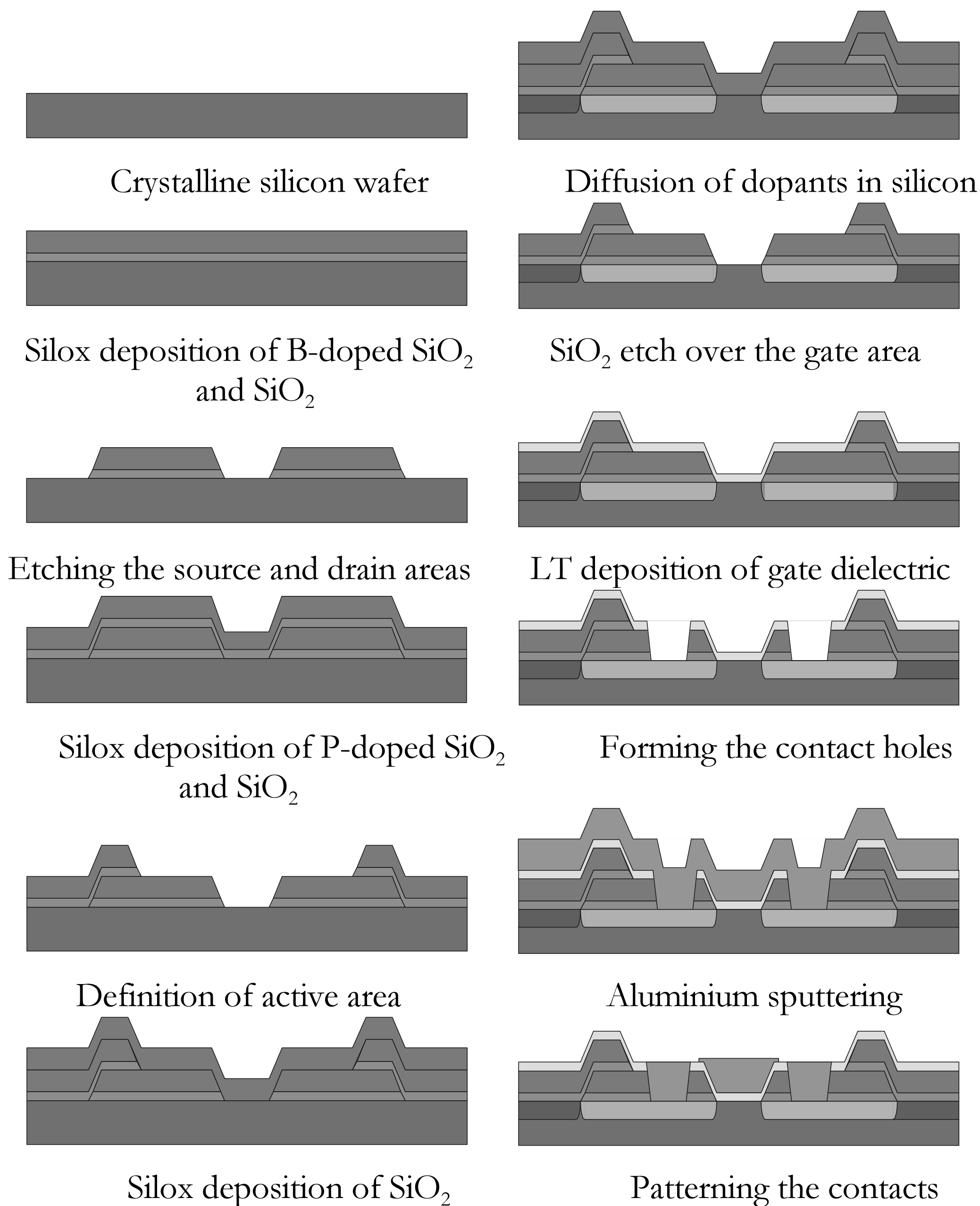

Figure 7.2. Process flow of PMOSFETs with near room temperature gate dielectric.

Another improvement was to protect the gate area during the furnace diffusion step. It is possible that dopant atoms diffuse out of the doped glass into the surrounding environment and are then re-deposited on the bare silicon surface where the gate dielectric will be deposited later on. To prevent this, besides capping all doped silox layers with an undoped SiO_2 layer, the gate area was protected with an undoped SiO_2 layer during the diffusion step.

Figure 7.2 shows the process flow for the transistors realised with near room temperature gate dielectric. The fabrication process is described in detail in annex A.2. The SiO_2 ECR PECVD film was obtained at a

microwave power of 400 W, with 5 sccm of SiH_4, 20 sccm of N_2O and at a pressure of 6 mTorr. The substrate was not intentionally heated and the thermocouple bonded in the holder indicated a temperature of 50ºC. Because no barrier layer was sputtered, the post-metallization annealing step was limited to 5 min.

7.3. MOSFET structures

Several test structures have been implemented on the wafer such as: MOSFETs, capacitors, gated diodes and Van der Pauw structures. The standard transistors have a gate length of 10 μm and 50 μm width as shown in figure 7.3. Overlaps of 5 μm and 10 μm were insured to prevent disastrous effects due to errors of alignment and overetching the layers.

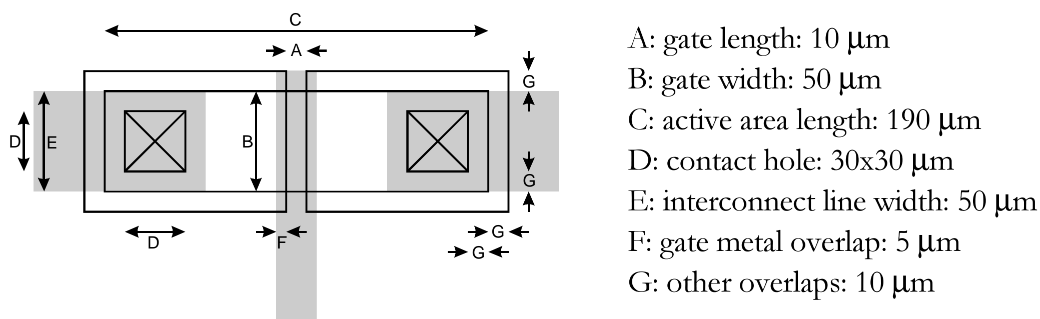

Figure 7.3. Transistor layout with the design parameters.

One die contains 24 of these transistors. Another type of die contains 20 transistors with various widths and lengths, which were used to study the effects of gate dimensions upon the transistor characteristics. The layout of this die is shown in figure 7.4.

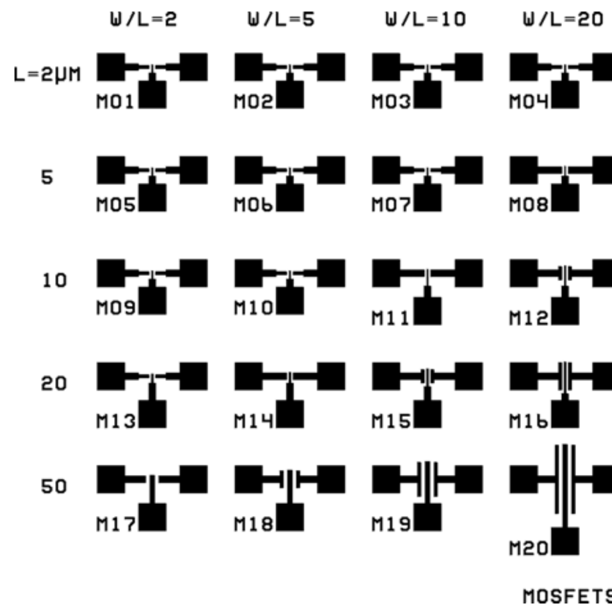

Figure 7.4. Layout of a die with transistors of various dimensions.

In figure 7.5 photographs are shown of the active area before the metallization step (a), and of the transistor after aluminium definition (b).

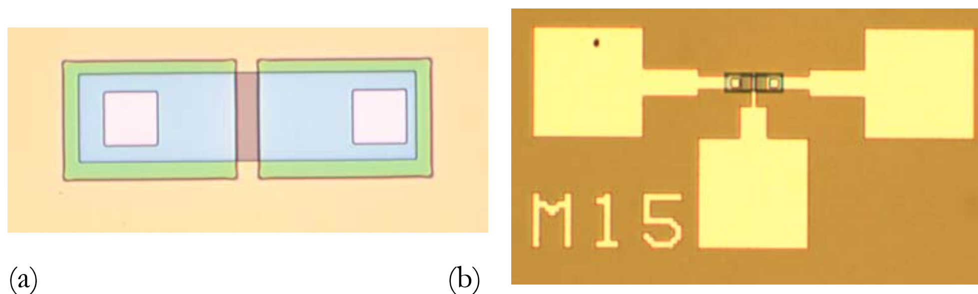

(a) (b)

Figure 7.5. Photographs of front-end and back-end of the MOSFETs.

7.4. *Transistors characteristics*

The output characteristics (figure 7.6) and the transfer characteristics (figure 7.7) of the built transistors have been measured. The transconductance (g_m) was calculated as the drain current (I_D) variation with a small gate voltage (V_G) variation while keeping the drain-source voltage constant (V_{DS}) [3]:

$$g_m = \left.\frac{\partial I_D}{\partial V_G}\right|_{V_{DS}} \tag{7.1}$$

From the intersection of the extrapolation of the g_m curve with the x-axis, the value for the threshold voltage (V_T) was extracted.

For $V_{DS} \geq V_G$-V_T, the MOSFET operates in the saturation regime, i.e. the drain current is approximately constant with V_{DS}:

$$I_D = \frac{\mu_h W C_{ox}}{2L}(V_G - V_T)^2 \tag{7.2}$$

where W and L are the width and the length of the transistor's gate and C_{ox} the gate dielectric specific capacitance.

The hole mobility (μ_h) was calculated based on the measured drain current for low $V_{DS} < V_G$-V_T and gate voltage of –7 V:

$$I_D = \frac{\mu_h W C_{ox}}{L}\left[(V_G - V_T)V_{DS} - \frac{1}{2}V_{DS}^{\ 2}\right] \tag{7.3}$$

The subthreshold swing (SS) can be measured from the transfer characteristics, when the transistor is in the subthreshold regime, i.e. $V_G < V_T$ and the channel is in weak inversion. It is defined as the gate voltage required for increasing the drain current with one decade:

$$SS = \ln(10)\left.\frac{\partial V_G}{\partial(\ln I_D)}\right|_{V_{DS}} \tag{7.4}$$

A good transistor should have a low threshold voltage, so that the transistor can be turned on, i.e. reach saturation regime at low gate voltages and exhibit high drain current. Furthermore, in order to reach large drain currents, it should also possess a high mobility. In addition, low subthreshold swing and off current are desired if the transistor is used as a switching device.

7.4.1. Gate dielectrics deposited at 500°C

First the transistors with 500°C ECR PECVD gate oxide have been investigated. The gate dielectric is a 60 nm SiO_2 ECR layer, deposited at 500°C, 20 mTorr and 150 W, with 5 sccm N_2O and 5 sccm 2% SiH_4 diluted in He and the dimensions of the gate are: W/L = 600 μm/100 μm. The measured output and transfer characteristics are shown in figures 7.6 and 7.7.

The drain current remains approximately constant after the transistor reaches the saturation regime, demonstrating the dielectric strength of the gate dielectric. This was confirmed by the measured low leakage current ($<10^{-12}$ A) between the gate and the substrate even for high positive gate voltages.

The transistors made with SiO_2 obtained at a higher deposition pressure exhibited a rising drain current at similar voltages (10-25 V). This effect was due to a higher leakage current for the dielectrics obtained at high pressure (see section 4.3.2).

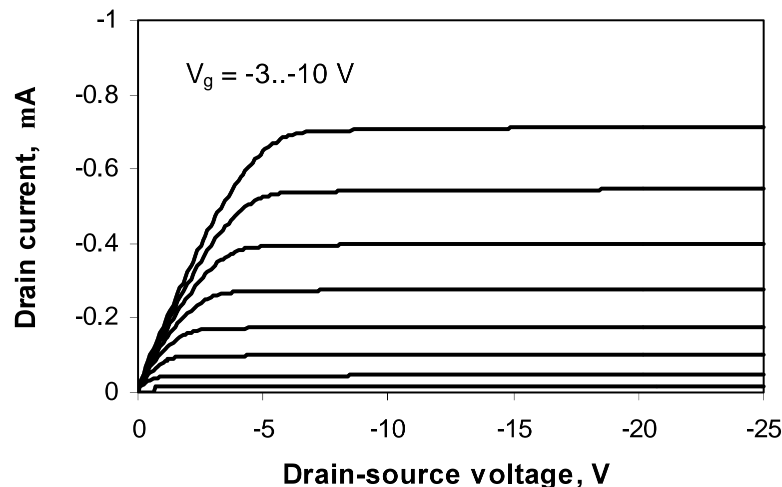

Figure 7.6. Output characteristics for PMOSFET with ECR PECVD SiO_2.

The MOSFETs electrical features were extracted from the output and transfer characteristics as described in the expressions 7.1-7.4 and are presented in table 7.1. The transistors exhibit a low off current, proving the quality of the gate dielectrics.

The threshold voltage, extracted from the transconductance graphic (fig.7.8) is around - 2.5 V and the mobility is 96 cm^2/Vs. These values are influenced by the oxide charge and interface trap density at the Si/SiO_2 interface [3]. The mobility is half of the holes mobility in a transistor with thermally grown oxide (table 7.2), while the threshold voltage is 1 V more negative.

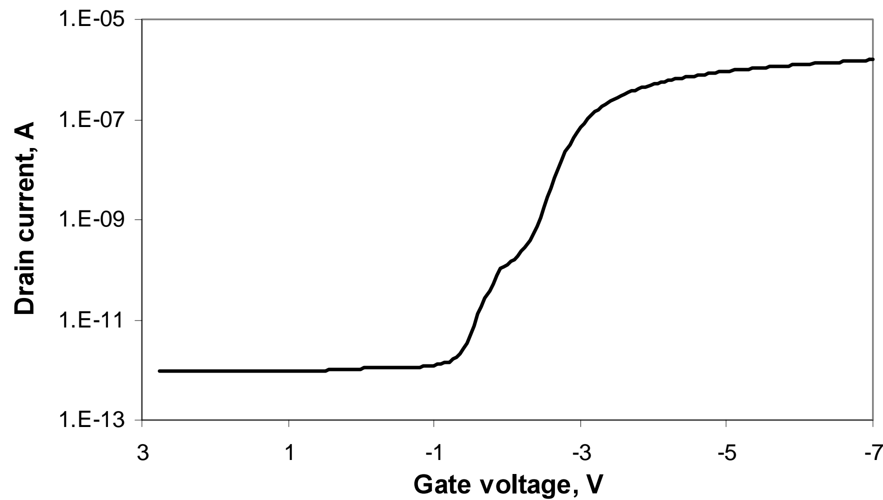

Figure 7.7. Transfer characteristics for a PMOSFET (V_D = 0.01V) with ECR PECVD SiO_2 obtained at 500°C.

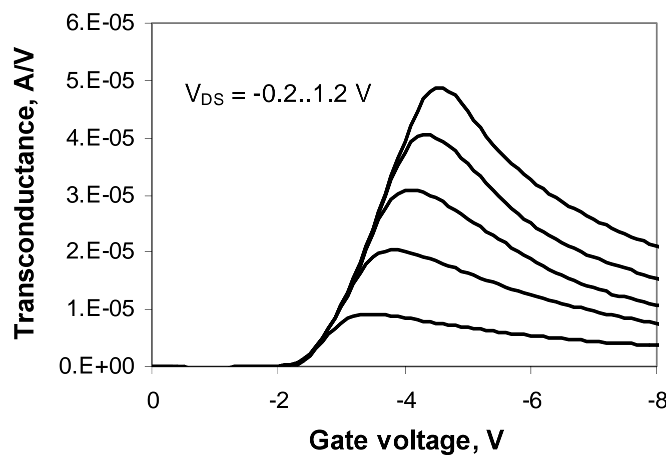

Figure 7.8. Transconductance of a PMOSFET with ECR PECVD SiO_2.

The subthreshold slope is also low, comparable with the value for the transistors with thermally grown oxide (Table 7.2). The I_{on}/I_{off} ratio is quite high: 10^6. A kink appeared in the transfer characteristics for the transistors made with the lay-out presented in figure 7.2.1. When the process flow was improved for the transistors made with near room temperature the kink disappeared (see figure 7.11), probably due to reducing the leakage current.

Table 7.1. Electrical characteristics for MISFETs with 500°C ECR PECVD gate dielectrics.

Gate dielectric	V_T (V)	μ_h (cm^2/Vs)	I_{off} (pA)	SS (V/dec.)
SiO_2	-2.5 ± 0.08	96 ± 5	0.9 ± 0.1	0.35 ± 0.06
Si_3N_4	-1.5 ± 0.06	51 ± 2	5 ± 1	0.5 ± 0.1

The ECR PECVD Si_3N_4 was also tested as a gate dielectric. The deposition conditions were: 20 mTorr pressure, microwave power of 150 W, 8 sccm N_2, 5 sccm diluted SiH_4, substrate heated to 500°C. The deposited dielectric was an oxynitride with a refractive index of 1.65. The oxygen contamination appeared due to the high pressure, low microwave power and low N_2 flow (see sections 5.3 and 5.4).

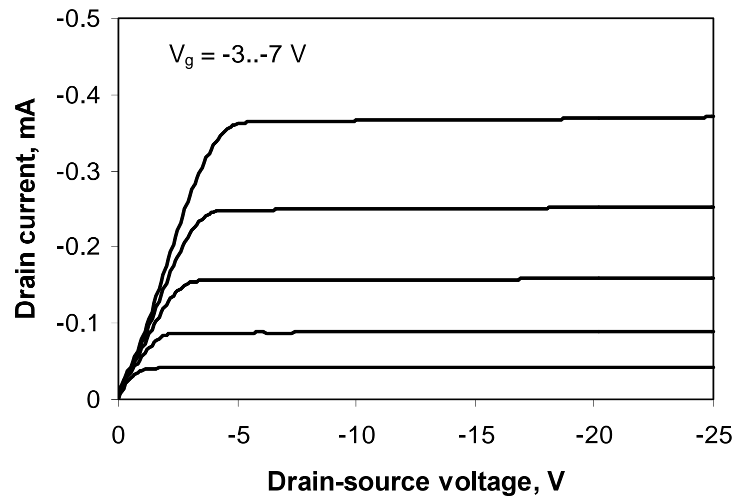

Figure 7.9. Output characteristics for a PMOSFET with a 60 nm ECR PECVD Si_3N_4.

Figure 7.9 shows the output characteristics for the transistor with Si_3N_4 as gate dielectric and the extracted parameters are listed in table 7.1. While the threshold voltage was less negative, the mobility was lower, in comparison with the transistors with SiO_2 ECR PECVD. The *C-V* curves made on the MOS capacitors present on the same wafer, showed that the positive charge was lower for the nitride film, therefore improving the transistor threshold voltage. However the interface trap density was higher causing the decrease in the carriers' mobility.

7.4.2. Room temperature gate dielectrics

The output characteristics for the transistors fabricated with near room temperature deposited dielectrics (Section 7.2.2) have been measured and presented in figure 7.10. For these transistors, the dopant density of the source and drain is quite high (10^{20} cm^{-3}) and source-body breakdown occurs for drain-source voltages of around 7 V, increasing the drain current.

The gate dielectric was deposited near room temperature, at 400 W, 10 mTorr, with 5 sccm diluted SiH_4 and 20 sccm N_2O.

A comparison between the transistors with near room temperature gate dielectric and thermally grown SiO_2 has been made and the electrical characteristics are shown in table 7.2.

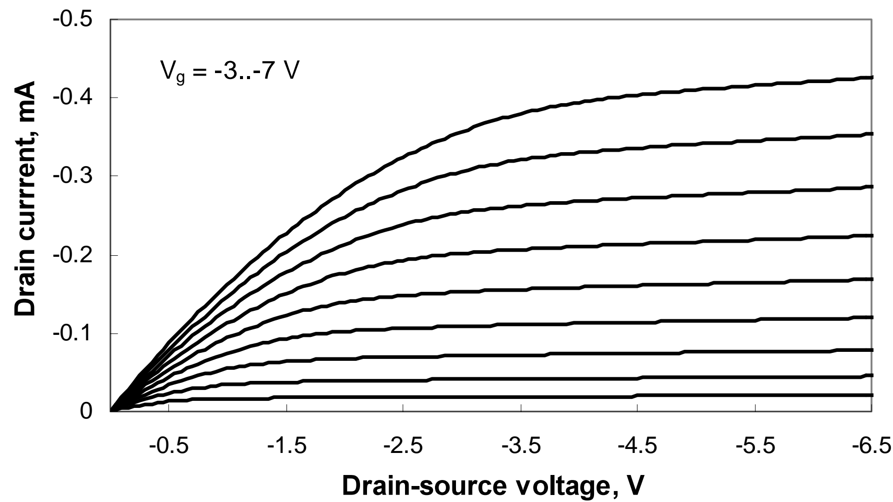

Figure 7.10. Output characteristics for a PMOSFET (W/L = 5), with a 50 nm SiO_2, deposited near room temperature.

Table 7.2. Transistor parameters for PMOSFETs fabricated with near room temperature ECR SiO_2 and reference PMOSFETs with thermally grown SiO_2.

Gate dielectric	V_T (V)	μ_h (cm^2/Vs)	I_{off} (pA)	SS (V/dec.)
ECR PECVD SiO_2	-1.25 ± 0.04	101 ± 3	1 ± 0.5	0.26±0.1
Thermally grown SiO_2	-1.5 ± 0.01	176 ± 2	0.2 ± 0.1	0.18 ± 0.04

The threshold voltages are similar for the two types of transistor. The mobility is lower than the mobility in the reference transistor, due to a higher positive charge and interface trap density (see section 4.2.7).

The transfer characteristics for transistors with two types of gate dielectric are presented in figure 7.11. The off current is higher and subthreshold slope

is lower for the PMOSFETs with near room temperature dielectric compared to the thermally grown oxides, but their values are quite good considering the deposition temperature.

Apparently, replacing the gate dielectric deposited at 500°C with the one at room temperature did not degrade the transistor properties. The subthreshold slope and threshold voltage were improved with decreasing the temperature while the off current was similar. However, because the process flows were not the same, a definite conclusion cannot be made.

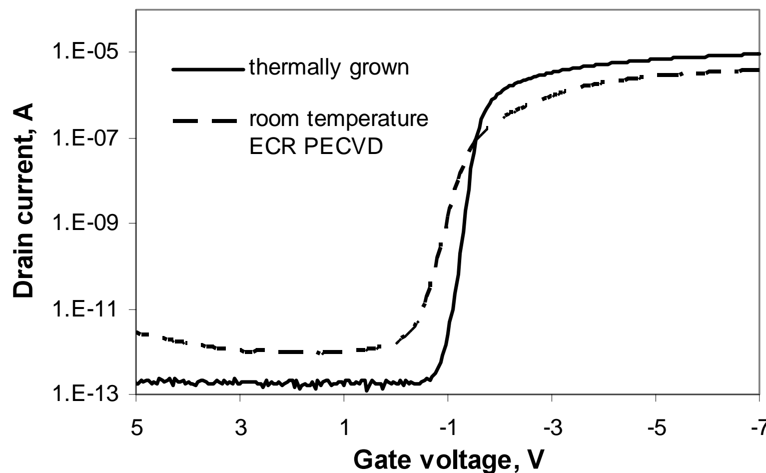

Figure 7.11. Transfer characteristics for PMOSFETs with W/L = 5 at V_D = 0.02V, with 50 nm ECR PECVD SiO_2 gate dielectric, obtained near room temperature and 40 nm thermally grown SiO_2 gate dielectric, obtained at 1050°C.

7.5. Thin film transistors

The high-mobility n-channel TFTs have been developed and fabricated by researchers at DIMES, Delft [4]. Only the gate dielectric was deposited in the multipolar ECR PECVD system.

The TFTs have been fabricated inside a single silicon grain with channel length and width of 3 μm and 4.3 μm, respectively. The large silicon grains were obtained by the grain-filter method [5]. Upon an insulator with a small diameter hole an amorphous silicon layer was deposited. The α-Si was planarised by reactive ion etching (RIE). Subsequently, the silicon film was melted by an excimer laser. The film solidification started from the grain-filter (hole) and large Si grains with diameter larger than 4 μm were produced above the grain filters.

The source and drain have been made by phosphorous implantation 30 keV with a dose of 10^{16} cm^{-2}. The dopant activation was made with an excimer laser at energy of 0.2 J/cm^2 [4].

The 40 nm SiO_2 layer used as gate dielectric was obtained by ECR plasma at near room temperature, a microwave power of 400 W, total pressure of 8 mTorr, with 5 sccm diluted SiH_4 flow and 20 sccm N_2O. Some layers were subjected to the post-deposition-annealing step described in section 2.5.

Aluminium was used as gate material and for interconnections. All the TFTs characteristics have been measured at DIMES. The TFTs parameters have been measured before and after 15 minute anneal in hydrogen plasma and presented in table 7.3 [4, 6]. The layers were not subjected to the PMA described in section 2.5, as were the capacitors studied in this thesis.

Table 7.3. Electrical parameters for large-grain Si TFTs with near room temperature ECR plasma SiO_2.

	V_T (V)	μ_e (cm^2/Vs)	I_{off} (A/μm)	SS (V/dec.)
No anneal	- 0.9	285	0.06 n	1.1
With plasma hydrogenation	-0.2 ± 0.6	354 ± 22	(13 ± 4) n	1.7 ± 0.92
With PDA and plasma hydrogenation	-0.8 ± 0.5	397 ± 45	(0.13 ± 0.04) μ	3.1 ± 0.5

The n-channel TFTs exhibited high electron mobilities (300-400 cm^2/Vs) and very good values for the threshold voltage. Both parameters were comparable to the values obtained for TFTs with thermal gate oxide. The electron mobility of the TFTs is much higher than the hole mobility measured for the MOSFETs, due to the fact that the electrons have a mobility three times higher than the holes. Furthermore the lay-out and dimensions of the transistors and the conditions in which mobility was measured were different.

For the devices fabricated without any annealing process, the measured off-current and subthreshold swing for the TFTs were reasonably low. Replacing the RIE planarisation with CMP planarisation has proven to decrease the off current and the subthreshold swing more than 10^4 times and 10 times, respectively [5]. However, the mobility decreases by 15% [4].

The off current and subthreshold swing were quite high for the TFTs measured after plasma hydrogenation. The cause of TFT deterioration after plasma annealing is not clear. The capacitors realised on c-Si wafers with the same dielectric layer were not degraded by plasma hydrogenation. More experiments for optimising the interface between the silicon grain and ECR oxide are needed. The plasma annealing increased the carrier's mobility by 25% [6].

7.6. Summary

PMOSFETs with gate dielectrics deposited by multipolar ECR plasma source at 500°C and near room temperatures have been fabricated with a simple and fast manufacturing process. The transistors exhibited low threshold voltage (-1.25 V, -2.5 V), reasonably high mobilities (101 cm^2/Vs), low off-currents (10^{-12} A) and subthreshold slopes (~ 0.3 V/dec.). Decreasing the deposition temperature of the gate dielectric did not considerably degrade the transistor parameters. The reference MOSFETs with thermally grown (1050°C) SiO_2 had superior characteristics. However, the transistors with low temperature dielectrics were reasonably good, considering the temperature used. Thin film n-channel transistors with large grain silicon and low temperature ECR gate dielectric exhibited high mobilities (300-400 cm^2/Vs) and low threshold voltage of -1 V. The off current of these devices was rather high.

7.7. References

1. R. Isihara, M. Matsumura, "Excimer laser produced single crystal silicon thin film transistors", Jpn. J. Appl. Phys., **36**, 6167 (4997).
2. P.S. Klaassen, "Electrical characterisation of gate dielectrics for thin film transistors", MSc. Thesis, Twente University, 2000.
3. S.M. Sze, Physics of semiconductor devices, 2nd edition, 1981.
4. Barry van Dijk, "Electrical characterization of c-Si TFTs fabricated by location-controlled laser crystallization", Ph.D thesis, Delft University, Netherlands, 2002.
5. P.Ch. van der Wilt, B.D. van Dijk, G.J. Bertens, R. Isihara, C.I.M. Beenakker, "Formation of location-controlled crystalline islands using substrate-embedded seeds in excimer-laser crystallization of silicon films", Appl. Phys. Letters, **79**, pp. 1819-1821 (2001).
6. Barry van Dijk, private communication.

Chapter 8 Conclusions and recommendations

8.1. Conclusions

Multipolar ECR PECVD is an excellent tool for obtaining dielectrics without heating the substrate.

Deposition kinetics:

- Deposition rate varied from 1 nm/min until 50 nm/min. Deposition rate was linear proportional with the SiH_4 partial pressure and increased with increasing the total pressure and microwave power.
- Deposition was dominated by surface chemistry, at low pressure and low microwave power. At high total pressure, deposition was limited by diffusion of precursor molecules to the substrate. Film deposition was not activated by the temperature of the substrate but was controlled by formation of precursor molecules in the gas-phase and ion bombardment of the growing film.

Silicon oxide (SiO_2) layers obtained by multipolar ECR plasma

- Stoichiometric SiO_2 films with refractive index of 1.46, low etch rate of 1.7 nm/s, and low H and N contaminations of 0.3 at.% and 0.2 at.% respectively, were deposited with a multipolar ECR plasma.
- At low total pressure and high microwave power dense SiO_2 layers with low hydrogen content, high refractive index and Si/O ratios of 1/2 were deposited, due to high energy transfer from the plasma to the layers. Si-H bonds were not present in the layer and only N-H bonds were visualised in the infrared spectra.
- The ECR SiO_2 films possessed high electrical quality, with critical field of 6 MV/cm, breakdown field of 10 MV/cm resistivity of 10^{16} $\Omega\cdot$cm, charge-to-breakdown of 1C/cm^2, net oxide charge density in the order of $10^{11}cm^{-2}$ and interface trap density of 10^{10} states/eVcm^2. These electrical properties are comparable with the ones of thermal oxide grown at 1050ºC, except for the positive charge, which is one order higher due to plasma damage.

- Films with low hydrogen content obtained by increased ion bombardment at low pressure and high microwave power exhibited higher dielectric strength. These films exhibited also increased positive charge at the interface. 400 W microwave power and 6 mTorr total gas pressure were found to provide SiO_2 layers with both good interface and bulk properties.
- A comparison between low temperature dielectrics revealed that ECR SiO_2 is better in terms of electrical properties than the rf-PECVD and LPCVD SiO_2 deposited at higher temperature.
- Porous SiO_2 layers with high silicon concentration were obtained with pure SiH_4. The usage of diluted silane, by decreasing the deposition rate improved seriously the film properties. The layers deposited with high SiH_4 flow exhibited higher leakage current, due to increased Si and H content
- The SiO_2 films obtained at low pressure and low SiH_4 flow exhibited Fowler-Nordheim tunnelling. For films deposited at higher flows or higher total pressures, the conduction mechanism is trap related. The current decreased during electrical stress because of electron trapping. Positive charges were measured at the interface for low electric stress while negative charges were trapped at high electric field. The SiO_2 reliability measurements confirmed that at low pressure and low SiH_4 flow films similar to thermally grown SiO_2 can be obtained.
- Decreasing the temperature from 500°C to near room temperature did not degrade the SiO_2 quality, proving that the multipolar ECR plasma is very efficient at low pressures.

<u>Silicon nitride layers obtained by multipolar ECR plasma</u>

- Silicon nitride films with a refractive index of 1.98, dielectric constant of 7.2, 2 at.% oxygen content and 0.6 at.% hydrogen content were deposited.
- The oxygen contamination was minimised by decreasing the pressure and increasing the microwave power. By this approach, the nitrogen dissociation in the plasma was improved due to a more efficient transfer of energy from the microwave source to the gas.
- The Si_3N_4 layers exhibited a breakdown field of 12 MV/cm, resistivity of 10^{16} Ωcm, charge to breakdown of 90 C/cm^2 and net charge density less than 10^{12} cm^{-2}. At lower pressure and higher N_2/SiH_4 ratio, films similar to 800°C LPCVD Si_3N_4 from the physical and electrical point of view were deposited.
- The extremely low hydrogen contamination was responsible for very good electric strength and film reliability, but also for degraded interface

properties. The effective charge and interface trap density, as well as the trap energy were very well correlated with the oxygen concentration.

Jet Vapour Deposition

- A 0.2 mm convergent-divergent nozzle has been designed to insure a supersonic jet of SiH_4/He.
- SiO_2 layers with a refractive index around 1.46 and stoichiometric O/Si ratio of 1.95 and less than 1% voids were deposited at room temperature by a multipolar ECR plasma source and a high-speed jet of SiH_4/He. The layers exhibited very good electrical quality: breakdown field of 12 MV/cm, net oxide charge density in the order of 10^{10} ions/cm^2 and interface trap density of 10^{11} $eV^{-1}cm^{-2}$.
- At lower pressure and higher He flow, due to increased energy transfer to the substrate, denser films with higher refractive index, less voids, stoichiometric composition and lower leakage current were deposited. The layers obtained with increased pressure in the SiH_4/He gas line possessed the best electrical quality even for high total pressure.
- Post-deposition anneal had no significant effect upon the film properties, while the post-metallization anneal step improved only the interface.

Transistors

- PMOSFETs with gate dielectrics deposited by multipolar ECR plasma source exhibited low threshold voltage (-1.25 V, -2.5 V), reasonably high hole mobilities (~ 100 cm^2/Vs), low off-currents (10^{-12} A) and subthreshold slopes (~ 0.3 V/dec). Decreasing the deposition temperature of the gate dielectric did not result in degraded transistor parameters. Although the reference MOSFETs with thermally grown (1050ºC) SiO_2 had superior characteristics, the transistors with low temperature dielectrics were good.
- N-channel thin film transistors with large grain silicon and low temperature ECR gate dielectric exhibited high mobilities (300-400 cm^2/Vs) and low threshold voltage of -1 V. The off current of these devices was rather high.

8.2. Recommendations for future work

- Improvement in the equipment in order to enable ECR plasma at very low pressures (1-5 mTorr) with higher gas flows (above 25 sccm) would extend the deposition conditions towards even better results. Under such conditions, due to the beneficial role of N_2O flow upon the oxide charge, improvement of interface properties may be possible without degrading the dielectric strength. A better vacuum may also solve the oxygen contamination problem in the Si_3N_4 films. In addition in case of high N_2 flow at low total pressures, the concentration of N radicals will be considerably increased, thus the oxygen contamination will be reduced.
- The mechanical translation and rotation construction for the chuck realised for JVD needs to be improved. The present construction has a very low lifetime ~ 10 hours of deposition. More JVD experiments need to be done with nozzles of different dimensions and at different distances from the wafer in order to further optimise the energy transfer and to obtain superior interface properties.
- The interface between the low temperature dielectrics and large grain silicon needs to be optimised by studying the effects of deposition parameters upon the TFTs characteristics.

ANNEX A.1.

Process Flowchart for Transistors with Gate Dielectric Deposited at 500°C

1. **Standard wafer cleaning (SWC):** beaker 1 fuming HNO_3 for 5 min, beaker 2 fuming HNO_3 for 5 min, rinsing in DI water, boiling HNO_3 69% 10 min, rinsing in DI water, spin dry.
2. **Silox deposition of boron-doped oxide** T = 425°C, N_2 = 3750 ml/min, 2% SiH_4 diluted in N_2 = 322 ml/min, 0.2% B_2H_6 in Ar = 280 ml/min, O_2 = 35 ml/min, time = 45 s, deposition rate 130 nm/min
3. **Silox deposition of undoped oxide:** T = 350 °C, N_2 = 3750 ml/min, 2% SiH_4 diluted in N_2 = 350 ml/min, O_2 = 35 ml/min, time = 6 min, deposition rate 40 nm/min.
4. **Definition of active areas:** *Photolithography step* (resist spinning 1.5 μm 907/17 4000 rpm, soft bake 60 s T = 95°C, exposure vacuum contact 6 s, after exposure bake 60 s T = 120 °C, developing 45 s, post bake 15 min T = 120 °C), Mask 1.
5. **Oxide etch:** HF/NH_4F 1:6 5 min, remove resist SWC + 1% HF dip.
6. **Dopant diffusion:** N_2 ambient 1 hr T = 1050 °C.
7. **Oxide etch, removal of oxide over gate area:** HF/NH_4F 1:6 1 min, remove resist SWC + 1% HF dip.
8. **LT deposition of ECR gate oxide:** 60 nm, P = 150 W, p = 18 mTorr, SiH_4/He = 5 sccm, N_2O = 3 sccm, T = 500°C.
9. **Anneal:** N_2 wet ambient 60 min T = 500 °C.
10. **Definition of contact windows:** *Photolithography step*, Mask 2.
11. **Oxide etch:** step 5.
12. **Metal deposition:** Oxford sputtering equipment 7000 W 350 V, Ti/W 20/80 barrier 70 nm, aluminium 1 μm.
13. **Metal patterning:** *Photolithography step* without boiling in HNO_3, Mask 3.
14. **Metal etch:** aluminium etch 1min, tungsten-titanium etch in H_2O_2 15 min, remove resist (beaker 1 fuming HNO_3 for 5 min, beaker 2 fuming HNO_3 for 5 min, rinsing in DI water).
15. **Back metal deposition:** resist spinning 1.5 μm 907/17 4000 rpm, post bake 15 min T = 120 °C, 1% HF dip, Oxford sputtering equipment aluminium 1 μm.
16. **Alloy step:** 30 min, T = 450°C in wet N_2 ambient.

ANNEX A.2.

Process Flowchart for Transistors with Gate Dielectric Deposited at near Room Temperature

1. **Standard wafer cleaning (SWC):** beaker 1 fuming HNO_3 for 5 min, beaker 2 fuming HNO_3 for 5 min, rinsing in DI water, boiling HNO_3 69% 10 min, rinsing in DI water, spin dry.
2. **Silox deposition of boron-doped oxide:** T = 425°C, N_2 = 3750 ml/min, 2% SiH_4 diluted in N_2 = 322 ml/min, 0.2% B_2H_6 in Ar = 280 ml/min, O_2 = 35 ml/min, time = 45 s, deposition rate 130 nm/min.
3. **Silox deposition of undoped oxide: :** T = 350 °C, N_2 = 3750 ml/min, 2% SiH_4 diluted in N_2 = 350 ml/min, O_2 = 35 ml/min, time = 6 min, deposition rate 40 nm/min.
4. **Definition of active areas:** *Photolithography step* (resist spinning 1.5 μm 907/17 4000 rpm, soft bake 60 s T = 95°C, exposure vacuum contact 6 s, after exposure bake 60 s T = 120°C, developing 45 s, post bake 15 min T = 120°C), Mask 1.
5. **Oxide etch:** HF/NH_4F 1:6 1 min, remove resist SWC + 1% HF dip.
6. **Silox deposition of phosphorous-doped oxide:** T = 350°C, N_2 = 3750 ml/min, 2% SiH_4 diluted in N_2 = 350 ml/min, 0.4% P_2H_3 in Ar = 5 ml/min, O_2 = 35 ml/min, time = 2.5 min, deposition rate 40 nm/min.
7. **Silox deposition of undoped oxide**: step 3.
8. **Definition of gate areas:** *Photolithography step*, Mask 2.
9. **Oxide etch**: step 5.
10. **Silox deposition of undoped oxide:** step 3.
11. **Dopant diffusion:** N_2 ambient 1 hr T = 1050°C.
12. **Oxide etch**, removal of oxide over gate area: step 5.
13. **LT deposition of ECR gate oxide:** 50 nm, P = 400 W, p = 6 mTorr, SiH_4/He = 5 sccm, N_2O = 20 sccm, T = 50ºC.
14. **Anneal:** N_2 wet ambient 60 min T = 500°C.
15. **Definition of contact windows:** *Photolithography step*, Mask 3.
16. **Oxide etch:** HF/NH_4F 1:6 1 min, remove resist SWC + 1% HF dip.
17. **Metal deposition:** Oxford sputtering equipment 7000 W 350 V, aluminium 1 μm.
18. **Metal patterning:** *Photolithography step* without boiling in HNO_3, Mask 4.
19. **Metal etch:** aluminium etch 1min, remove resist (beaker 1 fuming HNO_3 for 5 min, beaker 2 fuming HNO_3 for 5 min, rinsing in DI water)

20. **Back metal deposition:** resist spinning 1.5 μm 907/17 4000 rpm, post bake 15 min T = 120 °C, 1% HF dip, Oxford sputtering equipment aluminium 1 μm.
21. **Alloy step:** 5 min, T = 450°C in wet N_2 ambient.

SAMENVATTING

In de informatietechnologie is een duidelijke trend waarneembaar naar beeldschermen met een groot oppervlak, hoge resolutie, laag vermogen, lage kosten en een flexibele drager. LCD (Liquid Crystal Display) vlakke paneel beeldschermen (flat panel displays) hebben een breed toepassingsgebied en de verwachting is dat de markt voor deze beeldschermen de komende jaren een sterke groei zal doormaken.

Tegenwoordig worden veelal dunne film transistoren van het MOS (Metal Oxide Semiconductor) type in amorf silicium toegepast als schakelaars in LCD beeldschermen. Het nadeel van deze transistoren is de lage beweeglijkheid van de ladingdragers (elektronen of gaten) en bovendien zijn hun elektrische eigenschappen onvoldoende stabiel om elektronische schakelingen met deze componenten mee te integreren op glas of plastic substraten. Daarom is er behoefte aan transistoren met goede, stabiele elektrische eigenschappen, die gerealiseerd kunnen worden bij een temperatuur die laag genoeg is voor toepassing op goedkope glassubstraten of polymeer substraten.

Het gate diëlektricum is van essentieel belang voor een goed functionerende Metaal Oxide Silicium Transistor. Tot nu toe was de kwaliteit van het gate oxide slechter naarmate de realisatie temperatuur lager was.

De onderzoek uitdaging van dit promotieonderzoek was om een technologie te ontwikkelen waarmee, bij temperaturen rond kamertemperatuur, diëlektrische lagen op Silicium gedeponeerd kunnen worden met goede, isolerende eigenschappen. In het bijzonder zijn de MOST eigenschappen zoals interface stabiliteit en de elektrische doorslagsterkte van belang.

De oplossing is gezocht in een depositie methode, die bekend staat als "Electron Cyclotronic Resonance Plasma Enhanced Chemical Vapour Deposition" (ECR-PECVD). Voor dit proces wordt een microgolf plasma gecreëerd met behulp van elektroncyclotron resonantie in een plasma reactor, op afstand van het substraat. Vanuit dit plasma vindt de depositie plaats, terwijl het substraat zelf niet direct aan het plasma wordt blootgesteld. Er is een technologie ontwikkeld voor de depositie van siliciumoxide lagen en voor siliciumnitride lagen. Optimalisatie van de laag eigenschappen bleek

lastig doordat variatie van de depositieparameters strijdige uitwerking had op de diverse elektrische eigenschappen van de lagen. Naarmate het inzicht in de depositieprocessen groeide bleek het echter mogelijk om de processen zodanig te optimaliseren dat er siliciumoxide lagen en siliciumnitride lagen gegroeid kunnen worden op onverwarmde substraten, met eigenschappen die de klassieke thermische oxides en nitrides vrijwel evenaren.

Bij lage druk en hoge microgolfenergie is het ECR plasma erg energierijk en de ionen arriveren met een hoge kinetische energie op het substraat. Onder deze conditie kunnen dichte lagen met een laag waterstofgehalte en uitstekende diëlektrische eigenschappen worden gedeponeerd. SiO_2 lagen die met een dergelijk ECR plasma bij nagenoeg kamertemperatuur zijn verkregen vertonen een specifieke weerstand, doorslagveldsterkte en een lading voor doorslag (charge-to-breakdown) die vrijwel gelijk is aan die van thermisch gegroeide oxides. Erg hoge microgolfenergie en uiterst lage drukken blijken evenwel schadelijke effecten voor het grensvlak Si-SiO_2 op te leveren tengevolge van de hoogenergetische botsingen van de ionen op het oppervlak. Daarom was voor de optimalisatie van het proces een gedetailleerde studie nodig van de effecten van de verschillende depositieparameters op de film eigenschappen. De hoge opname van waterstof bij hoge druk en lage microgolfenergie bleek verantwoordelijk te zijn voor verhoogde lekstroom, hoge invangst van lading (trapping) en slechte betrouwbaarheid eigenschappen. Stoichiometrische Si/O verhoudingen werden verkregen bij sterke verdunning van de SiH_4 precursor in Helium.

Bij nagenoeg kamertemperatuur gedeponeerde Siliciumnitride lagen vertoonden ook uitstekende bulk eigenschappen en bleken een waterstof gehalte kleiner dan 1 at.% te hebben. De zuurstof contaminatie werd geminimaliseerd bij lage drukken om een verhoging van de dissociatiegraad van N_2 te bewerkstelligen. Zuurstof atomen hebben een heilzame werking voor het grensvlak tussen de gedeponeerde laag en het silicium, zonder dat de diëlektrische sterkte van de film nadelig wordt beïnvloed.. Hierdoor kan siliciumnitride een oplossing bieden voor het produceren bij nagenoeg kamertemperatuur van lagen met zowel goede grensvlak als bulk eigenschappen.

Om de film eigenschappen verder te verbeteren is ook de Jet Vapour Depositie technologie verkend. Hierbij wordt een hoge snelheid straal van Helium, waarin het SiH_4 wordt getransporteerd op de wafer gericht. De straalstroom (jet stream) wordt opgewekt in een convergerende-divergerende straalpijp. De beste vorm en afmetingen van de straalpijp werden verkregen uit simulaties van de gasstroom met technieken uit de vloeistof dynamica.

Proefondervindelijk is vastgesteld dat toename van de druk bij de ingang van het mondstuk, de schadelijke effecten van hoge drukken op de bulk eigenschappen kan tegengaan. De extra kinetische energie teweeggebracht door de supersonische straalstroom, zorgt voor verdichting van de gedeponeerde lagen. De diëlektrische sterkte van de lagen werd niet beïnvloed door de nabehandelingprocessen, hetgeen aantoont dat ECR-JVD plasma een geschikte technologie is voor het aanbrengen van lagen bij lage temperatuur.

Ten behoeve van het karakteriseren van de diëlektrische eigenschappen van de lagen zij er Metaal–Oxide-Semiconductor condensatoren gemaakt. De ECR en JVD lagen bleken beter dan LPCVD (Low Pressure Chemical Vapour Deposition) en rf-PECVD (radio-frequent Plasma Enhanced Chemical Vapour Deposition) diëlektrica.

Tenslotte zijn MOS-transistoren gemaakt en bemeten. Hiermee werd experimenteel bevestigd dat de kwaliteit van lage temperatuur diëlektrica ook met betrekking tot de drempelspanning en de hoogte van de ladingdragers mobiliteit goed is.

SUMMARY

The trend in information technology is toward large-screen, high-resolution, low-power, low-cost and flexible displays.

Flat panel displays have a large area of applications and it has been predicted that the display market is going to increase in the next years. Amorphous-silicon transistors, while widely used nowadays as switching devices in displays, have too low carrier mobility and poor stability for integrating the circuitry on glass or plastic substrate. Therefore, transistors with good characteristics need to be realized at low temperature, compatible with the cheep glass or polymer substrate.

The gate dielectric is fundamental for the good functioning of the transistor, however until recently the quality of the dielectric was degraded considerably with decreasing the temperature.

The challenge of this PhD research is to develop a technology for realizing a high quality dielectric in terms of interface properties and breakdown field at near room temperature.

A low-temperature deposition method called electron cyclotronic resonance (ECR) PECVD has been used for depositing silicon oxide and silicon nitride films. Optimising the film properties has proved to be difficult due to the opposite dependencies of electrical properties upon the deposition parameters. For low pressure and high microwave power, the ECR plasma was very energetic and the ions bombard efficiently the substrate. Therefore, for these conditions, dense layers with low hydrogen content and excellent dielectric strength can be produced. The ECR plasma deposited SiO_2 obtained at near room temperature exhibits resistivity, breakdown field and charge-to-breakdown similar to the ones of thermally grown oxide. However, very high microwave power and extremely low pressure have deleterious effects upon the interface due to ion bombardment. Therefore the film optimisation required studying in detail the effects of various deposition parameters upon the film properties.

The hydrogen incorporation at high pressure and low microwave power proved to be responsible for the increased leakage current, high trapping

behaviour and poor reliability. Stoichiometric Si/O ratios were obtained by highly diluting the SiH_4 precursor in helium.

Silicon nitride layers deposited at near room temperature exhibited also excellent bulk properties and under 1 at.% hydrogen content. The oxygen contamination was minimised at low pressures for an increased dissociation degree of N_2. Oxygen atoms have a beneficial role upon the films interface with silicon, without degrading the dielectric strength; therefore silicon oxynitride can be a solution for obtaining layers at near room temperature with both good interface and bulk properties.

In order to improve furthermore the film properties, Jet Vapour Deposition was explored. A high-speed jet of helium transporting the SiH_4 to the wafer was produced with a convergent-divergent nozzle. The shape and dimensions of the nozzle were obtained by simulating the gas flow, according too the fluid dynamics. Experiments have shown that increasing the pressure at the entrance of the nozzle can eliminate the deleterious effect that high pressure has upon the bulk properties. The extra kinetic energy brought by the supersonic jet densified the deposited films. Annealing processes did not modify the dielectric strength of the layers, showing that ECR –JVD plasma is suitable for low temperature deposition.

Metal–oxide –semiconductor capacitors were used mainly for investigating the dielectric properties. The ECR and JVD films were better than LPCVD and rf-PECVD dielectrics. Transistors made with low temperature dielectrics confirmed the high quality of the films in terms of low threshold voltage and high mobility.

ACKNOWLEDGEMENTS

This PhD dissertation is the result of the research I performed in the Semiconductor Components group, at MESA+ Research Institute of the University of Twente. The work was financially supported by the Dutch Foundation for Fundamental Research on Matter (FOM). During the research, I had support from many people and I am very grateful to all of them. I would especially like to thank:

- My promoter Hans Wallinga for continuous encouragement and support, and for helping me with organizing and writing this thesis.
- My daily supervisor Jisk Holleman for his guidance, for the many fruitful discussions and for his vast knowledge that he shared with me.
- Pierre Woerlee for the constructive talks we had, for his useful advices in the topic of conduction mechanisms and for his suggestions about my papers.
- Alexey Kovalgin from I which I learnt almost everything I know about CVD and dielectrics; who had the patience of introducing me into the subject of my thesis and answering all my annoying questions. *Alexey спасибо!*
- Cornel Cobianu for introducing me to University of Twente and for his encouragement in presenting my work.
- Ronald Dekker for introducing me into the Clean Room work; Tom Aarnick for his technical advices and for his pleasant presence; Ton Jenneboer for being always ready to help; Marcel Weusthof and Henk de Vries for their support in the testing room; Cor Bakker and Frederik Reenders for helping me communicate with my computer.
- Eddy Ruiter, Arie Kooy, Peter Linders, Huib van Vossen, Marion Groen, Stan Kruger, Jonny Sanderink and Samantha Geerdink for their technical support in the Clean Room; the technicians from the glass workshop for their help with the quartz lines; Peter and André, the technicians from the mechanical workshop for repairing for several times the chuck; Martin Siekman for his assistance in AFM measurements, Paul Kosters for his help with FTIR measurements and Albert van den Berg for the Auger and XPS measurements.
- Marie-Christine Predery, Annemiek Janssen, Joke Vollenbroek and Sofie Kreulen for their administrative assistance.
- Peter Klaassen for his work in transistors with low temperature dielectric.

- Ton Mouthaan, Fred Kuper, Herma van Kranenburg and Jurrian Schmitz for their support.
- My colleagues Andreea, Svetlana, Zichun, Nataša, Sheela, André, Hieu, Phuong, Viet, Radko and Jay for creating a wonderful atmosphere but also for helping me when I had problems.
- Berndt Stannowski from Utrecht University for the ERD measurements; Barry van Dijk from Delft University for making and measuring the large grain TFTs and Mircea Modreanu from NMRC, Ireland for the spectroscopical ellipsometry measurements.
- Loredana and Szabolcs Deladi, Rita and Octavian Petre, Codruta and Cosmin Marinica and Victor Popa for being my friends.

I am very grateful to all my family members for their permanent support. I miss you so much; you are in my heart and mind wherever I go. I am grateful especially to my late father Ioan for believing always in me, to my mother Constanţa for her unconditional love for me, to my brother Andu for his patience with me and to my cousin Andreea Mareş for helping me these last months while I was writing the thesis.

Finally and most importantly, I would like to thank my husband Bogdan and my daughter Ana for being my sources of joy and strength. Thank you for putting up with me these last years, while I was doing my PhD.

LIST OF PUBLICATIONS

Publications

- Kovalgin, A.Y., Isai, I.G., Holleman, J., Dekker, R., Woerlee, P.H., & Wallinga, H., *Characterisation of silicon oxide films deposited by means of ECR PECVD*, Proceedings of SAFE conference 1999, 24 November 1999, Mierlo, The Netherlands.
- Isai, I.G., Kovalgin, A.Y., Holleman, J., Woerlee, P.H., & Wallinga, H., *High quality, room temperature gate dielectrics for TFTs*, Proceedings of SAFE conference 2000, 29 November 2000, Veldhoven, The Netherlands.
- Isai, I.G., Kovalgin, A.Y., Holleman, J., Wallinga, H., Woerlee, P.H., & Cobianu, C., *Electrical characterisation of gate dielectrics deposited with multipolar electron cyclotron Resonance Plasma Source*, Proceedings of the 30th European Solid State Device Research Conference, ESSDERC 2000, 11 September 2000, Cork, Ireland, pp. 424-427.
- Isai, I.G., Kovalgin, A.Y., Holleman, J., Woerlee, P.H., & Wallinga, H., *High quality silicon oxide deposited with a multipolar electron cyclotron resonance plasma source*, Thin Film Technologies V, Volume 2000-31, pp. 169-175.
- Isai, G., Kovalgin, A., Holleman, J., Woerlee, P.H., & Wallinga, H., *Room temperature SiO_2 films deposited by multipolar ECR PECVD,* Journal de Physique IV, Volume 11, No. 3, 2001, pp. 747-753.
- Isai, G., Holleman, J., Woerlee, P.H., & Wallinga, H., *Electrical conduction processes in silicon oxide films obtained by ECR PECVD*, Proceedings of SAFE conference 2001, 29 November 2001, Veldhoven, The Netherlands.
- Isai, G., Holleman, J., Woerlee, P.H., & Wallinga, H., *Silicon nitride layers obtained by ECR PECVD,* Proceedings of SAFE conference 2002, 29 November 2002, Veldhoven, The Netherlands.
- Isai, G., Kovalgin, A., Holleman, J., Woerlee, P.H., & Wallinga, H., Electrical properties of room temperature SiO_2 deposited by a combination of jet vapor source and multipolar electron cyclotron resonance plasma, Thin Film Technologies VI, accepted for publication.
- Isai, I.G., Kovalgin, A.Y., Holleman, J., Wallinga, H., Woerlee, P.H., Cobianu, C., Modreanu, M., Physical properties of silicon oxide layers deposited at room temperature by a combination of ECR plasma and high-speed jet of silane, Proceedings of CVD XVI/ EUROCVD 14, Volume 2003-08, pp. 609, 27 April-1 May 2003, Paris, France.

- Isai, G., Holleman, J., Woerlee, P., & Wallinga, H., *Low hydrogen content silicon nitride films deposited at room temperature with a multipolar ECR plasma source,* Journal of the Electrochemical Society, submitted for publication.
- Isai, G., Holleman, J., Woerlee, P., & Wallinga, H., *Conduction and trapping mechanisms in SiO_2 films grown near room temperature by multipolar ECR PECVD*, Journal of Vacuum Science and Technology B, submitted for publication.

Oral presentations and posters

- Isai, G., Holleman, J., Woerlee, P.H., & Wallinga, H., *Room temperature silicon nitride films deposited with a multipolar electron cyclotron resonance plasma source,* EMRS conference, Strasbourg, France, 18-22 June 2002, oral presentation.
- Isai, I.G., Kovalgin, A.Y., Holleman, J., Dekker, R., Woerlee, P.H., & Wallinga, H., *Dielectric thin films deposited by means of ECR PECVD,* FOM Solid-State Physics conference, Veldhoven, The Netherlands, 20-21 December 1999, poster.

ABOUT THE AUTHOR

Gratiela Isai was born in Ploiesti, Romania on 24 September 1975. In 1994 she graduated the National College Sf. Sava from Bucharest, Physics - Chemistry Orientation. In September 1994 she was admitted to the Faculty of Physics at the University of Bucharest. She followed the Solid-State Physics courses and graduated the first in 1998 with a thesis on plasmon-phonon mode coupling in semiconductors. In October 1998 she began to work as a PhD student at the Department of Electrical Engineering on deposition at low temperature of high quality dielectrics for thin film transistors. This research work has resulted in the present thesis.